AD-A146 183 CENTER FOR DIELECTRIC STUDIES(U) PENNSYLVANIA STATE 1/2
UNIV UNIVERSITY PARK MATERIALS RESEARCH LAB
L E CROSS ET AL. MAY 84 N00014-82-K-0339

UNCLASSIFIED F/G 20/12 NL

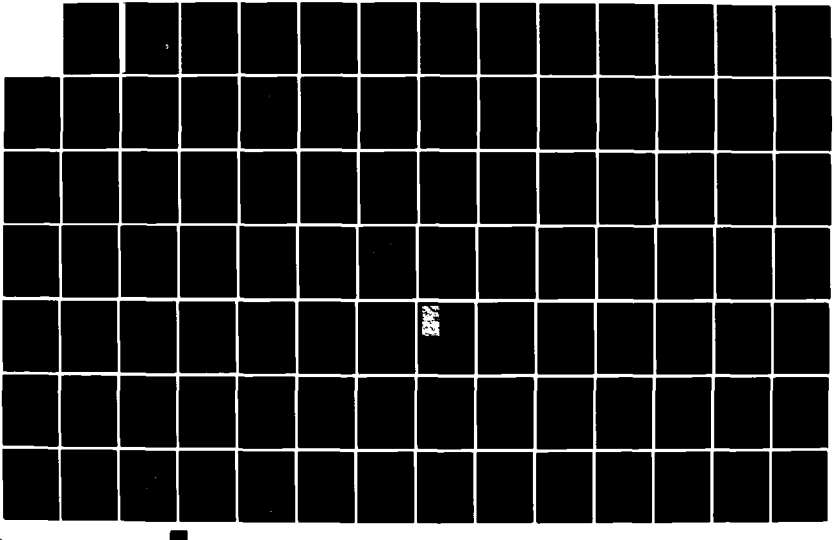

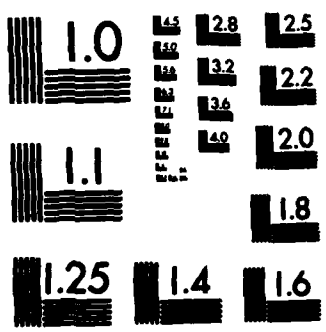

MICROCOPY RESOLUTION TEST CHART

(12)

CENTER FOR DIELECTRIC STUDIES

Contract No. N00014-82-K-0339

Sponsored by

The Office of Naval Research

L.E. Cross

R.E. Newnham

J.V. Biggers

May, 1984

THE MATERIALS RESEARCH LABORATORY

THE PENNSYLVANIA STATE UNIVERSITY

UNIVERSITY PARK, PENNSYLVANIA

DISCLAIMER NOTICE

THIS DOCUMENT IS BEST QUALITY PRACTICABLE. THE COPY FURNISHED TO DTIC CONTAINED A SIGNIFICANT NUMBER OF PAGES WHICH DO NOT REPRODUCE LEGIBLY.

TABLE OF CONTENTS

ABSTRACT

This report describes work carried out over the second year of support under ONR Contract No. N00014-82-K-0339 which was for partial support of a Center for Dielectric Studies at Penn State. It is very pleasing to be able to report that over this year we have built up a truly National Center for Dielectric Studies with ten major companies in full membership, and eleven in associate membership. The National Science Foundation recognized the Center with a Centers Grant funding. Over the year, the Office of Naval Research also initiated or continued funding of eight associated programs on closely related dielectric topics.

This report focuses upon the parts of the Center program which have drawn most extensively upon Navy funds. In the basic study of polarization processes in high K dielectrics, major progress has been made in understanding the mechanisms in relaxor ferroelectric in the perovskite structure families. A new effort is also being mounted to obtain more precise evaluation of the internal stress effects in fine grained ~~$BaTiO_3$~~ barium titanate. Related to reliability, studies of the effects of induced macro-defects are described, and preparation for the evaluation of space charge by internal potential distribution measurements discussed.

To develop new processing methods for very thin dielectric layers, a new type of single barrier layer multilayer is discussed, and work on the thermal evaporation of oriented crystalline antimony sulphur iodide describe.

In line with earlier reports, a brief narative description is given of ongoing work, and completed published studies are summarized in the technical appendices.

1.0 INTRODUCTION

This report describes work carried out over the second year of ONR Contract No. N00014-82-0339 which was a funding in partial support for the formation of a Center for Dielectric Studies at The Pennsylvania State University. It is very pleasing to be able to report that over the current contract year, from March 1, 1983, to March 1, 1984, the build up of a truly National Center for Dielectric Studies has been accomplished. In March, 1983, in response to a first solicitation, eight major companies came into full membership and three into associate membership. August of 1983, following on from a most useful planning grant, the National Science Foundation (NSF) announced the award of a National Centers Grant to Penn State, recognizing the initiation of a National Center for Dielectric Studies. By the end of the calendar year, there were ten companies in full membership and five in associate membership category. The current status of the Center, as of March 1, 1984, is summarized in Appendix 16 which gives the names of all companies in membership and their designated representatives to the Center.

In parallel, and coordinated with this effort, the Office of Naval Research has now funded eight associated programs on topics dealing primarily with the reliability of multilayer capacitors (MLCs) and their dielectrics. Work statements for the associated programs are given in Appendix 17.

Early in the contract year (May 24th and 25th), a preliminary organizational meeting was held with the Industry representatives at Penn State to plan in more detail the structuring of the Center, and the qualifications and conditions for Industrial membership. This planning process was concluded at the Annual meeting of the Center held November 7-9, 1983. This Annual Meeting was also coordinated with one full day of presentations on the associated programs.

In the following report, those parts of the Center program which have drawn extensively upon ONR supporting funds are highlighted. Following the established practice for ONR reporting, work in progress is covered in a compact narative style. Completed studies are attached as technical appendices.

2.0 SUMMARY OF TECHNICAL ACHIEVEMENTS

Topics for study were initially classified broadly under the titles Basic Science, Evolutionary Studies, and Revolutionary Approaches.

2.1 Basic Science

A problem which is necessarily of major concern is that of the polarization processes which contribute to the high dielectric polarizability in the ferroelectric type dielectrics which are of fundamental importance to the compact high capacitance MLCs. As was indicated in our first report, to make use of and build upon the foundation of earlier Navy sponsored programs, a major topic of our interest has been the ferroelectric relaxors, ferroelectrics with diffuse phase change at T_c which have also been of major interest as electrostrictive displacement transducers, but which because of their very high permittivity begin to find significant interest as capacitor dielectrics.

Here, however, the emphasis of the work is in developing basic understanding, and we believe that by a combination of approaches the group has made an important step forward in understanding these unusual relaxor systems.

It would appear now that in the systems, lead scandium tantalate, lead magnesium niobate and its solid solutions with lead titanate, and in the higher lanthanum containing lead lanthanum zirconate titanates (PLZTs), we can trace out the evolution of developing order from paraelectric, through

superparaelectric, critical superparaelectricity into the final ferroelectric ordered state. A discussion of these phenomena was given at the fall meeting of the American Ceramic Society in Grossingers, NY. A more complete summary of the evidence is given in the following.

A second very basic area of study has been concerned with a refined treatment of the effects of grain size upon the dielectric properties of pure $BaTiO_3$ ceramics. To permit an update and extension of the original simple Buessem, Goswami, Cross (BGS) internal stress model a refined thermodynamic analysis is being carried through in cooperation with the Ceramics Department in Leeds University. To permit description of the very wide temperature range now covered by the more recent Japanese experimental data[1] the Gibbs Free Energy function has been expanded to include all symmetry permitted sixth power terms in electric polarization.

To check the validity of the proposed function, it has been used to predict the electric field dependence of the ferroelectric:ferroelectric phase transitions, and gives excellent agreement with the experimental data by Fesenko[2].

To identify the average stress levels which occur due to the absence of 90° twins in the fine gain size ceramics, new x-ray measurements covering the temperature range down to 4°K are being carried out in Oxford, and the modified spontaneous strains compared to the strains in free powders. The measured strain will be converted to stress using the known elastic constants, and the modified permittivity calculated in tetragonal, orthorhombic and rhombohedral phases using the improved thermodynamic function.

2.2 Evolutionary Approaches

In the evolutionary approaches, two studies are involved. As a first attempt to provide experimental data for model studies, plastic inserts in the

green tape have been used to induce voids and delaminations of controlled shape and their influence on the dielectric properties studied. For the second, we are setting up to measure the potential distribution in 'thin' dielectric sheets by using probing electrodes tape cast into the multilayer structure. The former work has been completed and details are given in the M.S. dissertation of David Hardy, the abstract for which is included as a technical appendix. the latter study is now at the stage where the measuring equipment has been completed and first samples are now being studied.

2.3 Revolutionary Studies

For the revolutionary approaches, two topics are again of special interest. In the first, we have been exploring techniques for evaporating thin films of the ferroelectric antimony sulphur iodide (SbSI). The very low melting temperature of SbSI suggests that crystalline films may be deposited upon quite low temperature substrates. Initial studies have shown excellent promise, but are plagued with problems of reproducibility. The second study concerns an imaginative approach to developing a multilayer barrier layer capacitor. Rather than trying, with many other groups, to make a grain:grain boundary structure of a size which can be accommodated in the very thin dielectric layer of the MLC we have gone to a modification of the Corning ACE process to inject a fritted silver electrode into a reduced $BaTiO_3$ body so as to form surface barrier layers on each of the thin reduced $BaTiO_3$ layers.

Effective internal surface barrier layers have been demonstrated, and very high volumetric efficiencies appear possible if the injection technology for the electrode can be improved.

2.4 Publications and Presentations at Meetings

Over the current contract period, the following papers have been published or accepted for publication.

1. S.L. Swartz, T.R. Shrout, W.A. Schulze, L.E. Cross. 'Dielectric Properties of Lead Magnesium Niobate Ceramics.' J. Amer. Ceram. Soc. 67:311 (1984).
2. D.J. Voss, S.L. Swartz, T.R. Shrout. 'The Effects of Various B-Site Modifiers on the Dielectrics and Electrostrictive Properties of Lead Magnesium Niobate Ceramics.' Ferroelectrics 50:203 (1983).
3. T.R. Shrout, S.L. Swartz, M.J. Haun. 'Dielectric Properties in the $Pb(Fe_{1/2}Nb_{1/2})O_3$:$PbNi_{1/3}Nb_{2/3}O_3$ Solid Solution System.' Bull. Amer. Ceram. Soc. (June, 1984), in press.
4. Yao Xi, Chen Zhili, L.E. Cross. 'Polarization and Depolarization Behavior of Hot Pressed Lead Lanthanum Zirconate Titanate Ceramics.' J. Appl. Phys. 54:3399 (1983).
5. Chen Zhili, Yao Xi, L.E. Cross. 'Depolarization Behavior and Reversible Pyroelectricity in Lead Scandium Tantalate Ceramics Under DC Bias.' Ferroelectrics 49:213 (1983).
6. Chen Zhili, Yao Xi, L.E. Cross. 'Reversible Pyroelectric Effects in $Pb(Sc_{1/2}Ta_{1/2})O_3$ Ceramics Under DC Bias.' Ferroelectric Letters 44:271 (1983).
7. Yao Xi, Chen Zhili, L.E. Cross. 'Polarization and Depolarization Behavior in Hot Pressed Lead Lanthanum Zirconate Titanate Ceramics.' Ferroelectrics 54:163 (1984).
8. A.J. Bell, A.J. Moulson, L.E. Cross. 'The Effect of Grain Size on the Permittivity of $BaTiO_3$.' Ferroelectrics

9. A.J. Bell, L.E. Cross. 'A Phenomenological Gibbs Function for $BaTiO_3$ Giving Correct E Field Dependence of all Ferroelectric Phase Changes.' Ferroelectrics (in press).

10. P.K. Ghosh, A.S. Bhalla, L.E. Cross. 'Preparation and Electrical Properties of Thin Films.' Ferroelectrics 51:29 (1983).

11. Zhang, Liangying, Yao Xi, H.A. McKinstry, L.E. Cross. 'Quasi Static Capacitance and Ultra Slow Relaxation of Linear and Nonlinear Dielectrics.' Ferroelectrics 49:75 (1983).

12. A.S. Bhalla, C.S. Fang, L.E. Cross, Yao Xi. 'Pyroelectric Properties of Modified Triglycine Sulphate Crystals.' Ferroelectrics 51:9 (1983).

13. C.S. Fang, Yao Xi, A.S. Bhalla, L.E. Cross. 'The Growth and Properties of a New Alanine and Phosphate Substituted Triglycine Sulphate (ATGSP) Crystals.' Ferroelectrics 51:9-13 (1983).

14. D.C. Hardy. M.S. Thesis in Ceramics, 'The Modeling and Effects of Macrodefects in Monolithic Capacitors,' The Pennsylvania State University (Dec. 1983).

The following papers were presented at National and International Meetings.

ANNUAL MEETINGS OF THE AMERICAN CERAMIC SOCIETY

CHICAGO, APRIL 1983

1. R.E. Newnham. Keynote Address: 'Structure-Property Relations in Multilayer Ceramics.'

2. M.J. Haun, S.L. Swartz, T.R. Shrout. 'Dielectric Properties in the $PbFe_{1/3}Nb_{2/3}O_3$-$PbNi_{1/2}Nb_{1/2}O_3$ Solid Solution System.'

3. S.L. Swartz, D.J. Voss, T.R. Shrout. 'The Effects of Various Additives on the Dielectric Properties of Lead Magnesium Niobate Ceramics.'

4. D.C. Hardy, G.L. Messing, W.A. Schulze. 'Defect Modeling in $BaTiO_3$ Monoliths.'

5. C.S. Fang, Z.X. Chen, L.E. Cross, A. Bhalla. 'Growth and Properties of Lithium-Doped TGS Crystal.'

INTERNATIONAL SYMPOSIUM ON APPLICATIONS OF FERROELECTRICS

ISAF 83 NBS, GAITHERSBURG, WASHINGTON, JUNE, 1983

6. D.J. Voss, S.L. Swartz, T.R. Shrout. 'The Effects of Various B-Site Modifications on the Dielectric and Electrostrictive Properties of Lead Magnesium Niobate Ceramics.'

7. P. Ghosh, A.S. Bhalla, L.E. Cross. 'Preparation and Electrical Properties of Thin Films of Antimony Sulphur Iodide (SbSI).'

8. C.F. Clark, W.N. Lawless, S.L. Swartz. 'Quantum-Ferroelectric Pressure Sensor.'

9. C. Zhili, Y. Xi, L.E. Cross. 'Pyroelectric Property of $Pb(Sc_{1/2}Ta_{1/2})O_3$ Ceramics Under DC Bias.'

10. A.S. Bhalla, R.E. Newnham. 'Low Temperature Pyroelectric Properties.'

11. C.S. Fang, Y. Xi, Z.X. Chen, A.S. Bhalla, L.E. Cross. 'The Growth and Properties of a New Alanine and Phosphate Substituted Triglycine Sulphate (ATGSP) Crystal.'

FALL MEETING OF THE AMERICAN CERAMIC SOCIETY

GROSSINGERS, NY, SEPTEMBER, 1983

12. L.E. Cross. 'Relaxor Ferroelectrics.'

13. J.V. Biggers. 'Center for Dielectric Studies at The Pennsylvania State University.

3.0 BASIC STUDIES

3.1 Relaxor Ferroelectrics

3.1.1 Introduction

Over the last 40 years, an excellent detailed picture has emerged as to the manner in which cooperative ferromagnetic order builds up as the size of 'clusters' of interacting magnetic spins increase. For simple atomic species like iron (Fe), the picture is both qualitatively detailed and quantitatively precise. Proceeding from the isolated weakly interacting spins of the classical paramagnet, the qualitative picture of ordering as the cluster size increases is depicted schematically in Figure 3.1.

In the dilute system, the magnetic field must compete with the randomizing action of thermal motion and the level of imposed magnetic order is very weak as evidenced by the very low susceptibility of the weak paramagnets. If, however, magnetic ions (atoms) cluster as in very fine (50A) iron particles, (A) or for example by fluctuations in site occupancy in a cobalt zinc ferrite (B), at a critical size the spins ferromagnetically couple to form a large magnetic moment. Since, however, the magnetic anisotropy energy is lower than the energy of ordering, the spin cluster (and its larger moment) are unstable against thermal fluctuations.

The ordered spin cluster then behaves like a 'super dipole' since the H.M term is now much larger than H.m for an isolated spin, applied H fields can induce larger magnetic moments, higher susceptibilities, hence the term superparamagnet.

It may be noted that in contrast to more ordered states, when the field is removed, thermal motion will completely randomize the cluster moments and no remanence will occur. If, however, the density of spin clusters is increased, again above a critical value cooperative interaction may occur, so that the clusters themselves now order giving critical super paramagnetism,

FERROMAGNETIC ORDERING

Steps in the build up of magnetic order in different systems well characterized

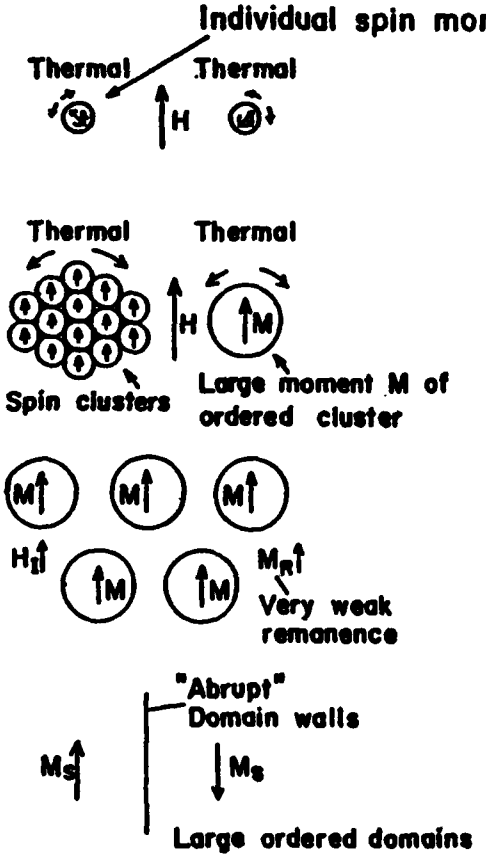

A. Spin clusters can be in very fine ferromagnetic particles e.g. Fe

<u>or</u>

B. Due to fluctuations in site occupancy as in Cobalt Zinc Ferrite

Figure 3.1. Schematic illustration of the build up of magnetic ordering with spin cluster size.

where a weak but measurable remanence will occur. Finally, one may expect that in a uniform system, where the spins are positioned on a lattice of suitable dimension for exchange coupling, the phenomena of normal ferromagnetism will occur where the ordered state is characterized by homogeneously magnetized domains separated by relatively narrow wall regions where the spins reorient continuously and over a short distance from one to the other direction of magnetization.

In a ferroelectricity the qualitative and quantitative picture of how the cooperative order builds up with size is nowhere near so complete.

It is clear that in many ferroelectric systems, long range dipole:dipole fields play a most important role in de-stabilizing the paraelectric form, but the exact balance of ordering forces is still unclear even in simple proper ferroelectrics. Unfortunately, the dipole:dipole field is much weaker and of longer range than exchange interaction, so that the role of free poles and consequent depolarization fields is correspondingly more important. We have no convincing evidence of ferroelectricity in amorphous or glassy systems and at least in the oxygen octahedron proper ferroelectrics a rather clear indication that one mode of deformation of the crystal lattice (the soft mode) carries most of the action for ferroelectric ordering.

Clearly, the problems of achieving proper size and scale are much more acute in the ferroelectric compounds than in some of the simple elemental magnetics. Question of how the chemistry and the surface structure change or reconstruct suggest that simple comminution to small nanometer size particles will be fraught with difficulties. In seeking to establish in analogue fashion the build up of ferroelectric order, it would then appear that a crystalline alternative (like type B in Figure 3.1) would be the most profitable to explore.

3.1.2 Relaxors with Perovskite Structure

It has been known since early work by Smolensky in 1958[3], that lead based perovskite type dielectrics with mixed cations of very different ferroelectric activity on the B sites of the ABO_3 structure, show peculiar diffuse phase transitions. Perhaps the first well authenticated example was $PbMg_{1/3}Nb_{2/3}O_3$ (PMN) where extensive work in the Soviet Union has documented

(a) That the temperature of the dielectric peaks near 0°C is a strong function of measuring frequency, moving to higher temperature with higher frequency. The lower temperature decay from the peak is also associated with a maximum in ε'' (tan δ) suggesting relaxation character, in spite of the fact that ε' maximum is more than 20,000 and thus in the range expected for a ferroelectric transition[4].

(b) Below the dielectric maximum, there is no evidence of macroscopic anisotropy and single crystals of PMN still appear cubic to both optical and x-ray test[5].

If, however, the crystal is cooled in a strong E field, macroscopic anisotropy is evident and the crystal may be left remanently in a state of rhombohedral symmetry much like $BaTiO_3$ below -90°C[6]. Moreover, abrupt reversal of the field produces switching by a domain wall motion as in conventional ferroelectrics. However, re-heating the poled state produced a loss of all remanence at temperature well below T_c the dielectric maximum[7].

(c) Detailed annealing studies show no evidence of long range order in the cation (Mg:Nb) arrangement upon the B sites, and one must presume that statistical fluctuations in site occupancy destroy perfect periodicity in these crystals[8].

It was recognized quite early that in these diffuse transition materials composition fluctuations could lead to a distribution of local Curie temperatures and to the co-existence of polarized and unpolarized regions over

a range of temperature around T_c, however, until recent work by Nava Setter in this Laboratory, the crucial role of the fluctuations in cation occupancy was not proven.

To verify superparaelectric behavior, two features must be proven.

(i) That there are polar micro-regions co-existing with a nonpolar matrix.

(ii) That the local electric dipole moments of these ordered regions are not fixed in space but are modulated by the thermal field.

3.1.3 Evidence for Superparaelectricity in Relaxor Ferroelectrics

3.1.3.1 Work on $Pb(Sc_{1/2}Ta_{1/2})O_3$ at Penn State. To prove the important role of fluctuations in cation occupancy on the B site of the lead based perovskite relaxors it is worth reiterating the experimental data of N. Setter upon the material $Pb(Sc_{1/2}Ta_{1/2})O_3$ (PST). From a careful tabulation of crystal chemical data for many perovskites with mixed B site cations, Nava was able to predict that PST would be right at the bound between structures in which the B site ions are ordered on a superlattice and structures in which B' and B'' are statistically disordered[9].

The important results from Nava's work in MRL[10-12] on PST are summarized in Figure 3.2. She was able to show by x-ray studies that in PST quenched rapidly from high temperature Sc and Ta ions are disordered as in 3.2(b) while by long annealing at temperatures of order 1000°C the Sc:Ta superlattice structure of 3.2(a) could be built up to better than 80% order. Here at last was a vehicle upon which to prove conclusively whether short range (100 to 1,000 A) fluctuations control the properties, and the answer is unequivocal. Dielectric properties of the ordered structure are those of a conventional ferroelectric with sharp first order phase change and an abrupt loss of P_s and optical anisotropy at T_c. The disordered crystal at identical

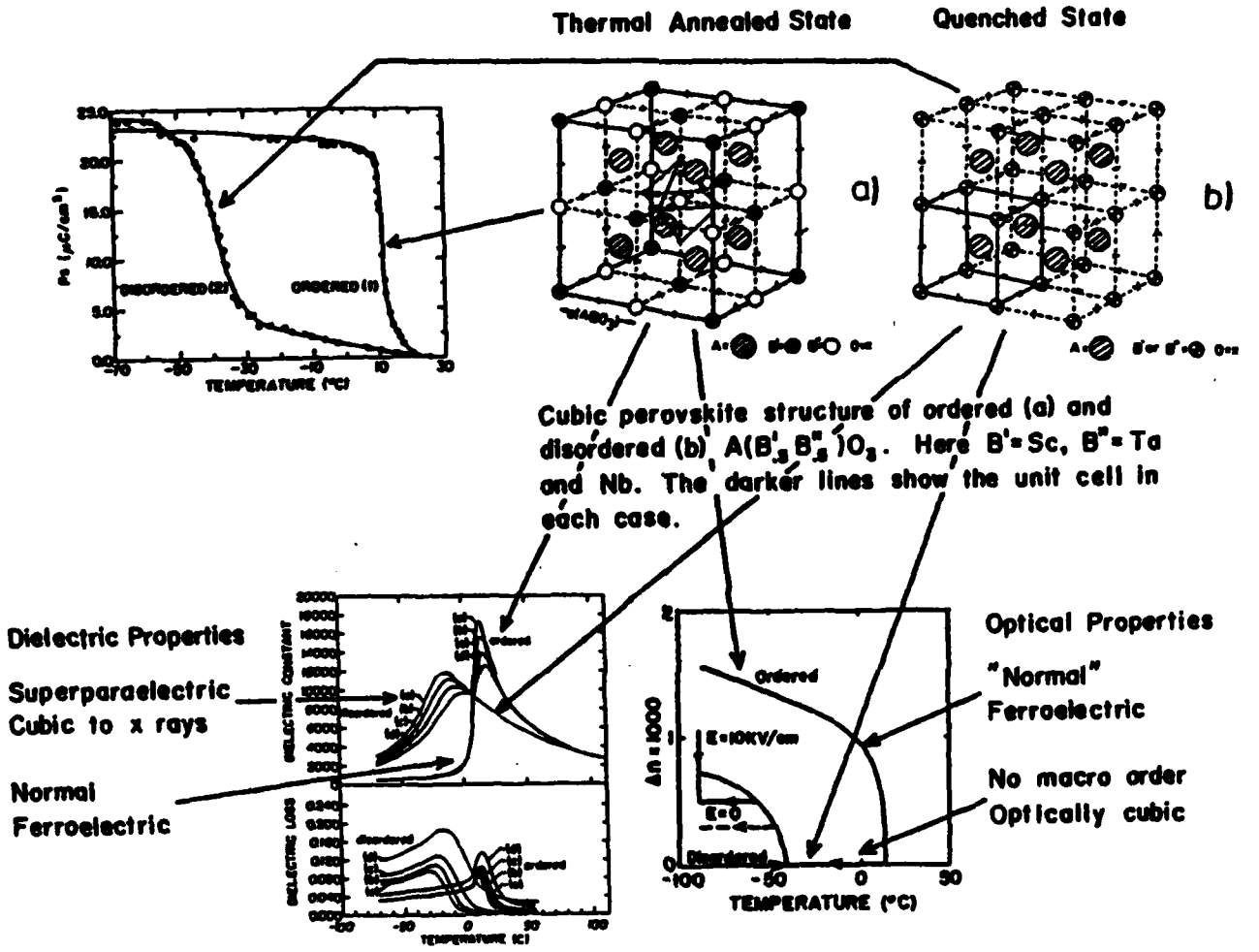

Figure 3.2 Evidence from work on lead scandium tantalate.

composition, however, shows classical relaxor behavior with a dielectric maximum whose temperature depends markedly on frequency, which has the associated lower temperature loss maxima and the expected loss of remanence at a temperature well below T_c as evidenced in the optical anisotropy. As in PMN, PST in the disordered cation state shows no optical or x-ray anisotropy if cooled without field, but a clear rhombohedral structure if cooled under bias. The ordered material, however, develops a macrodomain structure immediately below T_c with the expected rhombohedral anisotropy. The findings are summarized in Table 3.1 and the evidence is very clear that if the statistical fluctuations in Sc:Ta distribution of the disordered state are removed by annealing to form the perfectly periodic lattice of Figure 3.1(a) the relaxation (diffuse transition) behavior is lost.

In all very high permittivity paraelectric dielectrics, there will be fluctuations in the local dipole moment due to thermal motions which will become quite large as the system approaches its Curie temperature. For the ordered PST structure, since the lattice is perfectly periodic and all superlattice cells are identical in make up, these fluctuations must be random in both space and time, and up to the sharp Curie temperature T_c the time average of P at any location in the crystal must go to zero. Similarly, below T_c the structure will develop a spontaneous polarization, and the time average of P at all locations will be non-zero.

For cation disordered PST however, one unit cell is not identical to its neighbor either in composition or dimensions, and spacial homogeneity is lost over regions of order 100 to 1000 Å in size. Due to differences in composition, these local regions will have different Curie temperatures and even at temperatures well above this Curie region, the spacial homogeneity of the fluctuations will be lost.

CONCLUSION

In $PbSc_{1/2}Ta_{1/2}O_3$

For the Annealed Cation Ordered State — no cation composition fluctuations

Normal Ferroelectric Properties

(1) Sharp 1st order change at T_c

(2) Stable remanent polarization

(3) No frequency dependence at radio frequencies in ferroelectric state

(4) Stable birefringence

(5) Rhombohed

For the Quenched Cation Disordered State — must have statistical fluctuations in Sc:Ta distribution on B

Superparaelectric Properties

(1) Diffuse phase change

(2) No stable remanence

(3) Strong frequency dependence

(4) No stable birefringence

(5) Cubic macro symmetry to both X rays and optical frequencies

In Perovskite PLZT 8:65:35

Demonstrate Critical Superparamagnetism

Table 3.1.

In these cation disordered compositions, a critical question concerning the analogue with superparamagnetism is the following: In a local region of high T_c, once the polarization ceases to fluctuate periodically through zero, does the vector stabilize in orientation to form a microdomain, or does the orientation of the vector continually change in response to thermal fluctuations as in the superparamagnet.

More recently, to explore this important question an extensive series of measurements have been made of the polarization and depolarization behavior of PST.

It is clear from Figure 3.1 that after cooling under DC bias, both cation ordered and disordered PST samples build up a substantial remanent polarization, however, on heating the temperature dependence of P_R is quite different. The ordered samples retain high remanence up to T_c while disordered samples lose all remanence at a temperature well below T_c as judged from the dielectric maximum. Measurements by the Byer-Roundy[13] technique of the pyroelectric response confirm these differences (Appendix 1) and suggest that the polar micro-regions formed below T_c have a range of temperature over which their P_s is not stable in orientation, i.e. the crystal can be poled to a substantial pyro-coefficient, but after removing the poling field most of the pyroelectricity is lost.

In many macroscopic ferroelectrics, it may be observed that P_R is not stable at temperatures close to T_c as the poled sample breaks up into domains of different orientation. The data presented clearly show that P_s in the polar micro-region is not stable over time, however, it does not distinguish whether the mechanism by which remanence is broken up is superparaelectric or is one of domain instability close to the local T_c.

A further test which tends to confirm superparaelectricity is the measurement of the <u>reversible</u> build up and decay of polarization under DC bias

with very weak thermal cycling (Appendix 2). The technique used here was the Chynoweth[14] method of measurement in which a tiny flake of the sample is cycled over a minute temperature range at 5.5 Hz using a chopped infrared heating. Ferroelectric domain motion is hysteritic, and for very small thermal amplitudes it should not contribute to the reversible pyroelectric response. Superparaelectric thermal disordering is however reversible, and at the low cycling frequency used in the Chynoweth experiment, it should contribute a substantial extrinsic component to the pyroelectric response. Figure 5 in Appendix 2 shows the very strong enhancement of pyroelectric response evident in disordered PST as compared to the very small effect in an ordered sample. Strong evidence that at least part of the disordering process is reversible and thus is not likely to be domain originated.

3.1.3.2 Work Upon PLZT Relaxors. In view of the importance of polarization:depolarization studies for the characterization of superparaelectricity, it appeared worthwhile to extend our studies to the lead lanthanum zirconate titanate (PLZT) family in the range of compositions beyond 7 mole% La_2O_3 where there is obvious relaxation character in the dielectric response.

The 7:65:35 and 8:65:35 PLZT compositions which exhibit the so called α:β phase transition[15] at a temperature well below the dielectric permittivity maximum were the first object of study (Appendix 3). For the 8:65:35 it is again clear that cooling from high temperature in the absence of any electric field no macroscopic phase change appears and the ceramic is effectively cubic for both x-ray and optical probes. Cooling under even weak field, however, (3 kV/cm) leads to a rapid build up of remanent polarization at temperatures near 80°C (the so called α-β transition) which persists to all lower temperatures.

It is important to note that this poled state is completely non-dispersive in dielectric response in the radio frequency range.

Applying a moderate field (less than 8 kV/cm) to a freshly depoled sample already cooled to -75°C does not, however, remove dispersion, but leads to a new dielectric change to the non-dispersive state on heating. This 'transition' moves to lower temperature with either increasing field or decreased heating rate. Again the dielectric change is associated with a very obvious build up of a macroscopic remanent polarization (Appendix 3).

These unusual behaviors can we believe be accounted for very nicely by the model of superparaelectricity. It would appear that in the PLZT, inhomogeneities in the La, Pb and vacancy distribution lead to compositional heterogeniety and a distribution of Curie temperatures leading to the diffuse transition near T_c. In the Curie range, we suppose that the polar micro-regions are superparaelectric, but freeze out into a random ensemble of microdomains at the very low temperature. Clearly the average scale is such that the domains are below the resolution of the optical microscope or the coherence length of the x-ray. Presumably some micro-regions (presumably the smallest) retain mobility even at low temperature and preserve the dispersive character of the permittivity.

Under moderate electric field applied at high temperature, it would appear that enough order is superposed in the temperature region near 80°C (some 35°C below T_c) that the micro-regions build up into stable macro-domains which are stable to all lower temperatures. At very low temperatures in depoled samples, presumably the polar micro-regions are frozen out into an array of polar microdomains and the field is too weak to impose order. On warming however, thermal motion imparts mobility to the domains and macro-order can be built up. As would be expected, the larger the field and the

longer the time, the lower would be the temperature at which the macro-ordered state could be built up.

The qualitative behavior is close to that which would be expected for critical superparaelectricity, with the micro-regions now at a concentration on the brink of generating macroscopic ordering.

Studies extending measurements to samples in the range from 7 to 9.5 mole% La_2O_3 give what appears to be a continuous spectrum of response from superparaelectric to critical superparaelectric to ferroelectric behavior (Appendix 4).

Studies on these materials are now being extended to investigate their electro-mechanical and electro-optic character so as to obtain more information on the polarization process.

3.1.3.3 Nature of the Phase Changes in Perovskite Relaxors. It is perhaps interesting to speculate as to the proper terminology for the polarization processes in these mixed cation relaxors. In the evidence from Nava Setter's work, the scale of compositional heterogeneity, and consequent T_c modulation appears in the range 100 to 1000 A, at the edge of what may be properly characterized as a separate phase. Clearly, on this scale, when the micro-region changes from a non-polar to a polar condition a phase change must have occurred.

On a global scale of say 1 cc of the material, however, no clearly identifiable change has occurred. The polar micro-region is constantly reorienting so there is no macro-polarization, no macroscopic structure change and no abrupt change in any measurable extensive variable. For this 1 cc scaling, clearly the poling field is the agency which effects a phase change inducing a large (at low temperature stable) macroscopic polarization, and an obvious macroscopic structure change.

For the 8:65:35, on the global scale cooling under no field clearly traps the system in a metastable cubic state (macroscopically) and a shift to the more stable ferroelectric polar state can be induced by high E fields. A phenomenological thermodynamic model which quite properly treats the system in this way has been recently published by Jonker[16]. We believe there is absolutely no conflict between this model (for the equilibrium properties) and the microscopic model proposed here.

As with all thermodynamic models, the contribution to basic understanding is excellent, but the contribution to the understanding of the dynamics is minimal and the more detailed microscopic model is necessary to understand the relaxation behavior.

3.2 Practical Relaxor Dielectrics

3.2.1 Lead Magnesium Niobate Based Compositions

An important contribution to the use of relaxor lead magnesium niobate in electrostrictive micropositioners and in dielectric application has been the development and documentation of a process for fabricating this material in a form free from the troublesome pyrochlore phase. Details of this work are given in Appendix 5.

In brief summary, both $PbMg_{1/3}Nb_{2/3}O_3$ and its solid solutions with $PbTiO_3$ can be prepared in pure perovskite form by using a $MgNb_2O_6$ columbite structure precursor in the calcining reaction, and by adding a small excess of MgO. Permittivity values at the peak in excess of 18,000 for PMN and 31,000 for PMN + 10% PT can be realized using a small excess of MgO and a firing schedule which increases the grain size.

In a second more recent study, Voss, Swartz and Shrout (Appendix 6) have examined the effects of a wide range of minor aliovalent additives to $PbMg_{1/3}Nb_{2/3}O_3$. Briefly summarized, their conclusions are

(i) Additives which raise the Curie range (T_c) also raise the peak permittivity.

(ii) High permittivity samples all show high dielectric saturation under DC bias.

(iii) No general trends as to the effects of ionic size upon diffuseness of the phase change could be adduced from these studies.

(iv) In general, more diffuse phase transitions lead to lower values of the electrostrictive Q_{12} constant, but may be advantageous for the field related M_{12} of importance for micropositioners.

3.2.2 Lead Iron Niobate:Lead Nickel Niobate

Results of a preliminary study of the $x(Pb(Fe_{1/2}Nb_{1/2})O_3) - (1-x)Pb(Ni_{1/3}Nb_{2/3})O_3$ PFN:PNN solid solution has been completed (Appendix 7). Compositions with $x \geq 0.6$ were found to densify at sintering temperatures less than 1000°C and to provide peak dielectric relative permittivities $K' > 15,000$ and relatively low temperature coefficients of capacitance change. Additions of small amounts of MnO were found to increase the resistivity markedly and to reduce dielectric loss. Small addition of $PbTiO_3$ raised the Curie temperature and increased the maximum permittivity.

3.3 Grain Size Effects in Pure $BaTiO_3$

Following the methodology outlined in the previous report, a more refined thermodynamic function is being developed to describe the single domain dielectric piezoelectric and elastic properties of $BaTiO_3$ over the whole temperature range from well above the Curie temperature T_c to absolute zero. This work is in cooperation with Dr. A.J. Moulson and his student A. Bell at Leeds University.

Progress to date has included the refinement of the Buessem, Goswami, Cross Elastic Gibbs Function[17,18] by including the last permitted sixth

order term ($HP_1^2P_2^2P_3^2$) which was omitted from their function. Choosing a value of $H = 4.91 \times 10^9\ Vm^9c^{-5}$, the function now predicts all the lower temperature phase changes in their correct locations. As a check of the validity, the high electric field (field along 100) effects upon the temperatures of all the phase changes have been calculated and compared to recent excellent experimental data from Fesenko et al. The agreement between calculated and observed shifts is excellent. An unexpected prediction from the phenomenological calculation is that the pyroelectric effect in the induced tetragonal phase below 0°C should change sign at high E fields. Experiments are being planned to check this prediction. A more detailed account of this work is given in Appendix 8.

As a first exploratory study of the effects of internal stress upon the single domain dielectric permittivity, it was assumed that the internal stress would be proportional to the square of the electric polarization

$$x_{ij} = -K\, s_{ijkl} P_k P_l$$

and $\bar{\epsilon}$ was taken as the arithmetic mean of the three principle permittivities. Under these assumptions of K, values of 0.052, 0.082, 0.205 in tetragonal, orthorhombic and rhombohedral phases, respectively, mean permittivities up to $\epsilon_R = 6{,}000$ occur near room temperature and the shifts of the ferroelectric:ferroelectric phase transitions appear reasonable. The shift of the Curie temperature is a little larger than expected, but this is probably because of the sharp first order phase change which is assumed in the model, but is much rounded by local inhomogeneous stresses in the finer grained ceramics. More details of this work are given in Appendix 9.

Clearly assumptions as to the proportionality of the stress and polarization squared are highly suspect so that the data in Appendix 9 are

just a first cut at the problem. When the more refined x-ray data becomes available from measurements on ceramics and powders, it should be possible to deduce the actual average stress levels and thus to make a more quantitatively exact analysis.

4.0 EVOLUTIONARY APPROACHES

4.1 Effects of Space Charge on Electrical Degradation in $BaTiO_3$

Earlier studies upon the effects of space charge in MLCs (Schulze[19]) have suggested the need for a more precise evaluation of the nature and distribution of the charges involved. From the earlier study, it was speculated that the charge at lower temperatures was dominantly ionic and the most probable transporting species anion (oxygen) vacancies.

In the present proposed experiment, DC leakage current and potential distribution will be monitored simultaneously. An experimental aparatus has been designed to accomplish the monitoring using up to 10 carefully buffered potential probes which will be embedded in the sample at various distances from the active current electrodes (see Figure 4.1).

Samples for this experiment will be formed by tape casting the desired dielectric formulation into thin sheets, then laminating and firing the sheets to form a monolithic structure with the noble metal probes internal to the block. Initial studies will be concentrated upon high purity barium titanate, using high purity commercial powders and powder to be made at Penn State by the liquid mix process. Potential distribution and leakage current will be followed as a function of time at fixed temperatures. In later studies when the bounds of the method have been explored, we propose to vary the stoichiometry Ba/Ti ratio, examine the effects of dopants, electrode compositions, porosity and defects, etc. Earlier studies showed clear evidence of effective blocking of current flow at the lower temperatures. By

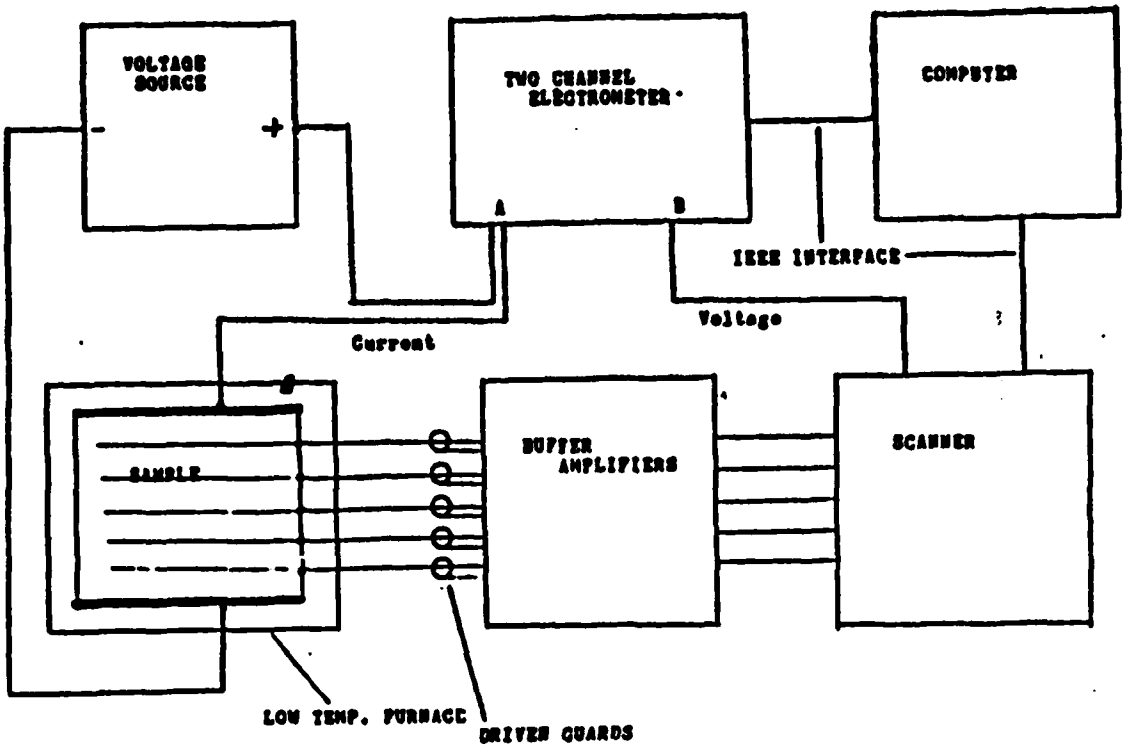

POTENTIAL PROBE BUFFERING

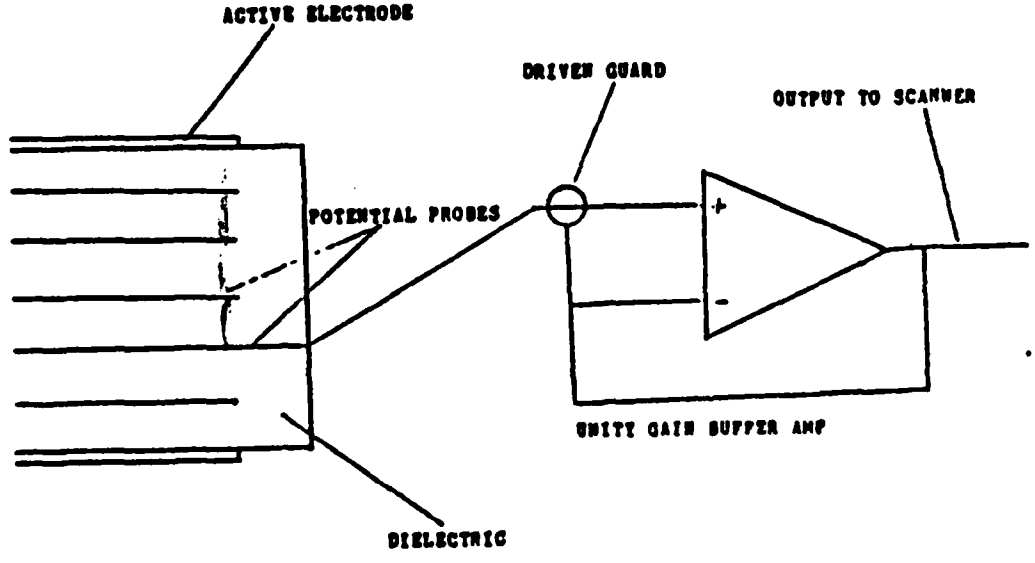

- High input impedance- 10^{13} ohms
- Driven gaurd- reduces capacitance
  - reduces leakage current
- Input voltage range ± 200 volts

Figure 4.1. Schematic of the measuring system.

these experiments, we may decide at once between bulk and grain:grain boundary blocking and identify the regions of high and of low field directly.

At the present time, the experimental equipment has been built and tested, the software is written to enable complete computer control of the data acquisition. Initial samples have been fabricated from pure $BaTiO_3$ made by the liquid mix process, and studies are now nearing completion to ascertain proper firing schedules for these internal probe multilayer structures.

4.2 Macrodefects in Multilayer Ceramics

An initial study of the effects of introducing macroscopic defects deliberately into MLC structures by using burnable plastic inserts has now been completed by David Hardy, this work was submitted for the M.S. degree in Solid State Science. The title and abstract for the thesis are included in Appendix 9. In very brief summary, it was shown that the macro-voids which were within the dielectric layers had an effect on weak field permittivity and loss which was indistinguishable from normal density defect due to accidental micro-voids and pores. For voids of different shape, spheres as expected appear most benign and longer acicular voids more lethal. An interesting finding was that larger voids induced at the interface between electrode and dielectric developed conductive surfaces during processing as evidenced by an enhancement of permittivity at low field.

Detailed interpretation from these initial studies was difficult from these initial concentration of micro-flaws in the dielectric and work is now in progress to improve the processing and reduce this background defect level.

5.0 REVOLUTIONARY APPROACHES

5.1 Introduction

Even superficial examination of the problems associated with developing capacitors of very high volumetric efficiency and compact form suggests that a

continuing trend must be towards thinner and more perfect dielectric layers. In VLSI circuits the voltage levels are now coming down to ~1 volt and even at 1 μ thickness of dielectric, the field (if uniform) is only 10^4 V/cm. It is well known that in most dielectric systems (certainly in polymers and ceramics) the breakdown field strength increases with decreasing thickness giving an additional benefit for thin systems.

For conventional ceramic processing, there is clearly still much that can be done, but it is rather difficult to believe that in any short time, the conventional processing methods can be improved to the point of generating micron or even submicron films. There is thus a pressing need to begin to explore alternative forming techniques for very thin dielectric films.

One method which is not at all new is that used in the old conventional single layer barrier layer, where a glass fritted electrode is used to re-oxidize the surface of a sintered pellet of highly reduced ferroelectric dielectric. In the current single layer barrier layer, more than 95% of the volume is occupied by useless electrode which simple acts as a padding resistor. It was our thought that the single layer barrier layer could be overfolded upon itself many times, by using a variation of the Corning ACE process to make many closely spaced (rough) large area internal surfaces. Potential advantages could be the self sealing effect of the frit step which would close cracks in the body of the part (now mostly conductor) and the rather efficient short path between barrier layers in the semiconducting titanate which would much reduce series resistance.

A second approach is perhaps more radical, but also more conventional. The crystals SbSI is a well known uniaxial ferroelectric and has been the object of concentrated research for many years, particularly in the USSR. The reason for our interest is the low melting temperature and high sublimation

rate in vacuum which suggest that crystalline films of SbSI might be reconstructed upon substrates cool enough not to destroy a fabricated IC device.

5.2 Single Barrier Layer Multilayers

A barium titanate based composition containing neodymium oxide and zirconia was chosen for the semiconducting ceramic. Neodymium functions as a reducing agent to facilitate the reaction $Ti^{4+} \rightarrow Ti^{3+} + e^{-}$ and zirconium is used as a Curie point shifter. Normal tape casting was used to produce 15 mil tapes for the semiconductor layers. Several methods were tried to develop the connected pore layers to interleave the semiconductor, the most successful incorporated a burnable polymer with a lower level of semiconductor loading to cast 7-8 mil thick sheets.

By careful regulation of the burnout, a suitably porous layer could be interleaved between the semiconductor monolithic sheets. Sintering was carried out in air at 1320°C for 2 hours, followed by a reduction treatment of 850°C in (5% H_2:95% N_2) gas.

The fritted electrode was forced into the porous layer using a vacuum chuck and positive over pressure. To form the barrier, the electrode was sintered in air at 780°C.

Initial dielectric studies show that an effective barrier structure can be fabricated which will maintain low power factor up to 10^5 Hz. Capacitance/square is slightly larger than a comparable area disk monolayer barrier layer due to the internal surface roughness. Total capacitance scales with the number of internal layers in precisely the manner expected.

Current work is concerned with improving the barrier capacitance and breakdown strength lowering the loss level by making the junction more abrupt.

Exploring the temperature variation of capacitance to characterize the barrier dielectric.

It is not intended to fabricate commercial type layer structures, but rather to completely and convincingly demonstrate feasibility and some of the advantages possible with this structure so that commercial developers may take up the extensive work required for commercial applicability.

5.3 Antimony Sulphur Iodide Thin Films

SbSI is a uniaxial ferroelectric crystal with most unusual and interesting dielectric, piezoelectric, pyroelectric and semiconducting properties. For these studies, thin films of SbSI were vacuum deposited by thermal evaporation. A variety of substrates including glass, gold coated glass, SnO_2 coated glass and silicon have been used. Films deposited at about 80°C showed poor crystallinity but subsequent annealing either in a closed container or in an iodine atmosphere produced highly oriented crystalline films. Needle shaped crystallites of order 0.2 μm in diameter can be discerned in SEM microscope images, and both SEM and x-ray diffraction studies confirm a high degree of orientation normal to the film surface.

Dielectric measurements show a peak in the permittivity near 10°C with relative permittivity K ~ 470, giving an effective capacitance of 0.5 $\mu F/cm^2$ and a loss factor less than 2% at frequencies down to 1 kHz.

The re-crystallized films could be poled under DC field to exhibit a substantial pyroelectric effect which peaks near 10°C confirming the ferroelectric character.

Current work is concerned with improving the reproducibility of the deposition process and the possibility of using a heated substrate to permit direct deposition of the crystalline form without subsequent annealing.

A more detailed account of these studies is given in Appendix 10.

6.0 DIELECTRIC MEASUREMENTS

Extension of the low frequency measuring range using the quasi-static constant voltage ramp method has temporarily stopped, pending the arrival of a new electrical engineering fellow to take up these studies. Work described in our earlier report was completed and is carried in published form as Appendix 11 to this report. It is anticipated that the work will be taken up again in July, 1984, when the focus will be upon separating the reversible and irreversible components of the polarization in soft PZTs.

Over the current contract year, the high frequency limitations of our measuring equipment have been relieved by the acquisition of a Hewlett Packard microwave measuring system comprising the 8350B sweep oscillator, with the 83592A plug in, this encompasses the range from .01 to 20 GHz. An HP 809C slotted line, coupled to the 8755C sweep analyser and 8750 storage normalizer permit impedance measurements on suitable components at frequencies up to 20 GHz.

During the coming year, the Laboratory will receive the full Hewlett Packard 8510T microwave network analyser, to permit impedance and full s parameter measurement at frequencies from 45 mHz to 26 GHz. In July, we shall be joined by Dr. Jin-Hun Kim, who is head of the EE Department in Sogang University, Seoul, and an experienced microwave engineer.

Taken together with our FFT ultra-long wavelength IR spectrometer, the Laboratory begins to have excellent measurement capability over the whole electromagnetic spectrum.

7.0 ANCILLIARY STUDIES

Over the contract year, personnel whose major commitment of time is to the Dielectrics Center program have participated in a number of interesting subsidiary projects relevant to the pyroelectric behavior of ferroelectric

crystals (Appendix 12, and Appendix 13), to the low temperature behavior of ferroelectrics and the relevance of electrostriction at these temperatures, to pressure sensing (Appendix 14).

REFERENCES

1. K. Kinoshita, Y. Yamaji, J. Appl. Phys. 47:371 (1976).
2. O.E. Fesenko, Y.S. Popov, Ferroelectrics 37:729 (1981).
3. G.A. Smolenskii, V.A. Isupov, Dokl. Akad. SSSR 9:653 (1954).
4. G.A. Smolenskii, V.A. Isupov, A.I. Agranovskaya, Sov. Phys. (Solid State) 1:150 (1959).
5. V.A. Bokov, I.E. Mylnikova, Soviet Phys. (Solid State) 3:613 (1961).
6. G.A. Smolenskii, Supplement to J. Phys. Soc. Japan 28:26 (1970).
7. G.A. Smolenskii, V.A. Isupov, A.I. Agranovskaya, S.N. Popov, Fiz Tverdago Tela 2:2906 (1960).
8. V.A. Isupov, Zh Tech. Fiz 26:1912 (1956).
9. N. Setter, L.E. Cross, J. Mat. Sci. 15:2478 (1980).
10. N. Setter, L.E. Cross, J. Appl. Phys. 51μ4356 (1980).
11. N. Setter, L.E. Cross, Phys. Stat. Sol. (a) 61:K71 (1980).
12. N. Setter, L.E. Cross, Ferroelectrics 37:551 (1981).
13. R.L. Byer, C.B. Roundy, Ferroelectrics 3:333 (1972).
14. A.G. Chynoweth, J. Appl. Phys. 27(1):78 (1956).
15. E.T. Keve, K.L. Bye, J. Appl. Phys. 46:810 (1975).
16. G.H. Jonker, Mat. Res. Bull. 18:301 (1983).
17. W.R. Buessem, L.E. Cross, A.K. Goswami, J. Amer. Ceram. Soc. 49:33 (1966).
18. W.R. Buessem, L.E. Cross, A.K. Goswami, J. Amer. Ceram. Soc. 49:36 (1966).
19. W. Schulze, U.S. Japan Study Seminar, Rapporgi, Ja_a , p. 7 (1982).

APPENDIX 1

DEPOLARIZATION BEHAVIOR AND REVERSIBLE PYROELECTRICITY IN LEAD SCANDIUM-TANTALATE CERAMICS UNDER DC BIASES

CHEN ZHILI*, YAO XI** AND L.E. CROSS
Materials Research Laboratory, The Pennsylvania State University, University Park, PA 16802

Abstract The depolarization behavior of ordered and disordered lead scandium-tantalate (PST) ceramics has been studied by Byer-Roundy and Chynoweth method. A sharp decrease of the spontaneous polarization takes place in a narrow temperature range very close to the Curie temperature T_c for the ordered PST materials. For the disordered PST materials, however, the depolarization takes place within a wide temperature range much lower than the temperature of maximum dielectric constant T_m. Evidence of microdomain activities has been observed in disordered materials. The reversible pyroelectric effect is discussed in terms of the micro-macro transition of the domains in disordered PST materials.

INTRODUCTION

Earlier studies have shown that in the lead scandium-tantalate $Pb(Sc_{1/2}Ta_{1/2})O_3$ (PST) single crystal and ceramics which are of simple perovskite structure, the B-site cations in the ABO_3 structure are close to the boundary of order and disorder[1]. The degree of ordering of the B-site cations can be controlled thermally. The quenched materials with disordered structures are relaxor ferroelectrics with diffuse phase transitions, while the well annealed materials with ordered structure exhibit "normal" sharp first order ferroelectric transition. The dielectric and ferroelectric properties of PST materials have been reported[2,3]. The dielectric and pyroelectric properties under DC biases have also been studied[4,5]. A reversible pyroelectric effect under DC bias in disordered PST ceramics has been explored.

In this paper, the depolarization behavior of order and disorder PST materials using both Byer-Roundy[6] and Chynoweth[7] method are given. The ordering of microdomain region is believed to be responsible for the reversible pyroelectricity. The microdomain activity in disordered PST ceramics is very similar to that explored in PLZT ceramics[8].

---

*Visiting Scientist from Shanghai Institute of Ceramics, Shanghai, China.

**Visiting Scientist from Xian Jiaotong University, Xian, China.

CHEN ZHILI, YAO XI, L.E. CROSS

EXPERIMENTAL PROCEDURES

Sample Preparation

Samples used in this work were prepared by conventional mixed oxide processing. Stoichiometric proportion of PbO, Sc_2O_3, Ta_2O_5 were ball milled in alcohol for 20 hours. The mixture was dried and precalcined at 800°C for 2 hours. After reground and pelletized, the samples were fired at 1300°C for one hour using $PbO+PbZrO_3$ as atmosphere controller. A final sintering was performed at 1560°C followed by rapid air quenching to induce disorder structure. The ordering of the B-site ions was achieved by thermal annealing at 1000°C for 24 hours. The degrees of ordering, S, for quenched and annealed samples are 0.40 and 0.87 respectively. The final density achieved was 94% theoretical with less than 3% weight loss.

The samples used in depolarization studies were 0.2-0.3 mm thick with sputtered gold electrode. The samples were heated to 150°C at first then poled at 30°C, 20 kV/cm for 10 min. and cooled under electric field down to -70°C. The temperature of dielectric constant peaks of disordered and ordered PST ceramics are 1.9°C and 17°C at 1 KHz respectively.

Depolarization Measurements

For the modified Byer-Roundy method, the sample in series with a bias voltage supply was connected to a picoammeter HP 4140B. The sample was heated in a temperature chamber, Delta 2300. Linear temperature ramping with specified ramping rate dT/dt can be achieved under computer control using the HP 9825A desktop computer. Pyroelectric coefficient, which is proportional to the thermal current, can be measured directly. The depolarization curve can be obtained by integration of the thermal current with respect to time.

A modified Chynoweth method has been used in this work. The sample in series with a bias voltage supply was connected to a phase lock amplifier model PAR HR-8 through a preamplifier and a blocking capacitor. The sample was heated by a chopped light beam with chopping frequency around 5.5 Hz. The pyroelectric signal, which can be read from the output voltmeter of the phase-lock amplifier, is proportional to p/KC_p, here p-- pyroelectric coefficient, K-- dielectric constant, C_p-- specific heat of the sample.

EXPERIMENTAL RESULTS AND DISCUSSION

Figure 1 and 2 are the pyroelectric coefficients and depolarization curves of the ordered and disordered PST materials under different bias fields using the Byer-Roundy method. Although the spontaneous polarization of the ordered and disordered samples are the same, the depolarization behaviors are quite different. For the ordered sample, a sharp decrease of spontaneous polarization takes place in a narrow temperature range very close to the Curie temperature T_c (17°C) at zero bias field. Higher bias field shifts the transition toward higher temperature. However, the

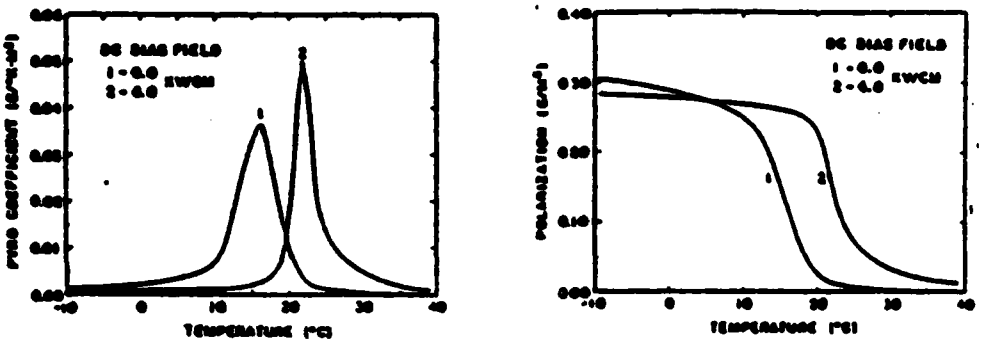

(a) (b)

Figure 1. Pyroelectric coefficient (a) and depolarization curve (b) of ordered PST ceramics.

shape of the depolarization curve has no significant change. A first order transition for the ordered material is quite evident. For the disordered materials, the depolarization takes place in a wide temperature range much lower than the temperature of maximum dielectric constant T_m (1.9°C) at zero bias field. Higher bias field also pushes the depolarization toward higher temperature range. However, a sharp decrease of the spontaneous polarization and an elongated tail section of the depolarization curve under bias field are quite evident. The effect of the bias field is more evident on the temperature dependence of the pyroelectric coefficient as shown in Figure 2(a). Under zero bias field a concealed terrace is clearly shown in the low temperature region of the pyroelectric coefficient curve. Under small DC bias field, the concealed terrace disappears, the temperature dependences of the pyroelectric coefficient become more "normal". In this respect, we can assume that a DC bias drives a diffused phase transition of a relaxor ferroelectric toward a normal first order transition.

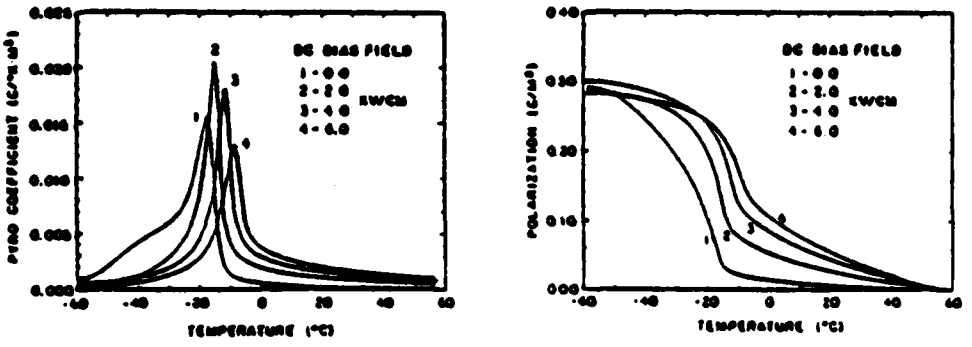

(a) (b)

Figure 2. Pyroelectric coefficient (a) and depolarization curve (b) of disordered PST ceramics.

The depolarization curves of ordered and disordered PST materials taken from Chynoweth method also exhibit the same characteristic, as shown in Figures 3 and 4. A very sharp decrease of the pyrosignal is clearly shown in Figure 3 for the ordered materials, while a rather wide temperature range of the decreasing of the pyrosignal is observed in Figure 4 for the disordered sample.

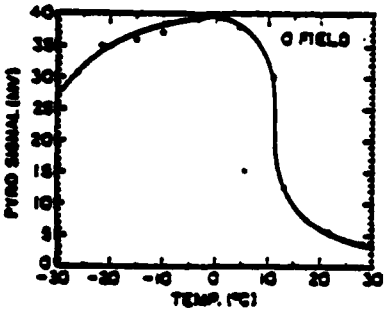

Figure 3. Pyrosignal of ordered PST ceramics (arbitrary scale).

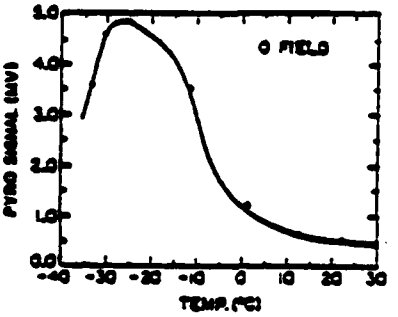

Figure 4. Pyrosignal of disordered PST ceramics (arbitrary scale).

A smooth and gentle decrease of the spontaneous polarization with respect to temperature change in the depolarization curve of a relaxor ferroelectric is very important for the reversible pyroelectric effect. It is in this temperature region that the highest enhancement of pyroelectric signal of disordered PST has been observed[5].

The detailed mechanism of the reversible pyroelectricity is still not yet known, however, it is believed that the microdomain activity is of vital importance.

In our early works, the evidence of microdomain activities in PLZT ceramics has been given[8]. The depolarization behavior of disordered PST materials also presents apparent trace of the microdomain activities. The splitting of highly polarized macrodomains into random oriented microdomains may be responsible for the smooth decreasing of the polarization and the appearance of the high terrace of the pyroelectric coefficient at zero bias field in Figure 2. A small DC bias field drives the random oriented microdomains into highly polarized metastable macrodomains keeping the material in high polarization level. The DC bias also plays as a restoring force of the polarization during temperature fluctuation. Therefore, a high enhancement of pyrosignal accompanied with reversible effect results.

The kinetics of the micro-macro transition of the domains in relaxor ferroelectrics is another critical point for the reversible pyroelectric effect. In disordered PST materials, the micro-macro

transition is fast enough to respond to a temperature fluctuation of 5.5 Hz (about 200 mS), while under the same condition no reversible ferroelectric effect has been observed in PLZT ceramics with composition 8:65:35. The experimental results on the kinetic behavior of the micro-macro transition in PLZTs[8] show that the transition is much slower than that of PST materials. An interesting question is how fast the micro-macro transition can respond to the temperature fluctuation. A detailed study on the kinetic behavior of the micro-macro transition of domains is now still continuing.

SUMMARY

The depolarization of ordered PST materials takes place in a narrow temperature range close to its Curie temperature, while for the disordered materials the depolarization takes place in a wide temperature range much lower than the temperature of maximum dielectric constant.

Evidence of microdomain activity has been observed in disordered PST materials. The micro-macro transition of domains in relaxor ferroelectrics is believed to be responsible for the reversible pyroelectric effect.

REFERENCES

1. N. Setter and L.E. Cross, J. Mat. Sci. 15, 2478-2482 (1981).

2. N. Setter and L.E. Cross, J. Appl. Phys. 51(8), 4356-4360 (1980).

3. N. Setter and L.E. Cross, Phys. Stat. Sol. (a) 61, K71 (1980).

4. Chen Zhili, Yao Xi and L.E. Cross, to be published.

5. Chen Zhili, Yao Xi and L.E. Cross, to be published.

6. R.L. Byer and C.B. Roundy, Ferroelectrics 3, 333 (1972).

7. A.G. Chynoweth, J. Appl. Phys. 27(1), 78-85 (1956).

8. Yao Xi, Chen Zhili and L.E. Cross, to be published.

APPENDIX 2

Ferroelectrics Letters, 1983, Vol. 44, pp. 271-276
0731-5171/83/4409-0271$18.50/0

REVERSIBLE PYROELECTRIC EFFECT IN $Pb(Sc_{1/2}Ta_{1/2})O_3$ CERAMICS UNDER DC BIAS †

CHEN ZHILI*, YAO XI** AND L.E. CROSS
Materials Research Laboratory, The Pennsylvania State University
University Park, PA 16802, USA

(Received for Publication December 27, 1982)

Abstract—It has been shown that quenched $Pb(Sc_{1/2}Ta_{1/2})O_3$ (PST) disordered ceramics and crystals show diffuse dispersive dielectric properties, while well annealed ordered materials exhibit normal sharp first order transition. The pyroelectric depolarization measurements taken using a Hewlett Packard Model 4140B picoammeter/DC Source under computer controlled heating cycle also have shown different behaviors between disordered and ordered materials.

In this work pyroelectric measurements by Chynoweth method under DC bias up to 1.8 KV/mm within a temperature range of 70°C around the temperature of maximum dielectric constant have been studied. A very significant enhancement of the pyroelectric signal under DC bias is observed in thermally quenched disordered samples. The largest enhancement of the signal appears at temperatures some degrees below the temperature of maximum dielectric constant.

The existence of microdomains in disordered materials is believed to be responsible for this new extrinsic component of reversible pyroelectricity.

The large reversible pyroelectric effect is a promising phenomenon for developing new pyroelectric devices.

1. INTRODUCTION

In PST single crystals and ceramics which are of simple perovskite structure the combination of B-site cations in the ABO_3 structure is close to the boundary between order and disorder[1]. The degree of ordering of the different B-site cations in these materials can be controlled thermally. Quenched disordered crystals and ceramics show diffuse dispersive dielectric properties, while well annealed ordered materials exhibit "normal" sharp first order ferroelectric transition. The influences of the ordering upon the dielectric, ferroelectric and elastoelectric properties of PST materials have been reported[2,3]. The effects of DC bias upon the dielectric properties of ordered and disordered PST ceramics have also been explored[4].

Pyroelectric depolarization studies showed that the polarization of disordered samples drops down more smoothly, while ordered samples depolarize abruptly within the transition region[2]. In this work pyroelectric measurements by Chynoweth method[5] under DC bias up to 1.8 KV/mm within a temperature range of 70°C around the temperature of maximum dielectric constant have been studied.

---

*Visiting scientist from Shanghai Institute of Ceramics, Shanghai, China.
**Visiting scientist from Xian Jiaotong University, Xian, China.

†Communicated by Professor L. E. Cross

2. EXPERIMENTAL

2.1 Preparation of Materials

All samples were prepared by conventional mixed oxide processing from stoichiometric proportion of PbO, Sc_2O_3, Ta_2O_5 and Nb_2O_5. Compositions were ball milled in alcohol for 20 hours. The mixture was dried, then calcined for two hours at 800°C. The calcine powders were reground and pelletized. Then the pellets were fired at 1300°C for one hour, using $PbZrO_3$ + PbO for atmosphere control. A final sintering was performed at 1360°C followed by rapid quenching to induce the disordered structure. The degree of ordering in the B-site cations were controlled by thermal annealing the sample at 1000°C. Final densities achieved were 94% theoretical, with no more than 1% weight loss.

The degree of ordering was established by comparing base and superlattice reflection intensity in the x-ray powder pattern and using the relation for the degree of ordering S

$$S^2 = \left(\frac{I_{superlattice}}{I_{base\ lattice}}\right)_{exp} / \left(\frac{I_{super}}{I_{base}}\right)_{theory} \quad \text{for } S = 1$$

The degrees of ordering are 0.87 for the samples annealed at 1000°C for 24 hours and 0.40 for the samples quenched at 1360°C to room temperature within 20 minutes.

2.2 Pyroelectric Measurements by Chynoweth Method

The pyro-signals were measured by a modified Chynoweth method. The schematic circuit for measurements is shown in Figure 1. The series circuit consists of a bias voltage supply, the sample, and a high resistance ($10^9\Omega$) across which a pre-amplifier was connected via a blocking capacitor (0.01 μf). The output of the pre-amplifier was connected to a phase-lock amplifier model PAR HR-8. The magnitude of the pyrosignal can be read from the output voltmeter of the phase-lock amplifier. A Tektronix 545A cathode ray oscilloscope was used to monitor the wave form of the pyrosignal. A disk radiation chopper was used to control the heating frequency of the detector so as to be close to the charge mode of operation. In this mode the pyroelectric signal at

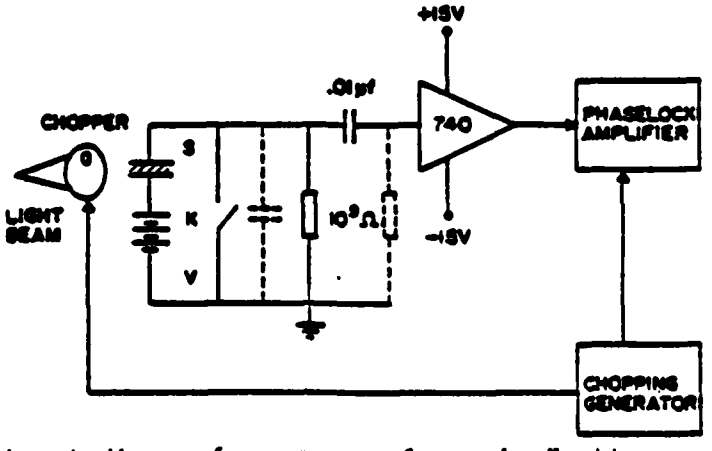

FIGURE 1. Schematic diagram of measurement. S - sample; V - bias source; 740 - pre-amplifier; K - charging switch.

fixed frequency is proportional to p/KC_p, here p - pyroelectric coefficient, K - dielectric constant, C_p - specific heat of the sample.

In all the experiments of this work the PST samples were about 0.25 mm in thickness. Circular gold electrodes were sputtered on to opposite faces of the samples, the diameter of the electrode was about 5 mm. Thin silver leads were attached to the gold electrodes by means of air-drying silver paste. An infrared projector lamp was used as the heat source to modulate the sample temperature. A Delta design MK 2300 environment chamber was used to change the ambient temperature about the bolometer chip.

Figure 2 shows the pyro-signal measured by Chynoweth method for the disordered and ordered PST ceramic samples without electric bias. The temperature range of measurement is 70°C around the temperature of the dielectric constant maximum T_m which is 1.9°C for the disordered PST ceramic sample, and is 17°C for the ordered one (Figure 3). It is obvious from the figures that the pyro-signal for ordered samples is much larger than that for the disordered one. The pyroelectric signal as a function of bias field at various temperatures is shown in Figure 4. If accurate absolute pyroelectric coefficients were needed, the pyro-signals would have to be corrected for the temperature variation of specific heat and the non-linearity departure of the rectifiers at small signal. These corrections were not performed since only relative magnitudes are to be used and thus they would not affect any of the interpretations and conclusions. It is clear that as the bias field increases the pyroelectric signal of the disordered PST sample increases more significantly than the ordered one. To compare the effect of electric bias field on the disordered and ordered materials the enhancement factor N_v, which is referred to as the ratio of the pyro-signal under a DC bias of 1.5 KV/mm and the pyro-signal under a DC bias of 0.1 KV/mm, is plotted as a function of the temperature difference $T-T_m$ (Figure 5). The following feature of the experimental results are obvious: (1) The enhancement factor of the pyro-signal under DC bias for the disordered material is higher than that for the ordered one within the whole temperature range of measurements. (2) The highest enhancement factor occurs at the temperatures different from T_m. For the disordered sample the highest enhancement factor appears at the temperature about 21°C below T_m, while for the ordered sample it appears at the temperature about 5°C above T_m.

In contrast with the results for the PST samples, the electric bias field shows no significant effect on $LiNbO_3$ single crystals at 23°C (Figure 6).

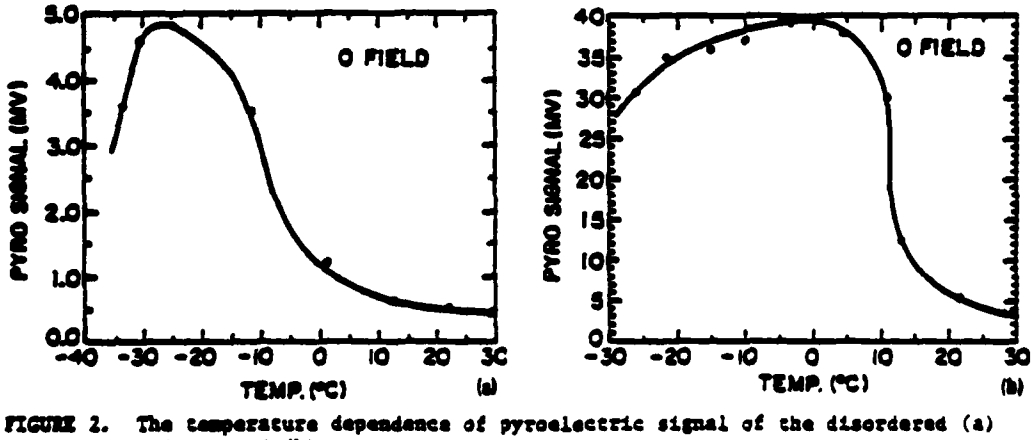

FIGURE 2. The temperature dependence of pyroelectric signal of the disordered (a) and ordered (b) ceramics.

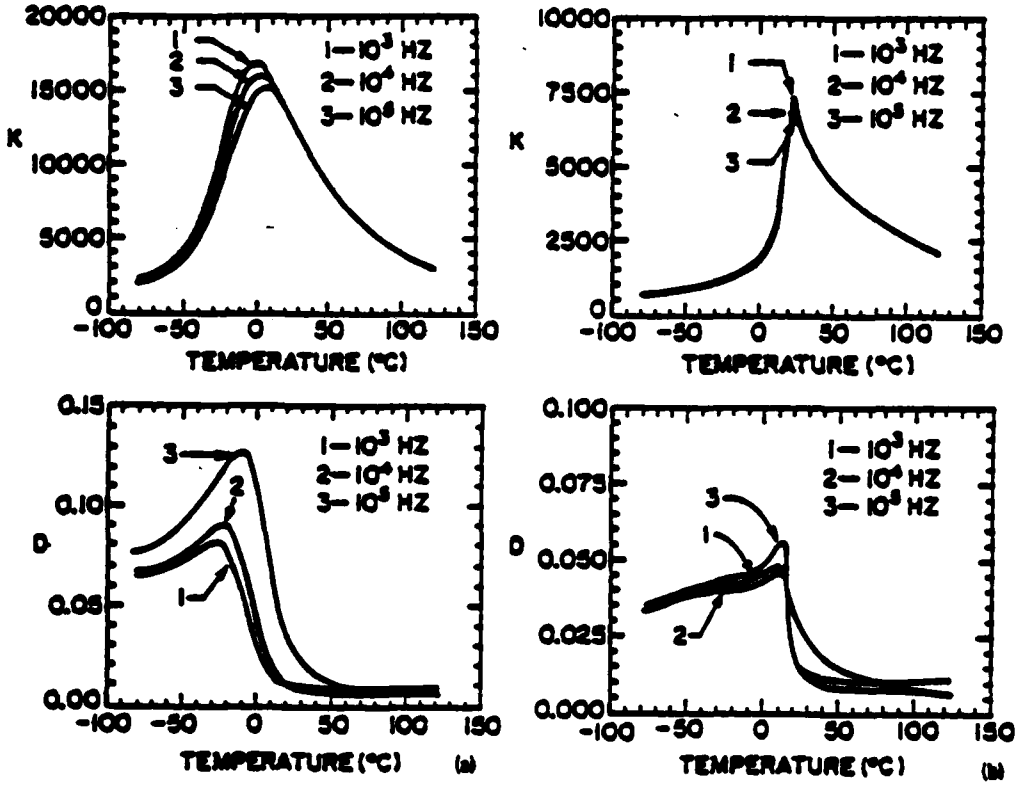

FIGURE 3. The temperature dependence of dielectric constant K and loss tangent D of the disordered (a) and ordered (b) PST ceramics.

3. DISCUSSION

The experimental results presented above show that the DC bias has a much stronger effect upon the pyroelectric behavior of disordered PST ceramic samples than the ordered one. An enhancement factor of 32 for the disordered PST sample was observed under a bias field of 1.5 KV/mm, while for the ordered one the highest enhancement factor is only 3. Since the pyro-signal measured in this work is proportional to the reciprocal of the dielectric constant K, the decreasing of K with respect to DC bias field for the ordered and disordered PST[4] should be partially responsible for the enhancement of the pyro-signal under DC biases. However, the ratio of the dielectric constants under DC biases of 0.1 KV/mm and 1.5 KV/mm is less than 3 within the entire temperature range of the measurement[4]. It would appear that a new extrinsic component of reversible pyroelectricity induced by DC bias must be responsible for the very significant enhancement of the pyro-signal of the disordered PST ceramics under DC bias. The existence of microdomains in relaxor ferroelectrics in the temperature region lower than the temperature of the dielectric maximum T_m is suggested to be the origin of this new extrinsic component of the reversible pyroelectricity. Under DC bias fields,

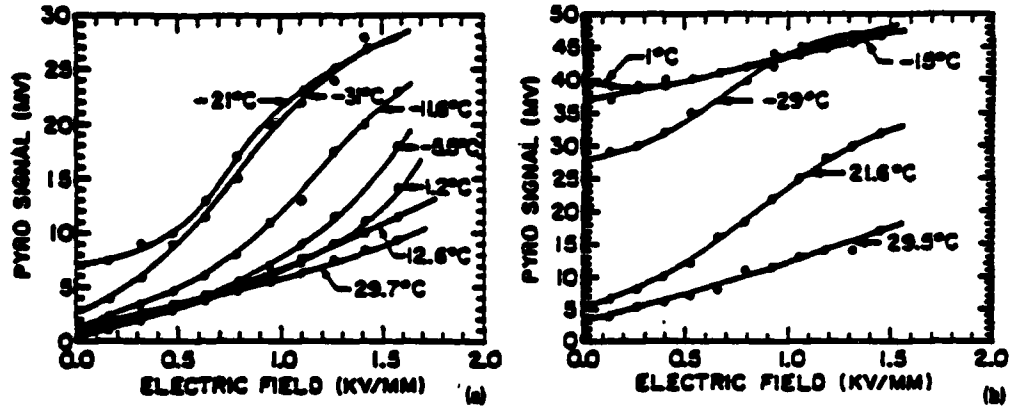

FIGURE 4. The pyroelectric signal as a function of bias field at various temperatures for the disordered (a) and ordered (b) PST ceramics.

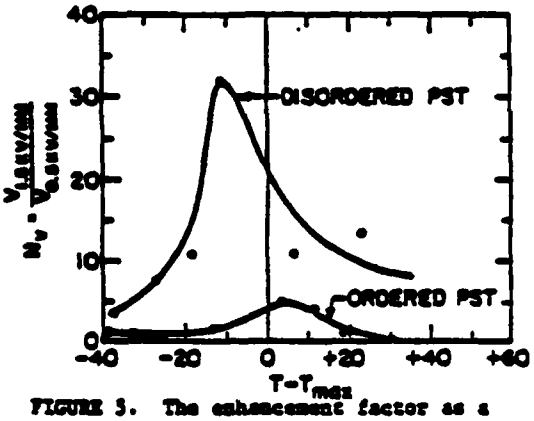

FIGURE 5. The enhancement factor as a function of the temperature difference T_m-T for the disordered and ordered PST ceramics.

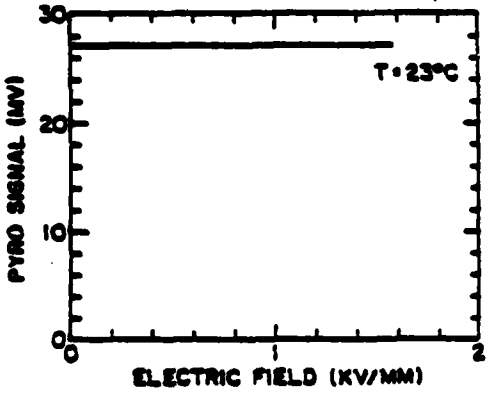

FIGURE 6. The pyroelectric signal as a function of bias field for $LiNbO_3$ single crystals.

the large dipole moments of the microdomains, which are oriented in a random way, will experience strong orienting force and build up into macrodomains. Since disordering of the micro regions is a thermalization process, small reversible temperature change can modulate the state of microdomain order and thus contribute a new extrinsic component to the temperature dependence of the induced polarization. In disordered PST material, the direct measurement of the pyroelectric coefficient by Byer-Roundy[6] technique shows that the pyroelectric coefficient peak appears at -37°C (Figure 7a), which

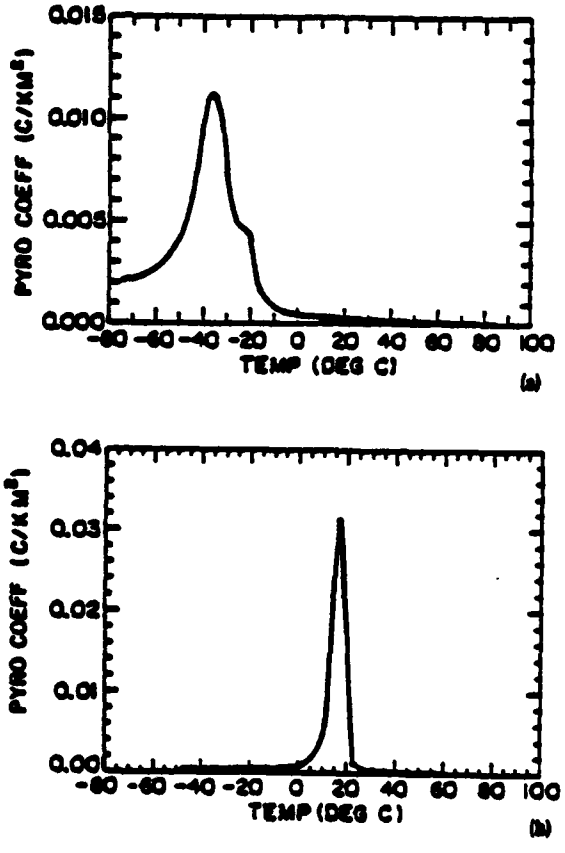

FIGURE 7. The temperature dependence of pyroelectric coefficient of the disordered (a) and ordered (b) PST ceramics.

is 39 degrees below T_m (1.9°C). The temperature region from -37°C to 1.9°C, which is supposed to be the most active temperature region of micro-domains, is well coincident with the temperature region of large enhancement of the pyro-signal for the disordered PST sample. while for the ordered PST material the pyroelectric coefficient peak is 14°C (Figure 7b), which is only three degrees below T_m (17°C). Since the ordered PST material exhibits more or less normal ferroelectricity, no significant microdomain activity can be traced. The fact that only a factor of five of the largest enhancements of pyro-signal at the temperature five degrees higher than T_m has been observed in ordered PST samples, means that the DC bias can only induce a rather small displacive polarization in the absence of the microdomains.

The large and field-controllable reversible pyroelectric effect is a promising phenomenon for developing new pyroelectric devices.

REFERENCES

1. N. Setter and L.E. Cross, J. Mater. Sci. 15, 2478-2482 (1981).
2. N. Setter and L.E. Cross, J. Appl. Phys. 51 (8), 4356-4360 (Aug. 1980).
3. N. Setter and L.E. Cross, Phys. Stat. Sol. (a) 61, K71 (1980).
4. Chen Zhili, X. Yao and L.E. Cross, to be published.
5. A.G. Chynoweth, J. Appl. Phys. 27 (1), 78-85 (1956).
6. R.L. Byer and C.B. Roundy, Ferroelectrics 3, 333 (1972).

APPENDIX 3

Polarization and depolarization behavior of hot pressed lead lanthanum zirconate titanate ceramics

Yao Xi,[a] Chen Zhili,[b] and L. E. Cross
Materials Research Laboratory, The Pennsylvania State University, University Park, Pennsylvania 16802

(Received 22 November 1982; accepted for publication 28 February 1983)

A detailed study of the polarization and depolarization behavior of 7:65:35 and 8:65:35 lead lathanum zirconate titanate transparent ceramics under dc bias and constant heating rates has been carried out. The dielectric permittivity exhibits a new anomaly near 0 °C in freshly thermally depoled samples which is associated with a buildup of macrodomains and the development of a remanent polarization. From continuity of the dispersive behaviors it is suggested that the dielectric change at the so-called α–β transition T_d is not a conventional phase change, but rather is a loss of macro-ordering and a decay back to a disordered microdomain texture.

PACS numbers: 77.60. + v

I. INTRODUCTION

The thermal depolarization behavior of electrically poled lead lanthanum zirconate titanate (PLZT) ceramics with compositions in the range of $PbZr_{0.65}Ti_{0.35}O_3$ with La_2O_3 additions of 6-, 7-, and 8-mole% La_2O_3 have been of interest for the behavior of the pyroelectric current, dielectric response, and electro-optic characteristics.[1–3] It was clear from the early studies of Keve[4] that depolarization of a short-circuited PLZT of composition 7:65:35 occurs at a temperature well below that of the dielectric permittivity maximum. Dielectric data of Salanek[5] suggest that the K' maximum is strongly dispersive as in ferroelectrics with diffuse phase transitions (relaxors). More recent measurements by Kimura, Newnham, and Cross[6] of the elastic shape memory effect suggest that the shape changing ferroelastic macrodomains are lost in these ceramics at the lower depoling temperature.

The present study was undertaken to explore more fully both the poling and depoling characteristics of transparent hot pressed PLZT's of 7:65:35 and 8:65:35 composition. Data presented here are for the 8:65:35 composition; however, the 7:65:35 material gives qualitatively similar results in every respect. To avoid, as far as possible, domain stabilization of the type demonstrated by Schulze, Biggers, and Cross,[7] all measurements were made on annealed and freshly thermally quenched samples.

II. SAMPLE PREPARATION

Ceramics used in these studies were originally prepared at the Shanghai Institute of Ceramics in China. The designations 7:65:35 and 8:65:35 indicate in the conventional manner a zirconia:titania ratio of 65:35 mole% and a substitution of 7 and 8 mole% of La_2O_3 for PbO. The samples were prepared from reagent grade nitrate salts of lanthanum and zirconium and reagent grade $TiCl_4$. The salts were dissolved in distilled water and the solutions mixed in the desired proportions. Mixed solutions were then coprecipitated by addition of ammonia to maintain a pH value of 8. After thorough washing to remove NO_3^- and Cl^- ions, the precipitates were spray dried at high temperatures. Reagent grade PbO powder in 10% excess of the required stoichiometric proportion was then added and the powders ball milled in polyethylene lined jars in acetone for 6 h. The slurry was again dried and cold pressed slugs of suitable dimensions were hot pressed in an O_2 atmosphere at 1150 °C for 16 h under a uniaxial stress of 200 kg/cm^2.

Boules of near theoretical density, high transparency, and a mean grain size of 2 μm resulted.

III. EXPERIMENTAL PROCEDURE

Samples of PLZT were cut with a string saw and then ground to the thickness used for dielectric measurements, generally 0.1 to 0.2 mm. Electrodes used were sputtered gold. The diameter of the electroded area was around 5 mm. Samples were annealed at 600 °C for 1 h and then followed by slow cooling.

The dielectric properties of PLZT were measured by a computerized automatic measuring system with Hewlett-Packard's new generation of microprocessor-based equipment. The biased temperature dependence of dielectric constant and loss tangent were measured by a multifrequency *LCR* meter, HP 4274A and 4275A in the frequency range of 10^2–10^7 Hz, with basic accuracy of 0.1%. The biased pyroelectric currents were measured with the HP4140B picoampere meter. A Delta Design model 2300 environment chamber covered the temperature range from −150 to 200 °C, using liquid nitrogen as a coolant. Temperatures were measured with a Fluke 8502A digital multimeter via a platinum resistance thermometer mounting directly on the ground electrode of the sample fixture. A HP 9825A desktop computer was used for on-line control of automatic measurement through a HP 6904B multiprogrammer interface. All the data were recorded on flexible magnetic discs. Special software was developed for automatic measurement. Linear temperature change with specified rates was easily achieved. The reproducibility of measurements was excellent.

All the measurements were made on freshly thermally

[a] Visiting scientist from Xian Jiaotong University, Xian, China.
[b] Visiting scientist from Shanghai Institute of Ceramics, Shanghai, China.

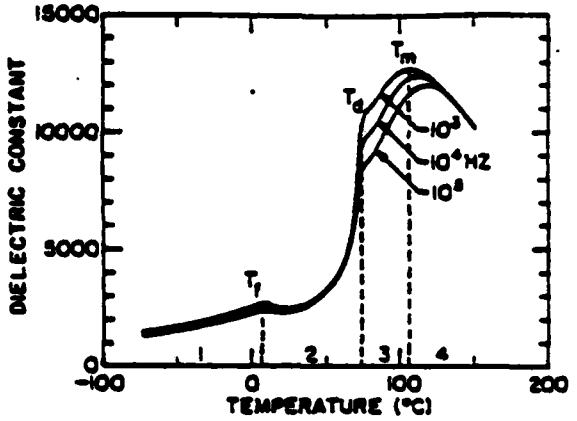

FIG. 1. Temperature dependence of dielectric constant of PLZT 8:65:35 under dc bias of 3 kV/cm at heating rate of 3 °C/min.

depoled samples. Samples were heated above 150 °C, then cooled down below − 75 °C. Bias was applied at − 75 °C and then the sample reheated from this temperature.

IV. EXPERIMENTAL RESULTS

The temperature dependence of the weak field dielectric permittivity at several frequencies applied to an 8:65:35 PLZT ceramic under a dc bias of 3 kV/cm applied at − 75 °C and measured on slow heating (3 °C/min) is shown in Fig. 1. The peak labeled T_f observed near 0 °C is a new phenomenon heretofore unobserved in this system, and appears to divide the response into four distinct regions. There

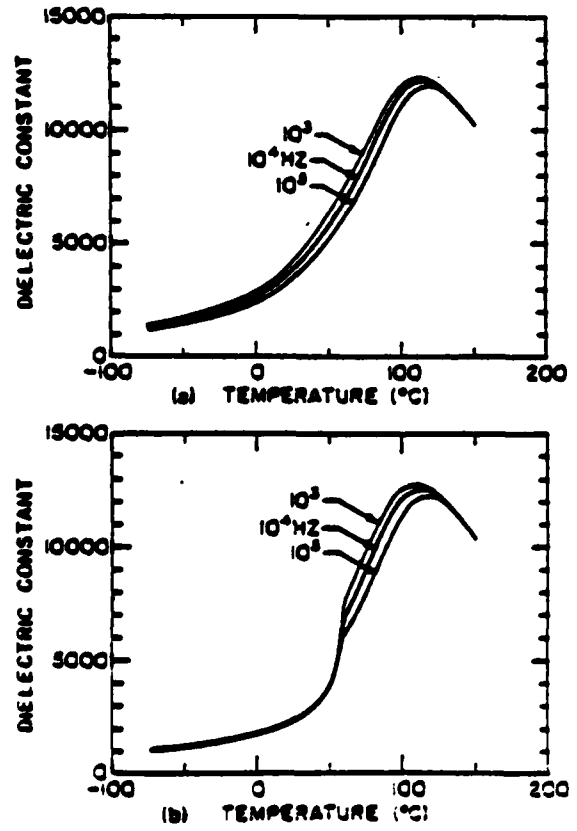

FIG. 2. Temperature dependence of dielectric constant of PLZT 8:65:35 (a) without and (b) under dc bias of 3 kV/cm at cooling rate of 3 °C/min.

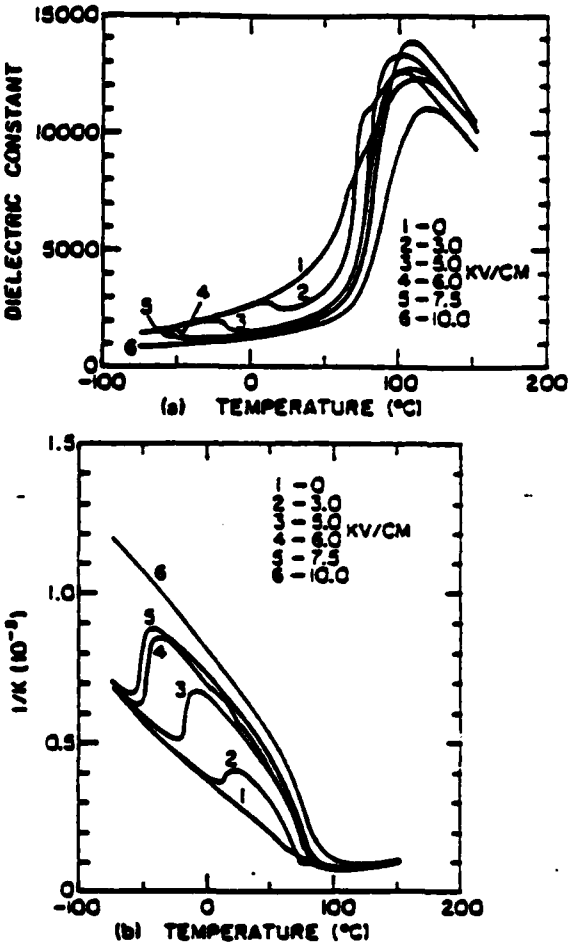

FIG. 3. Temperature dependence of (a) dielectric constant K and (b) dielectric stiffness $1/K$ of PLZT 8:65:35 under different bias field at constant heating rate.

is a dispersive region below T_f (1), a largely nondispersive region between T_f and T_d, a temperature often referred to as the α–β phase change (2), a second dispersive region between T_d and T_m the temperature of the dielectric maximum (3), and a second nondispersive region above T_m (4).

In a sample cooled without bias from above T_m, regions (1) and (3) cojoin filling the whole temperature range below T_m and appear to be of completely similar property [Fig. 2(a)]. On cooling under dc bias, however, T_d is reproduced.

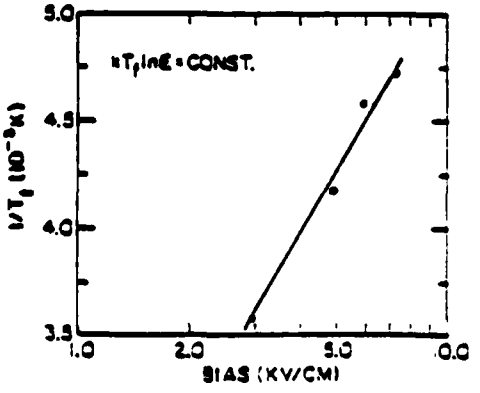

FIG. 4. Linear relation between logarithm of bias field ln E and reciprocal of transition temperature $1/T_f$.

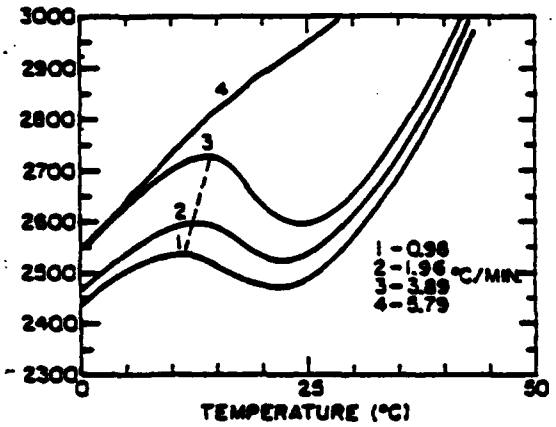

FIG. 5. Kinetic behavior of transition at T_f under different heating rates.

but region (2) now persists down to the lowest temperatures measured and region (1) is lost [Fig. 2(b)].

At a constant heating rate T_f shifts to a lower temperature with increasing bias [Fig. 3(a)] the "transition" being most obvious in the dielectric stiffness [Fig. 3(b)]. It would appear that the product $kT_f \ln E$ is approximately constant over the field range studied (Fig. 4). k is an arbitrary constant.

For field below 1 kV/cm no T_f peak was observed, but at intermediate field levels it was clear that the temperature T_f depends on the heating rate, increasing with faster heating, but being difficult to observe for rates above 5 °C/min (Fig. 5).

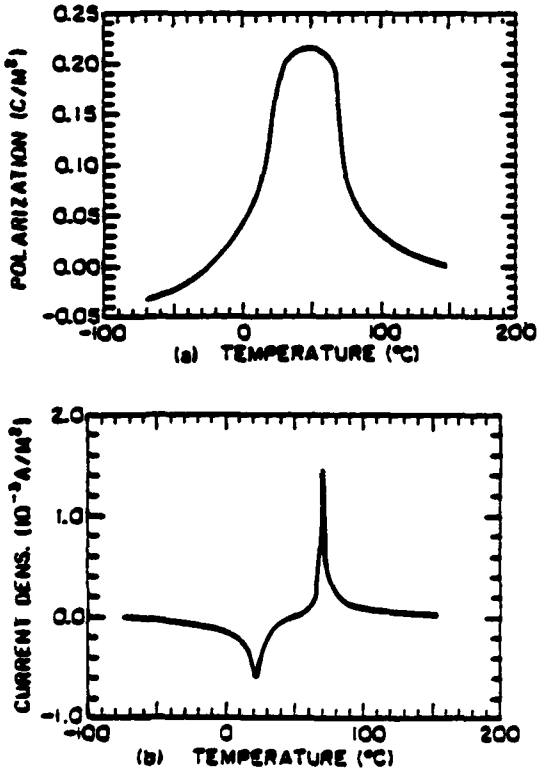

FIG. 6. The buildup and decay of (a) the remanent polarization and (b) associated charging and discharging current of PLZT 8:65:35 under dc bias of 3 kV/cm at constant heating rate.

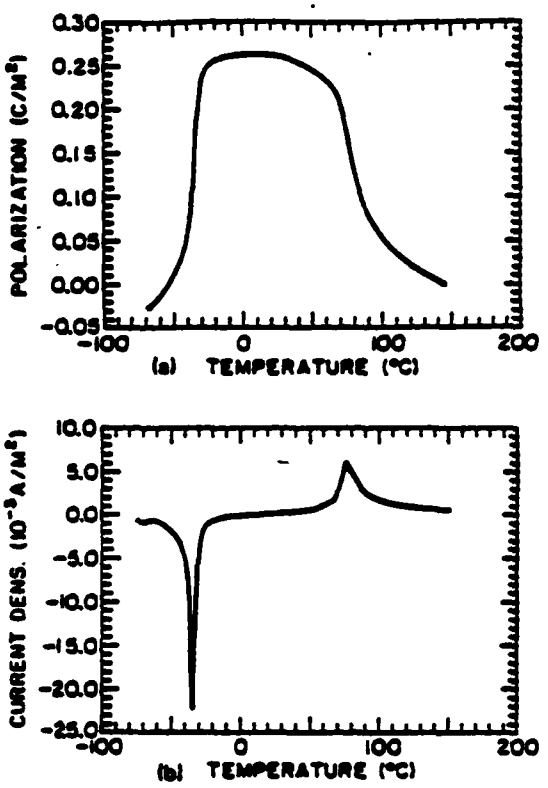

FIG. 7. The buildup and decay of (a) the remanent polarization and (b) associated charging and discharging current of PLZT 8:65:35 under dc bias of 5 kV/cm at constant heating rate.

Prepoled samples do not exhibit the T_f peak and in no sample could we detect this change on cooling from high temperature. A necessary preconditioning is that the sample be cooled in an unpoled state and the field applied at low temperature.

Aging the sample at temperatures below T_m appears to preferentially reduce the dispersive component of K (Ref. 7) and for such samples the peak at T_f was smeared. In long aging at low temperature the T_f peak was often to the point where the change was difficult to discern at all.

That the dielectric changes are associated with the buildup and decay of marcropolarization has been confirmed by pyroelectric measurements using the Byer–Roundey[8] technique.

The remanent polarization builds up rapidly in the vicinity of T_f for a sample heated from the depoled condition under a field of 3 kV/cm [Fig. 6(a)] and the charging current associated with this buildup is evident in the current curve in Fig. 6(b) and is in sharp contrast to the depoling current peak at T_d. Similar curves for a larger field of 5 kV/cm [Figs. 7(a) and 7(b)] confirm the dielectric trends for T_f and T_d.

The asymmetry on cooling is clearly evident in Figs. 8(a) and 8(b) which show that once the macropolarized state is established it does not decay again on cooling. Thus, only the poling current peak is evident in Fig. 8(b).

For a 3-kV/cm field the behavior of prepoled and depoled samples is contrasted directly in Fig. 9.

V. DISCUSSION

The evidence presented above suggests strongly that neither T_f nor T_d are associated with conventional phase changes in the dielectric. The dispersive character below T_m in the virgin state is similar to that observed in many relaxor ferroelectrics and is attributed to heterophase micro regions which are disordered in the thermally depoled state. Since these "domains" are on a scale much smaller than the x-ray coherence length or the wavelength of light, the structure appears cubic below T_m to most macroscopic tests.

Under bias fields, the large dipole moments of the microdomains will experience strong orienting force and apparently at T_d microdomains can build into macrodomains with consequent distortion of the structure, the manifestation of optical birefringence, and the emergence of the shape memory of ferroelastic macrotwins.

Once established below T_d, the ordered state will persist down to absolute zero, and no lower change is to be expected. Clearly, however, the kinetics of microdomain rearrangement will slow up with reducing temperature. We suggest that for thermally depoled samples in the region below 0 °C the kinetics is sufficiently slow that a dc bias is unable to effect reorientation in a reasonable time, and the disordered state persists. If, however, the biased disordered microdomain system is now heated at a constant rate, ordering can occur at a suitable temperature when the rates have speeded up sufficiently. Thus higher fields or slower heating rates will both serve to depress the temperature T_f of the change from micro- to macro-ordering.

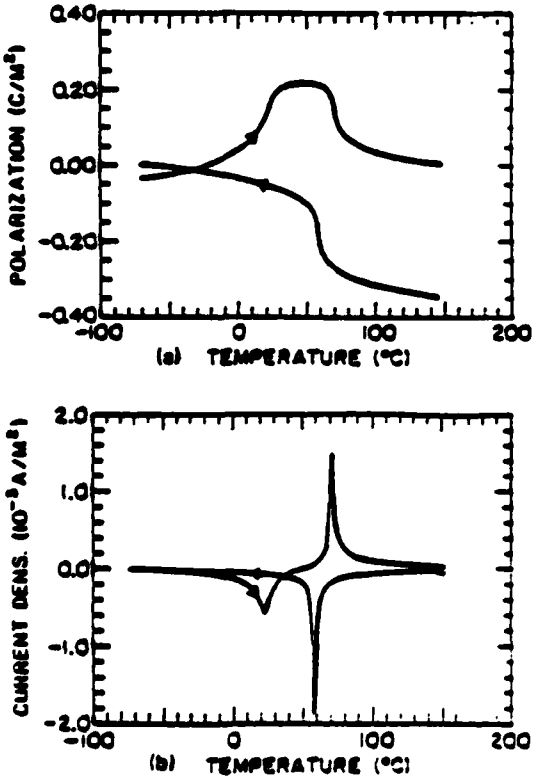

FIG. 8. (a) The remanent polarization and (b) charging-discharging current of PLZT 9:65:35 under dc bias of 3 kV/cm at heating and cooling measurement.

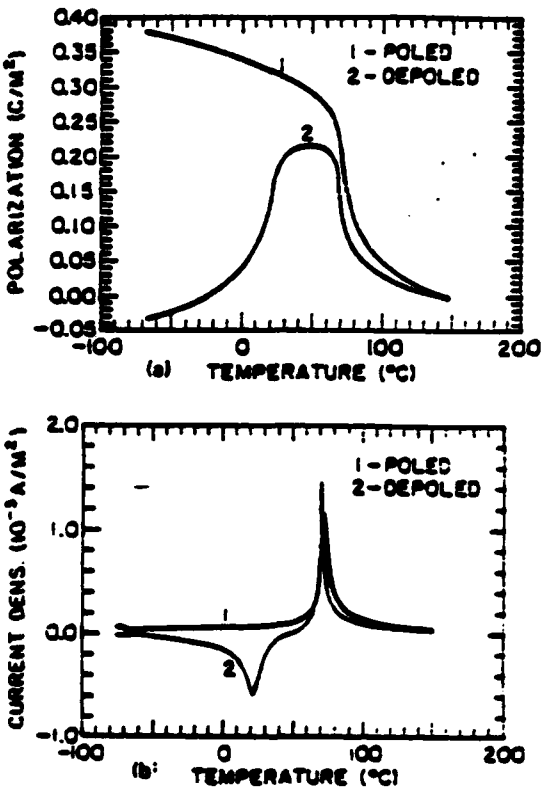

FIG. 9. (a) The remanent polarization and (b) charging-discharging current of prepoled and depoled PLZT 9:65:35 samples under dc bias of 3 kV/cm at constant heating rate.

The sequence of dielectric and pyroelectric observations are consistent with this suggested pattern. If T_d were an α-β phase change, as has been suggested earlier, then it would necessarily imply that the change at T_f was a conventional poling phenomenon. In this case the kinetics of the behavior would be difficult to explain, and the clear continuity of the dispersions in regions (1) and (3) for unbiased crystals would be a remarkable coincidence.

On balance we feel that the buildup and decay of macrodomains from polar microregions provide a valid description for all observed phenomena. A more subtle "phase change" explanation may be possible, however, bearing in mind the scale of the polar microregions postulated. Since the onset of a nonzero polarization will occur at a different temperature in each microregion over the temperature range of the dispersive dielectric permittivity peak, it may well be that on a global scale these local onsets should not be considered as phase changes.

In this view then, the crystal may be regarded as being macroscopically cubic over the whole temperature range. Below some temperature T_c between T_d and T_f, this "cubic" nonpolar phase becomes metastable with respect to a macroscopically polar phase and the crystal can be forced into the more stable state by a poling field. Thus T_d and T_c may be regarded as a field-forced phase change to a polar state and a thermal depoling into a macroscopically nonpolar state, respectively.

A question of major interest which remains unresolved is the nature of the subgrain heterogeneity in the PLZT which favors relaxor behavior. It may be suspected that the

very high levels of lanthanum doping could give rise to partially ordered planar defects which could serve to interrupt and limit the polarization on the appropriate scale, but much more detailed structure work is required to delineate this heterogeneity.

ACKNOWLEDGMENT

The authors wish to thank Mrs. Yin Weiping of the Shanghai Institute of Ceramics for providing the PLZT materials.

[1]A. H. Meitzler and H. M. O'Bryan, J. Am. Ceram. Soc. 55, 504 (1972).
[2]G. H. Haertling and C. E. Land, J. Am. Ceram. Soc. 54, 1 (1971).
[3]G. H. Haertling, J. Am. Ceram. Soc. 54, 303 (1971).
[4]E. T. Keve and K. L. Bye, J. Appl. Phys. 46, 810 (1975).
[5]W. R. Salaneck, J. Appl. Phys. 43, 4468 (1972).
[6]T. Kimura, R. E. Newnham, and L. E. Cross, Phase Transitions 2, 113 (1981).
[7]W. A. Schulze, J. V. Biggers, and L. E. Cross, J. Am. Ceram. Soc. 61, 41 (1978).
[8]R. L. Byer and C. B. Roundy, Ferroelectrics 3, 333 (1972).

APPENDIX 4

Ferroelectrics, 1984, Vol. 54, pp. 163-166
0015-0193/84/5401-0163$18.5000

POLARIZATION AND DEPOLARIZATION BEHAVIOR OF HOT PRESSED LEAD LANTHANUM ZIRCONATE TITANATE CERAMICS

YAO XI, CHEN ZHILI, AND L.E. CROSS
Materials Research Laboratory, The Pennsylvania State University, University Park, PA 16802

Abstract—Studies have been made of the polarization and depolarization behavior for lead lanthanum zirconate titanate ceramics with zirconia:titania ratio 0.65/0.35 and La_2O_3 content from 0.07 to 0.095 (7:65:35 to 9.5:65:35). Continuity of the dielectric dispersion on cooling unbiased freshly de-aged samples suggests that across this whole composition range for temperatures below the dielectric maxima, there are no macroscopic phase changes. Large remanent polarizations may be built up at low temperatures by cooling under suitable DC bias, but the ceramics will 'stand off' significant bias levels applied at low temperature and remain dispersive. Depoling on heating becomes progressively less abrupt with increasing La_2O_3 content but is always accomplished well below the temperature of the dielectric maximum. A model involving the ordering and disordering of polar micro-regions under electrical and thermal fields accounts well for the observed properties.

INTRODUCTION

The thermal depolarization behavior of electrically poled lead lanthanum zirconate titanate (PLZT) ceramics with compositions in the range of $PbZr_{0.65}Ti_{0.35}O_3$ with La_2O_3 additions of 6-, 7-, and 8-mole% La_2O_3 have been of interest for the behavior of the pyroelectric current, dielectric response, and electro-optic characteristics[1-3]. It was clear from the early studies of Love[4] that depolarization of a short-circuited PLZT of composi-tion 7:65:35 occurs at a temperature well below that of the dielectric permittivity maximum. Dielectric data of Salanek[5] suggest that the K' maximum is strongly dispersive as in ferroelectrics with diffuse phase transitions (relaxors). More recent measurements by Kimura, Newnham, and Cross[6] of the elastic shape memory effect suggest that the shape changing ferroelastic macrodomains are lost in these ceramics at the lower depoling temperature.

The present study was carried out to investigate more fully both poling and depoling characteristics of transparent hot pressed PLZTs covering the composition range from (7 to 9.5):65:35. Data for the 8% La_2O_3 composition have been presented earlier[7], but some are reproduced again here to compare with the 8.8 and 9.5% La_2O_3 compositions.

SAMPLE PREPARATION AND EXPERIMENTAL PROCEDURE

Ceramics used in these studies were provided by the Shanghai

Institute of Ceramics in China. Wafers used in the present study were cut from boules of near theoretical density, high optical transparency and mean grain sizes in the range 2 to 5 μm.

Dielectric properties were measured on a computerized automatic measuring system using the HP LCR meters HP 4274A and 4275A under HP 9825 computer control. Pyroelectric currents were measured with an HP 4140B picoamperemeter. A Delta Design 2300 environment chamber covered the range -150 to 200°C and temperature were measured with a platinum resistance thermometer on a Fluke 8502A digital multimeter. Special software was developed for automatic measurement and all data were recorded on flexible magnetic disks.

EXPERIMENTAL RESULTS

The temperature dependence of dielectric permmittivity in 8:65:35 PZT cooling under zero bias, and under a DC bias of 3 kV/cm for a cooling rate of 3°C/min is shown in Figure 1a and 1b. Suppression of the dispersive behavior (relaxor character) under bias is clearly evident at temperatures below 55°C. Similarly for an 8:65:35 PLZT sample cooled to -75°C then biased to 3 kV/cm and heated at 3°C/min (Fig. 2), the persistence of the dispersion up to a temperature T_f followed by a suppressed no dispersive region (2) a re-emergence of dispersion below T_m (3) and the conventional higher temperature non-dispersive regions (4) are quite evident. That T_f and T_m are poling and depoling temperatures is evidenced from the pyroelectric currents (Fig. 3), and the integrated current shows the corresponding build up and decay of macroscopic polarization.

Data has already been presented to show that T_f decreases with increasing bias field, and the kinetic nature of the change is evident from the dependence upon heating rate[7].

In the 8.8/65/35 PZT, on cooling a freshly de-aged sample again the dispersive character of a relaxor ferroelectric is clearly evidenced (Fig. 4a). Here, however, under even high DC bias of 15 kV/cm the relaxation is not completely suppressed and there is no evidence of an abrupt change such as that seen in the 8/65/35 compositions (Fig. 4b). That the polarization builds up and decays in a rather similar manner to that in the ceramics of lower lanthanum content is,however, evident from the integrated pyroelectric response for a sample cooled under field (Fig. 5[2]) as compared to that of a sample cooled without field to -100°C then biased to 3 kV/cm and heated at a constant rate of 3°C/minute (Fig. 5[1]).

It may be noted that the major changes with increased La_2O_3 content is that the polarization levels are lower, the changes are more gradual and occur at lower temperature.

In the 9.5:65:35 this trend is continued (Fig. 6) and here a higher field of 6.6 kV/cm was used to produce comparable polarization changes. Larger polarization levels can be induced in both 8.8 and 9.5% La_2O_3 compositions, but only by going to much higher field levels.

DISCUSSION

The continuity of the dispersion curves in all samples below T_m suggests that in the absence of a driving field none of the materials goes through a normal macroscopic phase change below T_m. This would appear to be confirmed by recent measurements in Shanghai of W. Yin and colleagues[8] who show that in grain grown PLZTs of the 8:65:35 composition the individual grains have isotropic optical properties below T_m in the absence of an external field.

For the 8.8:65:35 and 9.5:65:35, the dispersion and poling: depoling behavior are remarkably similar to those observed in $Pb(Mg_{1/3}Nb_{2/3})O_3$, $Pb(Sc_{1/2}Ta_{1/2})O_3$ and other relaxor ferroelectrics. It is thus tempting to apply the model of ordering of polar micro regions under field, and disordering under temperature to describe the observed build up and decay of polarization. That the 8:65:35 composition is optically isotropic grain by grain on cooling again suggests the model of disordered polar micro-regions. However, in this composition the disordering is rather abrupt and has many of the features of a phase change.

We suggest in speculation, that in analogy to magnetism, the PMN, PST, 8.8:65:35 and 9.5:65:35 compositions may be superparaelectric but that in the 8:65:35 the phenomena may be more analogous to that of critical superparamagnetism.

REFERENCES

1. A.H. Meitzler and H.M. O'Bryan, J. Am. Ceram. Soc. 55, 54 (1972).
2. G.H. Haertling and C.E. Land, J. Am. Ceram. Soc. 54, 1 (1971).
3. G.H. Haertling, J. Am. Ceram. Soc. 54, 303 (1971).
4. E.T. Keve and K.L. Bye, J. Appl. Phys. 46, 810 (1975).
5. W.R. Salaneck, J. Appl. Phys. 43, 4468 (1972).
6. T. Kimura, R.E. Newnham, and L.E. Cross, Phase Transitions 2, 113 (1981).
7. Yao Xi, Chen Zhili, and L.E. Cross, J. Appl. Phys. 54(6):339 (1983).
8. B.H. Chu, H.K. Ngao, X.S. Zheng, and Z.W. Yin, Joint US:China Seminar on Microstructure and Properties of Ceramic Materials, Shanghai, May, 1983 (to be published).

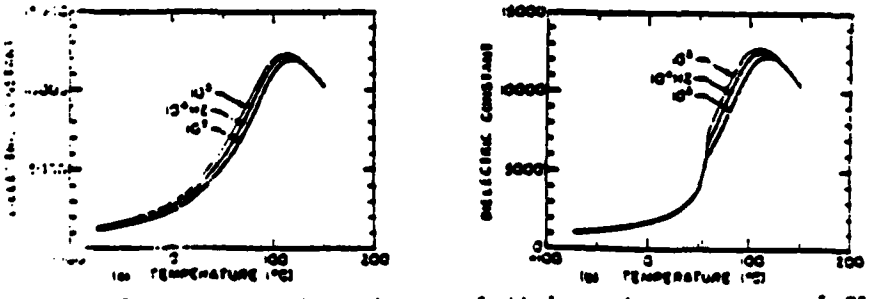

Figure 1. Temperature dependence of dielectric constant of PLZT 8:65:35 (a) without and (b) under dc bias of 3 kV/cm at cooling rate of 3°C/min.

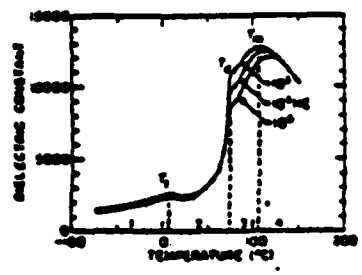

Figure 2. Temperature dependence of dielectric constant of PLZT 8/65/35 under dc bias of 3 kV/cm at heating rate of 3°C/min.

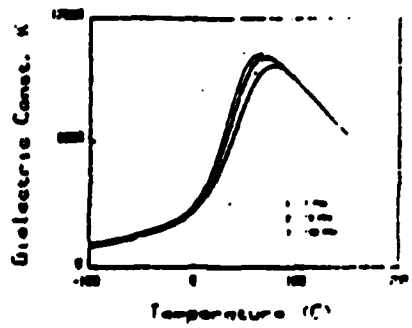

Figure 4(b). Dielectric permittivity in PLZT 8/65/35 at field 100 V/cm, in bias 15 kV/cm, cooling at 3°C/min.

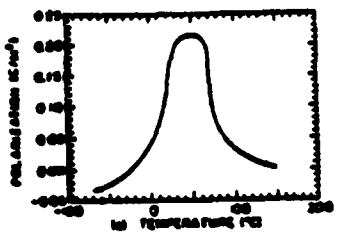

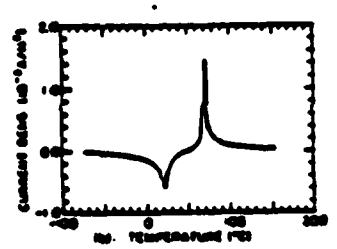

Figure 3. The buildup and decay of (a) the resonant polarization and (b) associated charging and discharging current of PLZT 8/65/35 under dc bias of 3 kV/cm at constant heating rate.

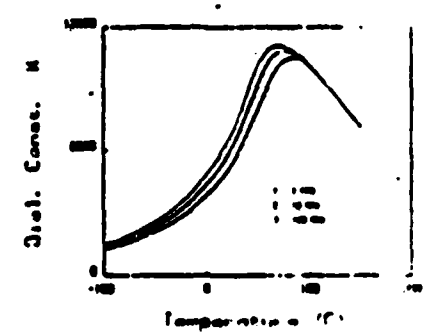

Figure 4(a). Dielectric permittivity in PLZT 8/65/35 E field 100 V/cm, cooling at 3°C/min.

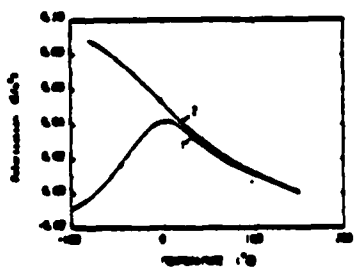

Figure 5. Polarization in PLZT 8.8/65/35
(1) Depoled sample heated at 3°C/min 1kV/cm
(2) Cooling under a field of 3 kV/cm.

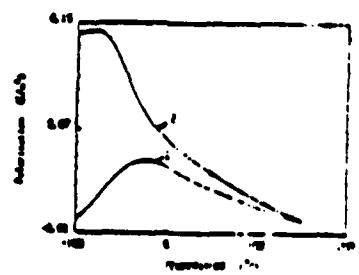

Figure 6. Poling and depoling in PLZT [illegible]
(1) Depoled sample heating [illegible]
under bias of [illegible]
(2) Depoling after [illegible]
under 30 kV/[illegible] in bias [illegible]
heating rate [illegible]

APPENDIX 5

Dielectric Properties of Lead-Magnesium Niobate Ceramics

S. L. SWARTZ,* T. R. SHROUT,*·* W. A. SCHULZE,*·† and L. E. CROSS*

Materials Research Laboratory, The Pennsylvania State University, University Park, Pennsylvania 16802

Dielectric properties are reported for lead magnesium niobate ($PbMg_{1/3}Nb_{2/3}O_3$) ceramics which were prepared as single phase (i.e., without pyrochlore) with an improved technique. Dielectric constants of 18 000 for pure PMN and 31 000 for PMN with 10% $PbTiO_3$ were achieved; these values are 50% larger than those reported in the literature. The dielectric constant of PMN ceramics was found to increase with both sintering temperature and excess MgO, and subsequent analysis of the microstructures confirmed that this was due to an increase in grain size. This grain-size dependence is explained as a consequence of low-permittivity grain boundaries.

I. Introduction

PEROVSKITE LEAD MAGNESIUM NIOBATE ($PbMg_{1/3}Nb_{2/3}O_3$, hereafter designated PMN) was first synthesized by Soviet workers in the late 1950s.[1] The dielectric properties of PMN have since been widely investigated in both the single-crystal[2-5] and ceramic[1,3-9] forms. The main feature of the dielectric properties of PMN, common to all of the above investigations, was a broad maximum of the dielectric constant‡ just below room temperature. The magnitude of this maximum (at 1 KHz, ≈12 000 for ceramic PMN and >20 000 for single-crystal PMN) decreased and the temperature of this maximum increased with increasing frequency. A corresponding frequency dispersion of the dissipation factor was also observed, but at a temperature range lower than that of the dielectric constant maxima. This behavior is typical of what are now commonly referred to as relaxor ferroelectrics.

Recently, there has been much interest in PMN and PMN-based materials for electrostrictive strain applications.[9-13] It has been reported that the electrostrictive strains generated in PMN-based ceramics are an order of magnitude larger than those of $BaTiO_3$-based ceramics[11] and are comparable to the piezoelectric strains of PZT ceramics.[13] This is due to the large dielectric constant of PMN, as the induced electrostrictive strains are proportional to the square of the polarization (and thus dielectric constant). PMN is not only an important candidate material for electrostrictive devices, but should also be promising for other applications requiring a large dielectric constant material, e.g., capacitors.

A limitation to the utilization of PMN in device applications has been the lack of a simple, reproducible fabrication technique for ceramic PMN. The fabrication of PMN is complicated by the formation of a lead niobate-based pyrochlore phase during the initial stages of reaction between mixed oxides.[14] The subsequent transformation of the pyrochlore phase to perovskite is sluggish and necessitates the use of repeated calcinations at relatively high temperatures for long times. Mixed-oxide processing rarely results in pyrochlore-free PMN and has associated problems of reproducibility and the control of PbO stoichiometry. At least part of the large discrepancy between the maximum dielectric constant values reported for ceramic and single-crystal PMN (12 000 vs 20 000) may indeed be explained on the basis of the fabrication problems.

In a recent investigation,[14] an improved process for the fabrication of pyrochlore-free PMN was developed. The technique consisted of prereacting magnesium and niobium oxides to form the columbite $MgNb_2O_6$, prior to reaction with PbO. Perovskite PMN thus formed via the reaction:

$$3PbO + MgNb_2O_6 \longrightarrow 3PbMg_{1/3}Nb_{2/3}O_3 \qquad (1)$$

The amount of pyrochlore phase was reduced to <2% by this method, as compared to ≈30% for a batch of mixed oxides given a similar calcination schedule. It was also shown that the pyrochlore phase can be completely eliminated by additions of excess MgO (≥2 mol%).

The purpose of this investigation was to study the microstructure and dielectric properties of sintered PMN ceramics fabricated using the above technique. Processing variables included deviation from the PMN stoichiometry, calcining temperature, and sintering temperature. The compositions investigated were based on pure PMN and PMN with 10 mol% $PbTiO_3$, which has a transition range closer to room temperature.

II. Experimental Procedure

Compositions were selected so that the effects of excess MgO and PbO stoichiometry could be determined. As previously reported,[14] excess MgO suppresses pyrochlore formation; however, its effect on dielectric properties should be examined. The effect of PbO stoichiometry becomes important when considering the problem of PbO volatility during sintering. Thus, compositions investigated in this study corresponded to the following: stoichiometric lead magnesium niobate (PMN-STD); 2 and 5 mol% excess MgO (PMN-*x*% MgO); 2 mol% excess PbO (PMN-2% PbO); and 2 mol% deficient in PbO (PMN-2% MN). Compositions with 10 mol% $PbTiO_3$ were also prepared as stoichiometric (PMN-10PT-STD) and with excess MgO (PMN-10PT-*x*% MgO).

The raw materials used throughout this investigation were reagent-grade oxides of lead, magnesium, niobium, and titanium. As described in Ref. 14, the fabrication process for PMN primarily consists of two steps: the preparation of $MgNb_2O_6$, followed by the addition of PbO and subsequent calcination. For the excess MgO compositions, the excess MgO was added prior to reaction with Nb_2O_5.

Accordingly, three $MgNb_2O_6$ batches were prepared with the stoichiometries: $MgO \cdot Nb_2O_5$ (for the STD, 2% PbO, and 2% MN compositions), $1.02MgO \cdot Nb_2O_5$ (2% MgO), and $1.05MgO \cdot Nb_2O_5$ (5% MgO). After ball-milling in ethanol for 12 h and subsequent drying, the $MgNb_2O_6$ batches were calcined in alumina crucibles at 1000°C for 6 h. X-ray diffraction (XRD) confirmed that the columbite structure of $MgNb_2O_6$ was obtained in each case.

The constituents, PbO and the appropriate $MgNb_2O_6$ batch, were weighed, mixed by ball-milling as above, and calcined in a closed alumina crucible at T = 800° or 870°C for a soak time of 4 h. After calcination, 2 wt% PVA binder was added and pellets (1.27 cm in diameter and 3 to 4 mm thick) were pressed. Following binder burnout at 500°C, the pellets were sintered at various temperatures (1200°, 1270°, and 1310°C) for 1 h. PbO loss was limited by the use of a sintered PMN source powder. Weight loss on sintering was typically held to <1% for the STD composition, <0.5% for excess MgO compositions, and <2% for the excess PbO composition; a slight weight gain was observed with the PMN-2% MN composition. The sintered pellets were analyzed by XRD and scanning electron microscopy (SEM).

Samples for dielectric measurements were prepared from the sintered pellets by polishing the faces parallel with 12 μm alumina, sputtering gold electrodes, and applying air-dried silver paint to

Presented at the Basic Science and Electronics Divisions Joint Fall Meeting, Cambridge, Massachusetts, September 15, 1982 (Paper No. 178-BE-82F). Received August 4, 1983; revised copy received December 12, 1983; approved January 16, 1984.

Supported by the Office of Naval Research under Contract No. N00014-78-C-0291.

*Member, the American Ceramic Society.

†Now with Sprague Electric Company, North Adams, Massachusetts 01247.

‡Now with Alfred University, Alfred, New York 14802.

§The term "dielectric constant" is used in this paper to describe the low-field relative permittivity.

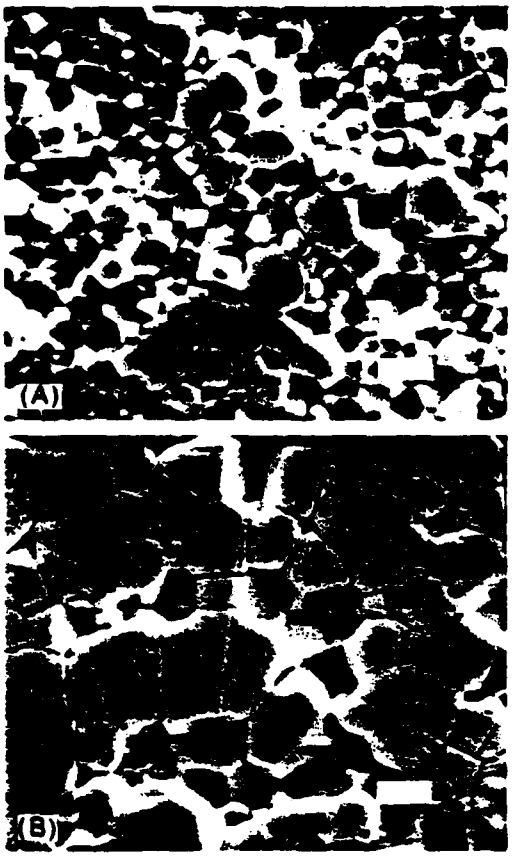

Fig. 1. Microstructure of (*A*) PMN-STD and (*B*) PMN-5% MgO, both calcined at 800° and sintered at 1200°C (bar = 5 μm).

Table I. Density and Grain Size of PMN Ceramics*

Composition	Sintering temp. (°C)	Density (g/cm³)	Grain size (μm)
PMN	1200	7.78	2.8
	1270	7.59	6.1
	1310	7.54	8.9
PMN-2% MgO	1200	7.77	3.7
	1270	7.61	6.0
	1310	7.56	10.2
PMN-5% MgO	1200	7.75	6.0
	1270	7.65	8.9
	1310	7.53	13.6

*Calcined at 800°C. ρ_{th} = 8.13 g/cm³.

improve electrical contact. Prior to electroding, the geometry and weight of each sample were measured and densities were calculated. Dielectric measurements were carried out on an automated system, whereby a temperature-control box[†] and LCR meters[‡] were controlled by a desk-top computer system.[**] Dielectric constant and dissipation factors were measured pseudocontinuously at various frequencies between 100 Hz and 1 MHz as the samples were cooled through the transition range at a rate of 0.75°C/min. Typically, 2 to 4 samples of each composition and thermal history were measured. The two parameters used for analysis of dielectric data were the maximum dielectric constant at 100 Hz and the temperature at which this maximum occurred. The dielectric constants were corrected for porosity by the equation governing parallel mixing:

$$K = K_{obs}(\rho_{th}/\rho_{obs}) \quad (2)$$

and averages were calculated.

Electrical resistivities of selected samples were measured at T = 250° to 550°C using a picoampmeter[††] with an appropriate field (≈0.1 to 0.5 kV/cm) being applied across the samples.

[†]Model 2300, Delta Design, Inc., San Diego, CA.
[‡]Models 4274A and 4275A LCR meters, Hewlett-Packard, Inc., Palo Alto, CA.
[**]Model 9825A, Hewlett-Packard, Inc.

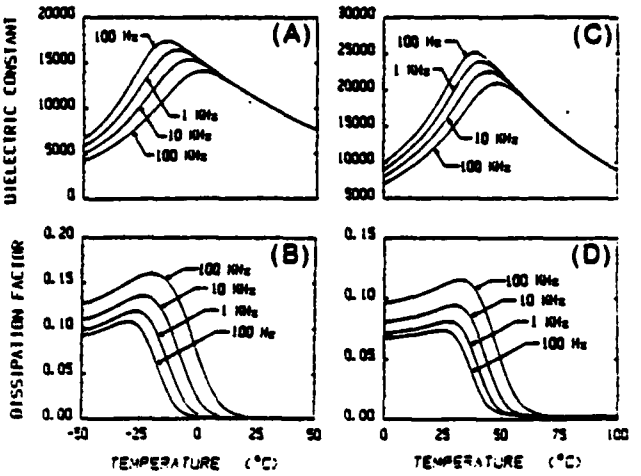

Fig. 2. Dielectric constant and dissipation factor vs temperature for (*A*), (*B*) PMN and (*C*), (*D*) PMN-10PT: STD compositions, calcined at 800°, sintered at 1270°C.

Table II. Effect of Processing Temperatures on 100-Hz Dielectric Properties of PMN-STD

Calcining temp. (°C)	Sintering temp. (°C)	K_{max} (100 Hz)	T_c (°C)
800	1200	15 900	−15
800	1270	18 200	−15
800	1310	16 400	−17
870	1200	14 900	−15
870	1270	15 800	−16

III. Results and Discussion

(1) *Microstructures*

Typical SEM micrographs are shown in Fig. 1, demonstrating the influence of excess MgO on the microstructure of PMN ceramics sintered at 1200°C. Table I gives the grain size (calculated by a linear intercept technique) and density as a function of composition and sintering temperature for sintered pellets made from PMN powder calcined at 800°C.

Two trends in the data presented in Table I were observed: (1) An increase in sintering temperature resulted in an increase in grain size and a corresponding decrease in density. (2) Excess MgO increased the grain size without appreciably changing the density. These two observations will become important when considering the results of the dielectric property measurements in the next section.

(2) *Dielectric and Resistivity Measurements*

Figure 2 shows typical plots of dielectric constant and dissipation factor vs temperature at various frequencies for pure PMN and PMN with 10% $PbTiO_3$. The 10% $PbTiO_3$ addition affects the dielectric properties of PMN in three ways:

[††]Model 4140B, Hewlett-Packard, Inc.

Table III. Effects of PbO Stoichiometry on 100-Hz Dielectric Properties of PMN*

Composition	Sintering temp. (°C)	K_{max} (100 Hz)	T_c (°C)
PMN-STD	1200	14 900	−15
	1270	15 800	−16
PMN-2% PbO	1200	14 500	−13
	1270	14 100	−14
PMN-2% MN	1200	13 200	−19
	1270	16 000	−19

*Calcined at 870°C.

Table IV. Effect of Excess MgO on 100-Hz Dielectric Properties of PMN*

Composition	Sintering temp. (°C)	K_{max} (100 Hz)	T_c (°C)
PMN-STD	1200	15 900	−15
	1270	18 200	−15
	1300	16 400	−17
PMN-2% MgO	1200	15 800	−13
	1270	17 800	−14
	1310	18 300	−15
PMN-5% MgO	1200	17 000	−13
	1270	19 400	−14
	1310	17 900	−15

*Calcined at 800°C.

(1) The transition range is shifted to higher temperature. The temperature of the 100 Hz dielectric constant maximum is increased from −15° for pure PMN to 40°C for PMN-10% $PbTiO_3$. A corresponding increase in temperature was observed at higher frequencies.

(2) The magnitudes of the dielectric constant maxima are increased by the addition of 10% $PbTiO_3$ from 14 to 18 000 (100 Hz) to 20 to 30 000, depending on processing conditions.

(3) The frequency dispersion of the dielectric constant maxima is decreased by $PbTiO_3$. The temperature difference between the 100 Hz and 1 MHz dielectric constant maxima is 23° for pure PMN and 13°C for PMN with 10% $PbTiO_3$.

The effects of the various experimental parameters (composition, processing temperatures, etc.) on the 100 Hz dielectric properties (K_{max} and T_c) of PMN and PMN-10% $PbTiO_3$ are presented in Tables II to VI.

Arrhenius plots of the resistivities of PMN-STD, PMN-2% MgO, and PMN-5% MgO, sintered at 1200° and 1270°C, appear in Fig. 3. The activation energies and extrapolated room-temperature resistivities are given in Table VII.

(3) Discussion of Results

In the following description of the results of the dielectric and resistivity measurements, each of the various topics will be taken up separately.

(A) Sintering Temperature: The effect of sintering temperature on the dielectric properties was pronounced and consistent over the entire set of compositions investigated. An increase in sintering temperature resulted in an increase in maximum dielectric constant. The effect of sintering temperature was most pronounced for the PMN-10PT-STD composition (Table V), for which the 100 Hz maximum dielectric constant (corrected for porosity) increased from 21 200 to 26 500 and 29 400 as the sintering temperature was increased from 1200° to 1270° and 1310°C, respectively, for powder which was calcined at 800°C. Relating this to the microstructures, a grain-size dependence of the dielectric properties is implied (i.e., an increase in dielectric constant with increasing grain size).

(B) Calcining Temperature: Using the criterion of maximum

Table V. Effect of Processing Temperatures on 100-Hz Dielectric Properties of PMN-10PT-STD

Calcining temp. (°C)	Sintering temp. (°C)	K_{max} (100 Hz)	T_c (°C)
800	1200	21 200	40
	1270	26 500	39
	1310	29 400	38
870	1200	19 900	40
	1270	25 500	39

Table VI. Effect of Excess MgO on 100-Hz Dielectric Properties of PMN-10PT*

Composition	Sintering temp. (°C)	K_{max} (100 Hz)	T_c (°C)
PMN-10PT-STD	1200	21 200	40
	1270	26 500	39
	1310	29 400	38
PMN-10PT-2% MgO	1200	29 300	41
	1270	27 300	39
	1310	33 100	40
PMN-10PT-5% MgO	1200	28 900	41
	1270	29 100	39
	1310	34 000	40

*Calcined at 800°C.

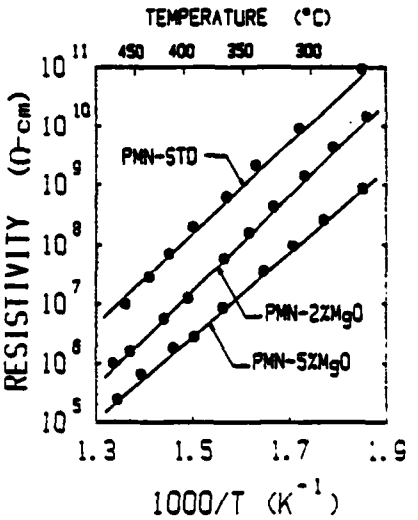

Fig. 3. Arrhenius plots of resistivity for PMN with excess MgO; calcined at 800°, sintered at 1270°C.

Table VII. Effect of Sintering Temperature and Excess MgO on Resistivity of PMN

Composition	Sintering temp. (°C)	$\rho_{25°C}$ (Ω·cm)*	Activation energy (×10⁻¹⁹ J/mol)
PMN-STD	1200	1.4×10^{23}	2.56
	1270	9.8×10^{22}	2.48
PMN-2% MgO	1200	2.2×10^{22}	2.40
	1270	1.6×10^{22}	2.56
PMN-5% MgO	1200	2.6×10^{19}	2.21
	1270	7.7×10^{19}	2.29

*Extrapolated from high-temperature data.

dielectric constant, it is apparent from the data presented in Tables II and V that 800°C is a better calcining temperature than 870°C for the PMN-STD and PMN-10PT-STD compositions. This might be explained on the basis of a pyrochlore content argument. In the calcining study described in Ref. 14, it was noted that, for the PMN-STD composition, the amount of pyrochlore phase increased with increasing calcining temperature (although the pyrochlore content for the highest calcining temperature was still <2%). However, the general trend of a lower dielectric constant with the 870°C calcining temperature (as compared to 800°C) was also noticed for compositions with excess MgO, which did not have a detectable amount of pyrochlore. Thus the exact nature of the apparent calcining temperature dependence of the dielectric properties of PMN cannot be fully explained at this time.

(C) PbO Stoichiometry: The importance of PbO stoichiometry was demonstrated by the data in Table III. Although the PMN-2% PbO composition experienced a large weight loss during sintering, which resulted in a PbO stoichiometry approaching that of the PMN-STD composition, a degradation of the dielectric constant was observed. The PMN-2% PbO composition had a 100 Hz transition temperature of −13°C, as compared to −15° for PMN-STD and −19° for PMN-2% MN. This result explains the slight decrease in transition temperature observed as the sintering temperature was increased. Increasing the sintering temperature, and thus PbO weight loss, would shift the stoichiometry of PMN toward the PMN-2% MN composition, and the transition temperature would be expected to decrease.

(D) Excess MgO: The data presented in Tables IV and VI show that the addition of excess MgO resulted in a significant enhancement of the dielectric constant of PMN ceramics. This was originally attributed to the elimination of the pyrochlore phase. Subsequent analysis of the microstructures confirmed that the increase in dielectric constant with excess MgO corresponded to an increase in grain size. Thus a grain-size dependence of the dielectric constant, similar to that observed with sintering temperature, seems a more probable explanation. However, two important questions remain to be answered: (1) How is the excess MgO responsible for an increase of grain size? (2) Is the excess MgO chemically incorporated into the perovskite grains, or does it exist as isolated grains or in grain boundaries?

(E) Grain-Size Dependence: The most important result of this investigation was the apparent grain-size dependence of the dielectric constant of PMN ceramics. This was evidenced by the substantial increase in dielectric constant observed with both sintering temperature and excess MgO. It must be stated, however, that the true grain-size dependence cannot be resolved, due to the difficulty in varying grain size without also changing the ceramic in other ways: density, PbO weight loss, microcracking, etc. Any deviation from the general trend of the dielectric data can be attributed to this problem.

A grain-size dependence of the dielectric constant of lead zirconate titanate ceramics has been reported.[19] It was shown that the room-temperature dielectric constant increased and the dielectric constant at the Curie temperature decreased with increasing grain size. This can be attributed to the clamping of domain walls in fine-grained PZT. This behavior can be contrasted to the grain-size dependence of $BaTiO_3$ ceramics. Internal stresses generated at the grain boundaries in $BaTiO_3$ ceramics cause the room-temperature dielectric constant to increase and the dielectric constant at the Curie temperature to decrease as the grain size decreases.[16]

The apparent grain-size dependence of the dielectric constant of PMN ceramics, as demonstrated by this investigation, was quite different from that of the preceding cases. The increase in dielectric constant with increasing grain size was observed in both the ferroelectric and paraelectric regions, suggesting that this is not a domain or stress effect. Thus it is likely that the grain-size dependence was actually caused by the influence of grain-boundary volume. If a second phase of low permittivity (pyrochlore, excess MgO, impurities, etc.) were to be distributed within the grain boundaries, the observed grain-size dependence would be satisfactorily explained. As the grain size increases, the number of boundaries in series with the grains decreases, and the large permittivity of the PMN grains becomes less affected by the low-permittivity grain boundaries. Therefore, the measured dielectric constant of the ceramic increases. This hypothesis is supported by indirect evidence obtained during the microstructural analysis. Scanning electron microscopy observations of fractured surfaces indicated primarily transgranular fracture, and polished and etched surfaces tended to have a large number of grain pullouts; these apparently weak grain boundaries suggest the presence of a different phase located in the grain boundaries. Also, neither the pyrochlore nor excess MgO phases were located by SEM EDS analysis, even though one or both phases were known to exist in all of the samples. Thus it might be assumed that both phases, if present, were located in the grain boundaries. However, the existence of the two phases in the grain boundaries is not a necessary requirement for the grain boundaries to have such an impact on the dielectric properties.

(F) Resistivity Measurements: Extrapolation of the resistivity data, shown in Fig. 3 and Table VII, to room temperature yielded resistivities on the order of 10^{20} Ω·cm. The extremely large values of resistivity and dielectric constant of PMN correspond to enormous resistance-capacitance time constants of $\approx 10^{13}$ s (10^5 yr). The PMN-5% MgO composition exhibited a significantly lower resistivity and a slightly decreased activation energy than the PMN-STD composition. However, the resistivities of both the PMN-STD and PMN-5% MgO compositions displayed no appreciable difference with sintering temperature, suggesting that the resistivity of PMN ceramic is not grain-size-dependent. The resistivity of the PMN-2% MgO composition decreased with increased sintering temperature, possibly indicating a change in the nature of incorporation of the excess MgO into the ceramics.

IV. Summary

The results of this investigation were: (1) A fabrication process has been developed which allows for the fabrication of pyrochlore-free lead magnesium niobate ceramics. (2) Increasing the sintering temperature results in an increase in grain size and a corresponding increase in dielectric constant. (3) Excess MgO completely eliminates the pyrochlore phase, increases the grain size, and results in an increase in dielectric constant. (4) The increase in dielectric constant with grain size can be explained by the influence of low-permittivity grain boundaries. (5) The resistivities of lead magnesium niobate ceramics are quite large and decrease with excess MgO but not with sintering temperature.

Acknowledgments: The authors thank P. Moses for help in the dielectric measurements, A. Narthasilpa for diligence in sample preparations, and B. Jones for SEM expertise.

References

[1]G. A. Smolenskii and A. I. Agranovskaya, "Dielectric Polarization and Losses of Some Complex Compounds," *Sov. Phys. Tech. Phys.*, 3, 1380–82 (1958).
[2]V. A. Bokov and I. E. Myinikova, "Electrical and Optical Properties of Single Crystals of Ferroelectrics with a Diffused Phase Transition," *Sov. Phys. Solid State*, 3 [3] 613–23 (1961).
[3]W. A. Bonner, E. F. Dearborn, J. E. Geusic, H. M. Marcos, and L. G. Van Uitert, "Dielectric and Electro-optic Properties of Lead Magnesium Niobate," *Appl. Phys. Lett.*, 10 [5] 163–65 (1967).
[4]J. W. Smith, "Dielectric Properties of Lead Magnesium Niobate", Ph. D. Thesis, The Pennsylvania State University, 1967.
[5]V. Y. Frisberg and P. A. Fritsberg, "Dielectric Properties of Lead Magnesium Niobate Under High Hydrostatic Pressures Near a Phase Transition Point," *Sov. Phys. Crystallogr.*, 24 [4] 492–93 (1979).
[6]G. A. Smolenskii, A. I. Agranovskaya, and S. N. Popov, "On the Mechanism of Polarization in Solid Solutions of $Pb_2NiNb_2O_9$-$Pb_2MgNb_2O_9$," *Sov. Phys. Solid State*, 1 [1] 147–48 (1959).
[7]G. A. Smolenskii and A. I. Agranovskaya, "Dielectric Polarization of a Number of Complex Compounds," *Sov. Phys. Solid State*, 1 [10] 1429–37 (1959).
[8]G. A. Smolenskii, V. A. Isupov, A. I. Agranovskaya, and S. N. Popov, "Ferroelectrics with Diffuse Phase Transitions," *Sov. Phys. Solid State*, 2 [11] 2584–94 (1961).
[9]S. J. Jang, "Electrostrictive Ceramics for Transducer Applications", Ph. D. Thesis, The Pennsylvania State University, 1979.
[10]K. Uchino, S. Nomura, L. E. Cross, S. J. Jang, and R. E. Newnham, "Electrostrictive Effect in Lead Magnesium Niobate Single Crystals," *J. Appl. Phys.*, 51 [2] 1142–45 (1980).
[11]L. E. Cross, S. J. Jang, R. E. Newnham, S. Nomura, and K. Uchino, "Large

Electrostrictive Effects in Relaxor Ferroelectrics," *Ferroelectrics*, 23, 187–92 (1980).
[12]S. J. Jang, K. Uchino, S. Nomura, and L. E. Cross, "Electrostrictive Behavior of Lead Magnesium Niobate Based Ceramic Dielectrics," *Ferroelectrics*, 27, 31–34 (1980).
[13]S. Nomura and K. Uchino, "Electrostrictive Effect in $Pb(Mg_{1/3}Nb_{2/3})O_3$-Type Materials," *Ferroelectrics*, 41, 117–32 (1982).
[14]S. L. Swartz and T. R. Shrout, "Fabrication of Perovskite Lead Magnesium Niobate," *Mater. Res. Bull.*, 17, 1245–50 (1982).
[15]K. Okazaki and K. Nagata, "Effects of Density and Grain Size on the Elastic and Piezoelectric Properties of $Pb(Zr\text{-}Ti)O_3$ Ceramics," *J. Soc. Mater. Sci., Jpn.*, 4, 404–12 (1972).
[16]W. R. Buessem, L. E. Cross, and A. K. Goswami, "Phenomenological Theory of High Permittivity in Fine-Grained Barium Titanate," *J. Am. Ceram. Soc.*, 49 [1] 33–36 (1966).

APPENDIX 6

THE EFFECTS OF VARIOUS B-SITE MODIFICATIONS ON THE DIELECTRIC AND ELECTROSTRICTIVE PROPERTIES OF LEAD MAGNESIUM NIOBATE CERAMICS

D.J. VOSS, S.L. SWARTZ AND T.R. SHROUT
Materials Research Laboratory, The Pennsylvania State University, University Park, PA 16802

Abstract Sintering characteristics, dielectric properties, and electrostrictive Q_{12} coefficients are reported for fourteen dopant cations incorporated in the perovskite $A(B',B'')O_3$ structure of lead magnesium niobate [$Pb(Mg_{1/3}Nb_{2/3})O_3$]. Two trends in the dielectric properties were found: the maximum permittivity appears to be directly proportional to the transition temperature, and secondly, the percent change in capacitance at 20 kV/cm is proportionally larger for the higher permittivity samples.

Two methods to estimate the frequency dependence of the diffuseness of the phase transition showed good correlation with each other, but revealed no general trend with ionic size or valence of the modifier cations. Electrostrictive Q_{12} coefficients were found to generally decrease with increasing diffuseness of the phase transitions.

INTRODUCTION

Perovskite lead magnesium niobate [$Pb(Mg_{1/3}Nb_{2/3})O_3$, hereafter abbreviated PMN] is a well-known relaxor ferroelectric exhibiting the characteristic frequency dispersion of the dielectric maximum, i.e., the maximum permittivity increases and shifts to lower temperatures as the frequency is decreased. This relaxation character has been attributed to a statistical inhomogeneity in the distribution of the Mg^{+2} and Nb^{+5} cations in the PMN structure[1] creating microregions of varying transition temperatures (Tc).

A wide variety of properties have been measured in polycrystalline samples of PMN and numerous homotypes[2] revealing that the PMN family are promising candidates for both dielectric and electrostrictive strain applications[3,4]. Crystallographic studies of the PMN family have shown that ordering in the B sites of the perovskite $A(B',B'')O_3$ structure depends on the relative differences in the sizes and valences of the B' and B'' cations[5]. However, the magnitudes of other physical properties, particularly the dielectric properties, have not been satisfactorily correlated to the ionic size, valence, or other properties of the various cations.

For this reason, the purpose of this study was to introduce various cations into the B site of the PMN structure in hopes of

possibly correlating resultant dielectric properties with characteristic properties of the cations. Upon analysis, these results should be helpful in selecting PMN-based materials having optimum properties for various dielectric and electrostrictive applications.

The properties examined included the sintering characteristics, the frequency-related diffuseness, temperature and E-field dependence of the permittivity, resistivity, and electrostrictive behavior.

EXPERIMENTAL PROCEDURE

A very successful method to fabricate polycrystalline samples of perovskite PMN with minimal pyrochlore phase has been reported[6]. The first step is to prereact the refractory oxides MgO and Nb_2O_5 to form columbite $MgNb_2O_6$; this product is then reacted with PbO to form perovskite $Pb_3MgNb_2O_9$ (PMN). This fabrication scheme was employed for the following +2-valent cations used in this study: Ni, Mg (pure PMN), Ca, Co, Zn, Mn and Cd. The columbite precursors were prepared by ball milling reagent-grade oxides or carbonates with optical grade Nb_2O_5 in ethanol for 12-24 hr, drying the slurries, and reacting the powders in open Al_2O_3 crucibles at 800°-1000°C for 2-8.5 h. X-ray diffraction confirmed the products were single phase.

The following cations were also investigated and are grouped according to valence: (+1) Li; (+3) Al, Cr, Fe, Sc, and Tl; (+4) Ge, Mn, Ti, Mo, W, Te, Sn, Hf, Zr and Ce; (+5) V and Ta; and (+6) W. Of these, precursors were prepared for the following five: Li^{+1} as $LiNbO_3$, Cr^{+3} as $CrNbO_4$, Fe^{+3} as $FeNbO_4$, Ti^{+4} as $PbTiO_3$ and Ta^{+5} as $MgTa_2O_6$.

Following precursor formation, appropriate amounts of the oxides and/or precursors for the modifier cations were mixed and reacted with PbO in a similar procedure as described above. The substitution of all B-sites was 3.3 mol% [this corresponds to 90 mol% PMN + 10 mol% $Pb(X^{+2}_{1/3}Nb^{+5}_{2/3})O_3$] for the seven cations with +2 valency. All non-+2 cations were introduced on 10 mol% of all B sites. Other dopant levels tried were Cd^{+2} at 5 mol% and Zn^{+2} at 10 mol%. The amount of substitution was limited to low levels to minimize distortion of the perovskite structure yet produce detectable changes in the macroscopic properties.

The calcinations were performed once at 800°C for 4 h, except for Al^{+3}, Cr^{+3} and Mo^{+4} which were reacted at 700°C for 4 h. X-ray analysis of the products showed that Tl^{+3} and Mn^{+4} yielded less than 50% perovskite phase by intensity ratios.

Pellets, 1.59 cm in diameter and 3-4 mm thick, were pressed from the other twenty-four calcined products to which 3 wt% of a polyvinyl alcohol binder was added. A PbO atmosphere was maintained during sintering to minimize PbO loss. Surfaces were ground parallel with 12 μm Al_2O_3 powder and geometrical densities were calculated. Densities less than 90% of theoretical were obtained for all sintered Mo^{+4}-doped pellets. A polished surface of the sintered pellets was x-rayed for phase analysis.

Dielectric Measurements

The faces of those pellets with densities greater than 90% of theoretical were electroded, first with sputtered Au and then with air-dry Ag. The weak-field dielectric measurements were made from 100 to -75°C with a cooling rate of 3°/min. The measurement system has been described elsewhere[4].

For ferroelectrics with a diffused phase transition, the law $1/\varepsilon \propto (T-T_o)^2$ has been shown to hold over a wide temperature range instead of the normal Curie-Weiss law. Uchino et al. have shown that when the local Curie temperature distribution is Gaussian, the diffuseness and/or broadness of the phase transition can be measured by the diffuseness parameter δ[7]. The temperature difference between the Tc's measured at 0.1 and 100 KHz is a second estimation of the frequency dependence of the diffuseness.

The broadness of the dielectric maximum can also be realized from the temperature dependence of the dielectric permittivity. For this, the magnitudes of the decreases in the permittivity 60°C above and 15°C below the KHz T_c were normalized with the maximum value found at T_c. This particular temperature range was chosen because it corresponds to the range of 10°C to 85°C being normalized with room temperature, commonly used for capacitor materials.

The dielectric permittivity as a function of E-field was determined on samples being maintained at their respective 10 KHz T_c. This temperature was arbitrarily chosen for comparison basis only. The permittivity was recorded with increasing and decreasing field; the maximum field being 20 KV/cm.

The electrical resistivity (ρ) was measured by applying 100 volts across selected samples being maintained at ∿100°C. Current values were recorded 10 min. after application of the voltage.

Electrostrictive Measurements

The electrostrictive Q_{12} coefficients were indirectly measured from induced piezoelectric resonance of the ceramic disks by the application of dc fields of various strengths. The selected samples were maintained in air at approximately 50°C above their respective 10 KHz T_c's, being far removed from possible nonlinear effects commonly found near T_c. Details of this method are described by Nomura et al.[8].

RESULTS AND DISCUSSION

Relatively broad, frequency-dependent permittivity-temperature curves were obtained for all modifier cations. However, not all cations were successfully incorporated into the PMN structure. This was evident from an insignificant change in T_c as compared to pure PMN, and the presence of other phases, primarily pyrochlore, in the x-ray analyses. These samples typically had low dielectric maximum (<5000) which can be attributed to the low-permittivity second phase(s). Interestingly, however, these compositions had low dissipation factors, relatively high resistivities, and low temperature

coefficients of dielectric constants which does not preclude their use for possible dielectric application.

The dielectric behavior, resistivity, and other properties for the samples in which the modifier cations were successfully incorporated into the structure are presented in Table 1. Most compositions were found to densify (>90% theoretical) at sintering temperatures as low as 1050°C with the compositions containing Cd^{+2}, Sn^{+4}, W^{+6} and 10% Zn being densified at $\leq$ 950°C.

Resistivities at 100°C were relatively high with the exceptions of Fe^{+3}-, Co^{+2}, and Mn^{+2}-doped specimens. The low value for these particular ions may be due to electronic conduction made possible by multiple valence states.

The dielectric properties, particularly K, were found to be a function of sintering conditions, particularly for the modifier Ti^{+4} in which K greatly increased with increasing sintering temperature. One possible explanation for such findings is a grain size dependency as reported by Swartz et al.[9]. In the compositions having Cd^{+2}, Zn^{+2} and Co^{+2}, T_c was found to decrease with increasing sintering temperature. This suggests that less of the cation is being incorporated into the PMN structure, further evidenced by an increasing amount of pyrochlore phase at the high sintering temperatures.

A wide range of T_c's are found in Table 1 with the T_c for W^{+6} being the lowest near -55°C and the T_c for Ti^{+4} being the highest near +50°C. Likewise, there is a correspondingly wide range of maximum permittivities. Figure 1 shows good correlation between T_c and the largest of the K_{max} values listed for each ion in Table 1. There also appears to be a corresponding increase in the temperature coefficients of the permittivity with increasing dielectric maximum.

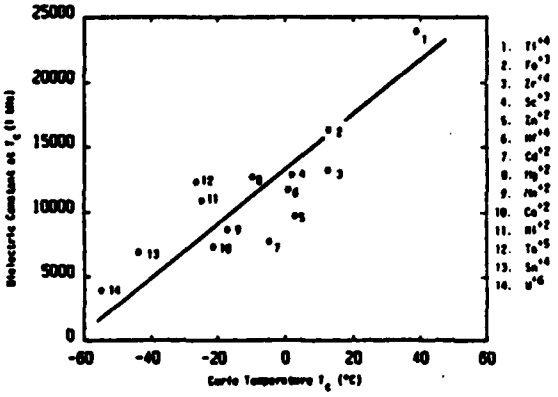

Figure 1. Dielectric constant at T_c (1 KHz data for fourteen compositions in Table 1.

A strong correlation of K_{max} with the percentage change in permittivity at a field strength of 20 KV/cm is shown in Figure 2. This shows the difficulty in finding a single phase material exhibiting a high K along with good field stability.

The main characteristic of a relaxor ferroelectric is the temperature breadth of the dielectric maximum at different frequencies. Listed in Table 1 are the differences in temperature at the 0.1 and 100 KHz T_c's for the various cations. Another measure of the frequency dependence of the diffuseness is the diffuseness coefficient δ which is

Table 1. Properties of Doped PMN.

Ion*	Sintering Temperature (°C)	T_c (1 kHz) (°C)	ΔT_c (0.1 and 100 kHz) (°C)	K_{max} (1 kHz)	$\frac{K(T_c-15°)-K_{max}}{K_{max}}$ (1 kHz) (%)	$\frac{K(T_c+60°)-K_{max}}{K_{max}}$ (1 kHz) (%)	δ (°K)	ρ (100°C) (Ω-cm)	$-Q_{12}$ ($\times 10^3$ m^4/C^2)
Ni^{+2}	1000	-20	15	8,100	-11	-38	60		
	1150	-25	11	10,000	-16	-37	59		
	1250	-25	17	10,900	-18	-43	56	8×10^{10}	54
Mg^{+2}	1000	-8	14	10,900	-10	-44	53		
	1150	-9	15	11,900	-17	-45	51	4×10^{11}	
	1250	-10	15	12,700	-19	-47	52	1×10^{12}	50
Co^{+2}	1000	0	3	6,400	-5	-36	60	2×10^{7}	
	1150	-10	7	8,500	-6	-36	58	6×10^{7}	
	1250	-21	17	7,300	-12	-39	55	1×10^{8}	52
Zn^{+2}	1000	4	14	11,100	-16	-46	52		
	1150	2	14	11,200	-16	-44	54	5×10^{11}	
	1250	1	14	11,700	-18	-46	52	6×10^{11}	50
10 mol%	950	30	11	10,300	-16	-42	50	3×10^{11}	
	1000	34	11	15,300	-16	-50	47	3×10^{10}	
	1150	33	12	13,000	-14	-47	50	2×10^{10}	
Mn^{+2}	1000	19	1	3,300	-3	-27	73		
	1150	29	2	4,000	-3	-31	66		
	1250	-17	11	8,000	-8	-36	58	8×10^{7}	
Cd^{+2}	900	2	18	6,000	-11	-31	70	6×10^{10}	
	1000	-1	18	6,100	-11	-30	72	9×10^{10}	
	1150	-6	19	7,700	-13	-34	68	8×10^{11}	50
	1250	-13	18	6,900	-13	-36	65	4×10^{10}	
5 mol%	900	9	21	7,900	-12	-32	75	3×10^{11}	
	1000	3	21	7,200	-12	-31	74	2×10^{11}	
Fe^{+3}	1150	13	12	16,300	-18	-52	43	2×10^{6}	
Sc^{+3}	1250	2	14	12,800	-20	-47	51	8×10^{11}	46
Ti^{+4}	1000	51	7	7,700	-5	-37	54		
	1150	41	10	13,500	-14	-46	48		
	1250	30	10	23,900	-24	-63	36	7×10^{11}	61
Sn^{+4}	900	-37	19	5,400	-11	-28	71		
	1000	-30	20	4,700	-9	-23	79		
	1150	-41	20	6,900	-13	-30	68		47
	1250	-44	21	6,900	-15	-30	73	3×10^{10}	
Hf^{+4}	1250	3	13	9,700	-12	-40	59	4×10^{11}	48
Zr^{+4}	1150	28	8	7,000	-4	-37	58		
	1250	13	14	13,200	-16	-47	51	6×10^{11}	50
Ta^{+5}	1150	-24	18	10,900	-18	-46	52		
	1250	-27	16	12,300	-19	-47	51	1×10^{11}	48
W^{+6}	950	-80	19	3,400	-11	-23	87	9×10^{9}	
	1000	-93	19	3,800	-12	-25	81		
	1150	-88	20	3,900	-15	-24	88		49
	1250	-84	19	2,900	-12	-23	88		

*For +2-valent ions, amount of substitution on total B-sites was 3.3 mol% except where noted for Zn^{+2} and Cd^{+2}. Amount of substitution was 10 mol% of total B-sites for cations with +3 or higher valence.

also listed in Table 1. These two parameters show good correlation with each other in that a wide T_c or large δ indicate a wide Gaussian distribution of T_c's and thus lower temperature coefficients of the permittivity.

The values of δ for the fourteen samples used in Figure 1 have been plotted in Figure 3 as a function of the ionic radii[10] of the modifier cations. When grouped according to common valences, there

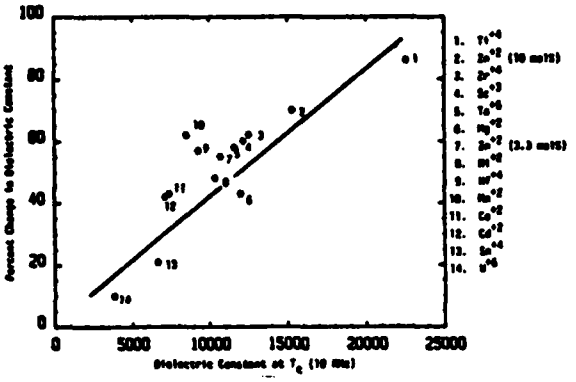

Figure 2. Decrease in dielectric constant at an E-field of 20 KV/cm. Samples were maintained at 10 KHz T_C's during measurement.

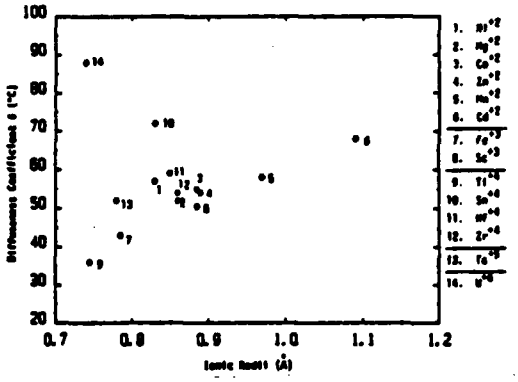

Figure 3. Diffuseness coefficient δ as a function of ionic radius for 14 compositions in Table 1.

appears to be only a slight increase in the magnitude of δ with increasing ionic radius.

The single data points for the cations with +5 and +6 valency are insufficient to show any trends. However, upon consideration of ionic size alone, no general trend was observed.

The electrostriction Q_{12} coefficients are also reported in Table 1 with a Q_{12} value of $-0.0050\ m^4/C^2$ for pure PMN. In general, the larger the δ coefficient, the smaller the Q_{12}.

REFERENCES

1. V.A. Bokov and I.E. Myl'nikova, Sov. Phys. Solid State 3, 613-623 (1961).
2. Landolt Bornstein, Ferroelectrics and Related Substances, New Series, Vol. 16 (1981).
3. B.A. Malkov and Y.N. Venevtsev, Inorg. Mat. 13, 1189-1192 (1977).
4. L.E. Cross, S.J. Jang, R.E. Newnham, S. Nomura and K. Uchino, Ferroelectrics 23, 187-192 (1980).
5. F. Galasso and J. Pyle, Inorg. Chem. 2, 482-484 (1963).
6. S.L. Swartz, T.R. Shrout, Mat. Res. Bull. 17, 1245-1250 (1982).
7. K. Uchino, S. Nomura, L.E. Cross, S.J. Jang and R.E. Newnham, J. Appl. Phys. 51(2), 1142-1145 (1980).
8. S. Nomura, K. Tonooka, J. Kuwata, L.E. Cross and R.E. Newnham, Proc. Second Meeting Ferroelectric Materials and Their Applications (FMA2), Kyoto, Japan, 133-138 (1979).
9. S. Swartz, T. Shrout, W. Schulze and L.E. Cross, (submitted for publication).
10. O. Muller and R. Roy, The Major Ternary Structural Families, Springer-Verlag, New York (1974).

APPENDIX 7

DIELECTRIC PROPERTIES IN THE $Pb(Fe_{1/2}Nb_{1/2})O_3$-$Pb(Ni_{1/3}Nb_{2/3})O_3$ SOLID SOLUTION SYSTEM

Thomas R. Shrout, Scott L. Swartz and Michael J. Haun
Materials Research Laboratory, The Pennsylvania State University
University Park, PA 16802

Abstract

Compositions in the $(x)(Pb(Fe_{1/2}Nb_{1/2})O_3-(1-x)Pb(Ni_{1/3}Nb_{2/3})O_3$ (PFN-PNN) solid solution system were prepared and their dielectric properties determined. Compositions with $x \geq 0.6$-0.8 were found to densify at sintering temperatures less than 1000°C having peak dielectric constants, $k>15,000$, and a relatively low temperature coefficient of capacitance change.

Additions of small amounts of MnO were found to greatly increase the electrical resistivity and reduce the dielectric losses. Additions of $PbTiO_3$ were found to shift the Curie temperature upward and to increase the dielectric constant.

Introduction

Many of today's multilayer ceramic capacitors employ costly precious metal internal electrodes. In some high capacitance parts, the precious metal can make up to 50 to 60% of the selling price of the capacitor. To reduce the cost of such capacitors, less expensive electrodes such as Ag or high Ag-Pd alloys are desired. Thus there has been an extensive search for dielectric materials which can be fired at temperatures less than 1000°C. Along with low firing capability, such dielectrics should have a high dielectric constant (k>5,000), low dielectric loss, low temperature dependence of capacitance, good insulation resistance, and good life performance.

This communication reports the preliminary results of studies on the sintering and dielectric properties of compositions in the $Pb(Fe_{1/2}Nb_{1/2})O_3$-$Pb(Ni_{1/3}Nb_{2/3})O_3$ and/or $PbTiO_3$ binary and ternary systems for possible capacitance applications. The above system was selected based on the low firing characteristics of $Pb(Fe_{1/2}Nb_{1/2})O_3$ (<900°C) and the relatively high dielectric constants exhibited by all three end members.

Experimental Procedure

It has been reported (1-2) that the ABO_3 structure perovskites $Pb(Fe_{1/2}Nb_{1/2})O_3$ and $Pb(Ni_{1/3}Nb_{2/3})O_3$ (hereafter designated PFN and PNN, respectively) are difficult to fabricate as single phase ceramics due to the appearance of a stable lead-niobate pyrochlore phase on calcination. Swartz and Shrout(3) and Voss et al. (4) reported that by first pre-reacting the B site refractory oxides of such $Pb(B'_{1/2}B''_{1/2})O_3$ and/or $Pb(B'_{1/3}B''_{2/3})O_3$ perovskites to form the appropriate columbite $B'B''_2O_6$, or wolframite $B'B''O_4$, compounds, and then followed by reaction with PbO, the amount of pyrochlore phase is greatly reduced. In this investigation, the pre-reacted compounds or precursors were wolframite, $FeNbO_4$, and columbite, $NiNb_2O_6$.

The precursors were prepared by ball milling the appropriate amounts of reagent grade oxides Fe_2O_3* or NiO* with optical grade Nb_2O_5** in distilled water for 12 hours using zirconia milling media. The resultant slurry was dried and placed in alumina crucibles whereby reaction was carried out at 1000°C for 4 hours.

These products were mixed, as above, with reagent grade PbO*** (yellow) and/or reagent grade $PbTiO_3$—. The powders were then calcined at temperatures from 750 to 800°C for 4 hours. The resultant calcined slug was then sufficiently ground to pass a 60 mesh sieve using a mortar and pestal. Disks 1.59 cm in diameter and 3-4 mm in thickness were pressed in which a 3 wt% polyvinyl alcohol binder had been added. Following binder burnout at 500°C, the disks were fired in closed alumina crucibles at temperatures ranging from 850°C to 1000°C and at various times. No atmospheric source of PbO was required.

Prior to electroding, the sintered disks were analyzed by X-ray diffraction to insure that little or no pyrochlore phase was present.

The sintered disks were then ground parallel with 12 μm Al_2O_3 powder and geometrical densities were calculated. Electrodes of sputtered on gold and air-dry silver were applied.

Dielectric measurements were carried out on an automated system whereby a Delta design model 2300 temperature control box—, and Hewlett Packard Model 4274A LCR meter were controlled by a Hewlett Packard 9825A desktop computer system———. The dielectric constant (k) and loss (tan δ) were measured

*Fischer Scientific Co., Pittsburgh, PA.
**Teledyne Wah Chang, Albany, OR.
***Hammond Co., Pittsburgh, PA.
—Alfa Products, Inc., Danvers, MA.
—Delta Design, San Diego, CA.
——— Hewlett Packard Co., 1-50-1 Yoyogi, Tokyo, Japan 151.

pseudocontinuously at 0.1, 1, 10 and 100 KHz upon cooling from 150°C at a rate of 3°C/min.

The electrical resistivity (ρ) was determined by applying 100 volts across selected samples at room temperature using a Hewlett Packard Model 4140B pico-ampmeter, with the current value being recorded after 1 minute.

Results and Discussion

Analysis of x-ray diffraction patterns confirmed that ceramics in the binary system PFN-PNN were single phase since a complete solid solution was formed for the whole range of binary compositions. The crystal system of the various compositions was presumed to be cubic or pseudocubic as reported elsewhere (5,6).

Figure 1 shows the dielectric behavior as a function of temperature for various compositions across the PFN-PNN binary system. It is evident from Figure 1 that PNN exhibits a frequency dispersion of the dielectric maximum, i.e., the maximum dielectric constant increases and shifts to lower temperatures as the frequency is decreased. Such compositions are referred to as 'relaxor' ferroelectrics. This relaxor characteristic has been attributed to a statistical inhomogeneity in the distribution of the B-site cations creating microregions of varying transition temperatures (T_c). It is interesting to note that compositions near to PFN showed virtually no relaxational character, but with increasing amounts of PNN, the dielectric maximums decreased and showed more and more frequency dispersion. Figure 2 shows the relationship between T_c's (at various frequencies) as a function of the composition. The relationship was found not to be linear as one would expect for a complete solid solution system. It can be clearly seen that if the T_c for samples having compositions near PNN were measured at very low frequencies, e.g., 0.1 Hz, then a linear relationship would probably exist.

This nonlinear behavior of T_c's was also reported by Yonezawa et al. (5) for the $Pb(Fe_{2/3}W_{1/3})O_3$-$Pb(Fe_{1/2}Nb_{1/2})O_3$ solid solution system.

Compositions high in PNN were also found to require higher sintering temperatures than those near the PFN side. Compositions having greater than 60% PFN were found to sinter at temperatures lower than 1000°C. Along with low firing capability, these compositions had large dielectric maxima as mentioned above; however, compositions near PFN had progressively higher dielectric losses and lower resistivities.

For the remainder of this investigation, the composition 0.6 PFN-0.4 PNN (x=0.6), having a low firing capability, relatively high k and broad maxima near room temperature and relatively low loss was selected for further optimization.

Firstly, in order to improve the dielectric loss and resistivity, small amounts of MnO were added, as reported elsewhere (6). Since such additions are typically small, e.g., 0.01 wt%, the MnO was added in the form of a water solution containing $MnSO_4xH_2O$* and during the milling process.

The effect of the MnO additions on resistivity for various firing conditions is presented in Figure 3. The resistivity was found to decrease with increasing firing temperature. This is believed to be due to the partial reduction of Fe^{+3} to Fe^{+2} leading to the increased electron hole conductivity commonly associated with Pb compounds (7). For both firing conditions shown in Figure 3, a very large increase in resistivity was found for additions of MnO as low as 0.005 wt% with further improvements being realized with increasing amounts of MnO. Amounts greater than 0.05 wt% were yet to be investigated, but have been reported to degrade the dielectric properties in similar systems (6). Figure 4 shows the effect of MnO additions on the

*Alfa Products, Inc., Danvers, MA.

dielectric loss as a function of temperature. Clearly, it is shown that MnO additions reduce dielectric loss, particularly the low frequency losses which are attributed to conduction processes. The MnO additions were also found to aid in the sintering process, further reducing the firing temperature.

Effects of the firing conditions on the density, T_c, dielectric constant and loss for samples having the composition 0.6 PFN-0.4 PNN with MnO additions are presented in Table 1. Also in Table 1 are the temperature coefficients of the dielectric constant at -30°C, 10°C, and 85°C with reference to the value at 25°C. All the samples reported in Table 1 had resistivities greater than $1x10_{10}$ ohm-cm. As evident from Table 1, the T_c was found to be slightly dependent on the firing temperature, that is, T_c increased with increasing firing temperature. No explanation can be given at this time. The dielectric constant k and density were also found to increase with firing temperature. A similar behavior was observed with sintering time.

Upon SEM microstructural analysis, it was found that the average grain size and uniformity increased with sintering temperature and time. An average grain size of 0.5 to 1.5 microns was observed for samples fired at 900°C or less for short durations ($\lesssim$2 hrs), with the grain size increasing to a maximum of about 4 microns for samples fired at 900°C to 10 hours and/or 1000°C for 5 hr. This behavior was also observed by Yonezawa et al. (5) in the $Pb(Fe_{2/3}W_{1/3})O_3$-$Pb(Fe_{1/2}Nb_{1/2})O_3$ system and by Swartz et al. (10) in $Pb(Mg_{1/3}Nb_{2/3})O_3$. The latter attributing the grain size dependence of k on a grain boundary volume phenomena in which a second phase of low k (pyrochlore, incompletely reacted phases, impurities, etc.) was distributed within the grain boundaries. As the grain size increases, the number of boundaries in series with the grain decreases, and the large dielectric constant of the grains would become less affected by a low dielectric constant grain boundary.

Samples that had increased dielectric constants also had increased temperature coefficients (T.C.'s). The coefficients could also be modified simply by varying the T_c with additions of $PbTiO_3$ (PT). The dielectric properties of 0.6 PFN-0.4 PNN with 0.04 PT samples fired at various times and temperatures are also reported in Table 1. These compositions were also found to densify at low temperatures and had grain size effects similar to that of 0.6 PFN-0.4 PNN. In general the dielectric constants were found to be greater than those without PT, with peak values greater than 20,000 being reported for samples fired as low as 1000°C and as high as 30,000 for samples fired at 1150°C for 1 hour, but exhibited exceedingly large temperature coefficients (not presented in Table 1). Further, the T_c and thus temperature coefficients could also be varied by simply varying the PFN-PNN ratio.

Summary

(1) The $Pb(Fe_{1/2}Nb_{1/2})O_3$-$Pb(Ni_{1/3}Nb_{2/3})O_3$ system appears to form a complete solid solution series. However, the relationship between the Curie temperature and composition was found not to be linear due to the ferroelectric relaxor behavior of compositions near PNN.

(2) Compositions high in PFN ($\geq$0.6 mole %) were found to have low firing capability (<1000°C), high dielectric constants, and relatively low temperature coefficients of capacitance change, but high dielectric losses and low electrical resistivities. The dielectric losses (tan δ) and resistivity could however, be greatly improved by small additions of MnO, which also was found to be a sintering aid.

(3) A grain size dependence on the dielectric constant was found, being a function of sintering time and temperature.

(4) With $PbTiO_3$ additions the transition temperature (T_c) was shifted higher with improved dielectric constants being achieved. The full extent of $PbTiO_3$-PFN-PNN solid solutions has yet to be investigated.

Future work will involve ways to increase the grain size, and to try other additives to further reduce dielectric loss and increase electrical resistivity. Also, the compatibility of Ag and Ag-Pd electrodes for possible multilayer capacitor capability should be investigated.

References

1. M. Lejeune and J.P. Boilot, 'Formation Mechanism and Ceramic Process of the Ferroelectric Perovskites: $Pb(Mg_{1/3}Nb_{2/3})O_3$ and $Pb(Fe_{1/2}Nb_{1/2})O_3$,' Cer. Int. 8 (3), 99-104 (1982).
2. L. Veitch, 'Dielectric Properties of $Pb(Ni_{1/3}Nb_{2/3})O_3$,' B.S. Thesis, The Pennsylvania State University (1982).
3. S.L. Swartz and T.R. Shrout, 'Fabrication of Perovskite Lead Magnesium Niobate,' Mat. Res. Bull. 17, 1245-1250 (1982).
4. D.J. Voss, S.L. Swartz, and T.R. Shrout, 'The Effects of Various B-site Modifications on the Dielectric and Electrostrictive Properties of Lead Magnesium Niobate Ceramics,' to be published in Ferroelectrics.
5. M. Yonezawa, K. Utsumi, and T. Ohno, 'Properties of $Pb(Fe_{2/3}W_{1/3})O_3$-$Pb(Fe_{1/2}Nb_{1/2})O_3$ Ceramics,' Proc. 1st Meeting on Ferroelectric Materials and Their Applications, Kyoto, Japan, 297-301 (1977).
6. K. Furukawa, 'High Dielectric Constant Type Ceramic Compositions Consisting Essentially of $Pb(Fe_{1/2}Nb_{1/2})O_3$-$Pb(Mg_{1/3}Nb_{2/3})O_3$,' U.S. Patent 4,216,102 (1980).
7. B. Jaffe, W.R. Cook, Jr., and H. Jaffe, Piezoelectric Ceramics, pp. 237-242. New York: Academic Press (1971).
8. Landolt-Bornstein, Ferroelectrics and Related Substances, New Series Vol. 16, Springer-Verlag Berlin, Heidelberg, New York (1981).
9. V.A. Bokov and I.E. Myl'nikova, Sov. Phys. Solid State 3, 613-623 (1961).
10. S. Swartz, T. Shrout, W. Schulze and L.E. Cross, J. Amer. Ceram. Soc. (submitted for publication).

Figure Captions

Figure 1. Temperature dependence of the dielectric constant (100 KHz) in the $(x)Pb(Fe_{1/2}Nb_{1/2})O_3-(1-x)Pb(Ni_{1/3}Nb_{2/3})O_3$ binary system.

Figure 2. The Curie temperature as a function of frequency in the $(x)Pb(Fe_{1/2}Nb_{1/2})O_3)-(1-x)Pb(Ni_{1/3}Nb_{2/3})O_3$ binary system.

Figure 3. The effect of MnO additions on the electrical resistivity for the composition 0.6 PFN-0.4 PNN.

Figure 4. The effect of MnO additions (wt%) on the dielectric loss (tan δ) as a function of temperature for the composition 0.6 PFN-0.4 PNN. The samples were fired at 900°C for 2 hours.

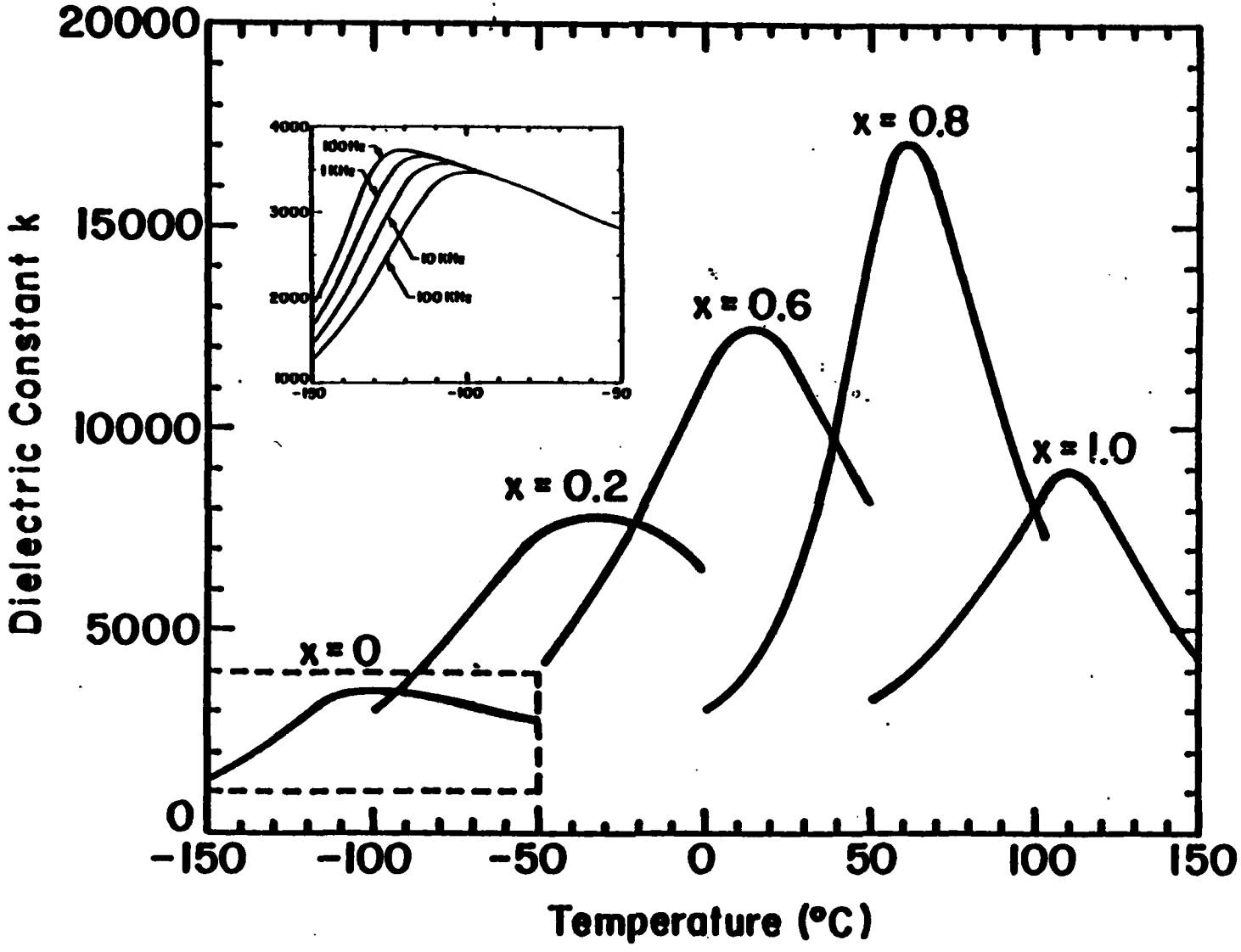
20000
15000
10000
5000
0
Dielectric Constant k
-150
-100
-50
0
50
100
150
Temperature (°C)
x = 0
x = 0.2
x = 0.6
x = 0.8
x = 1.0
4000
3000
2000
1000
100Hz
1KHz
10KHz
100KHz
-150
-100
-50

FIG. 1

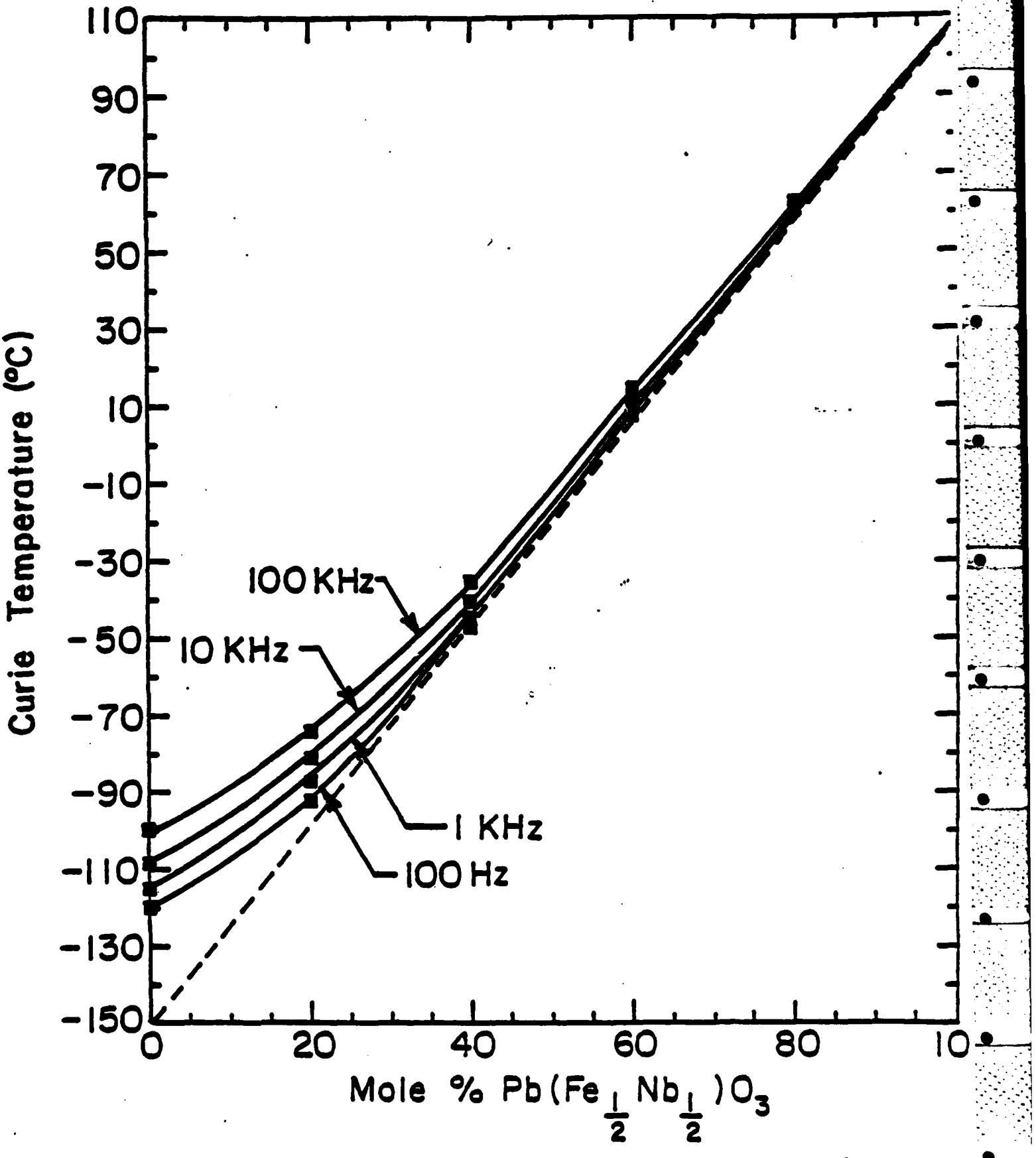
110
90
70
50
30
10
-10
-30
-50
-70
-90
-110
-130
-150
Curie Temperature (°C)
100 KHz
10 KHz
1 KHz
100 Hz
0
20
40
60
80
10
Mole % Pb(Fe 1/2 Nb 1/2)O3

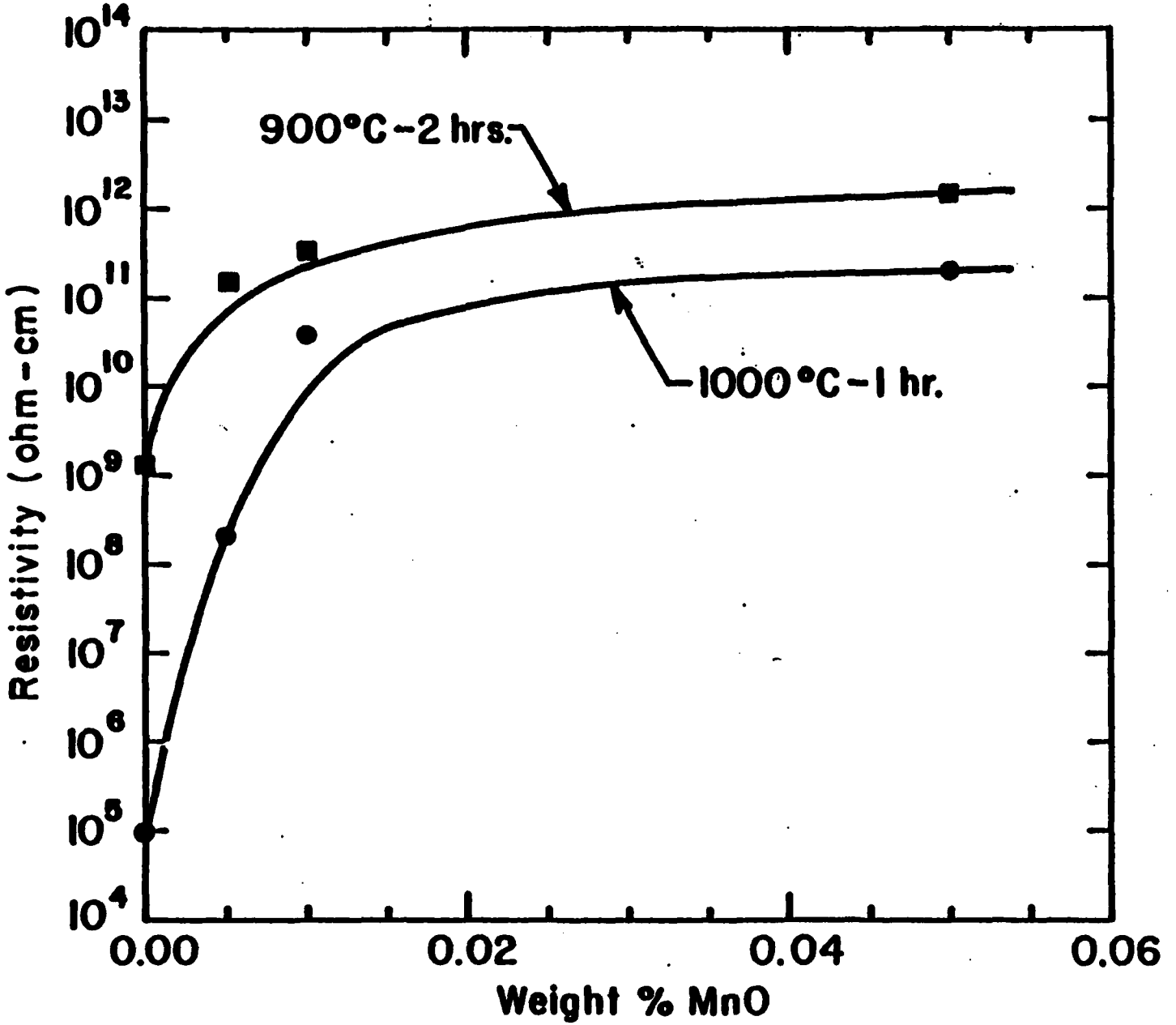
Resistivity (ohm-cm)
10^{14}
10^{13}
10^{12}
10^{11}
10^{10}
10^{9}
10^{8}
10^{7}
10^{6}
10^{5}
10^{4}
900°C-2 hrs.
1000°C-1 hr.
0.00
0.02
0.04
0.06
Weight % MnO

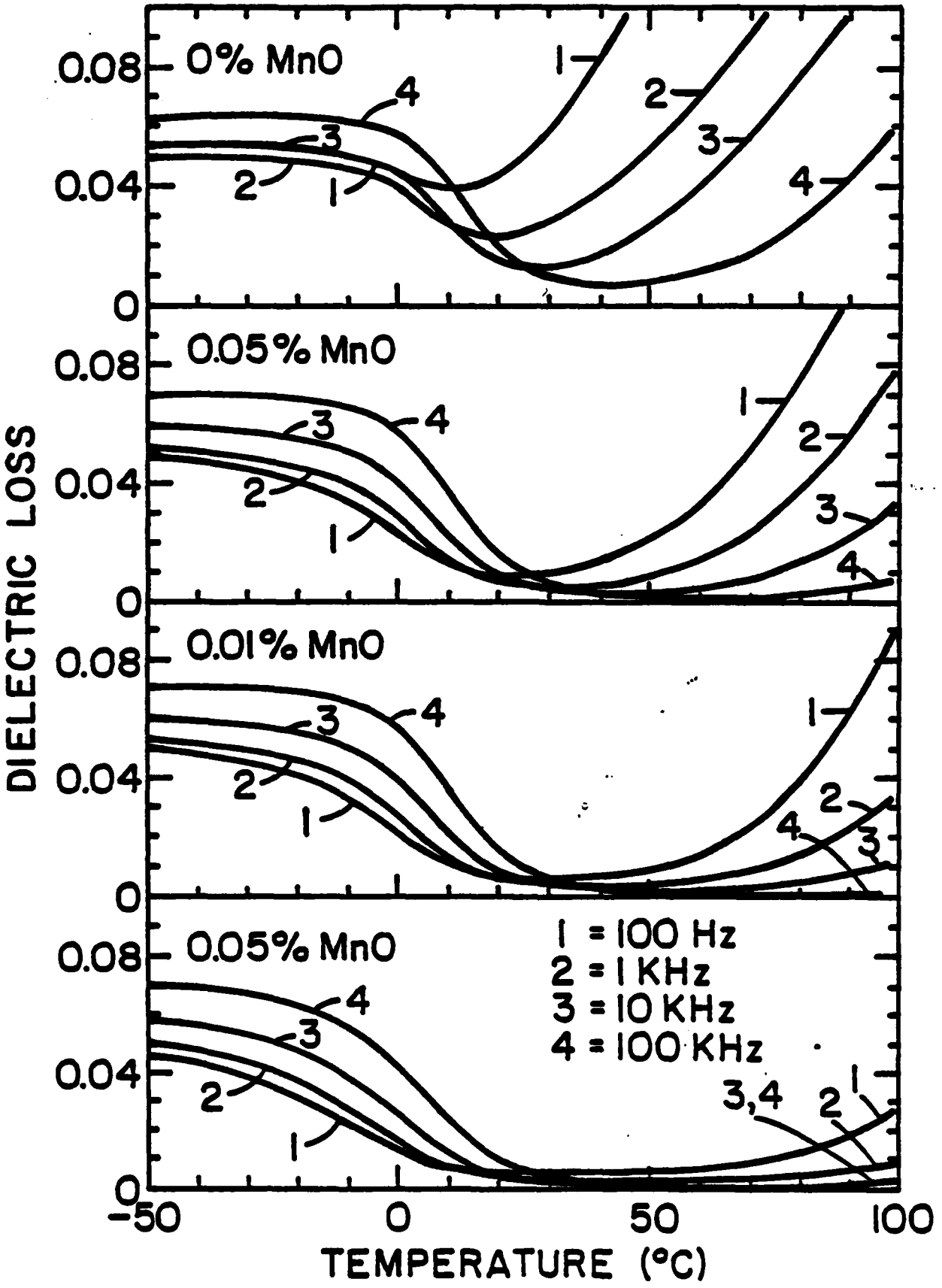
0% MnO
0.05% MnO
0.01% MnO
0.05% MnO
0.08
0.04
0
DIELECTRIC LOSS
1 = 100 Hz
2 = 1 KHz
3 = 10 KHz
4 = 100 KHz
3,4
−50
0
50
100
TEMPERATURE (°C)

Table 1. Dielectric Properties as a Function of Firing Condition.

Composition	Firing Condition	% Theoretical Density**	T_c (°C)	Dielectric Constant (1 KHz) K (25°C)	tan δ (%)	K (max)	Temperature Coefficient, T.C.* (%) -30°C	10°C	85°C
0.6 PFN-0.4 PtN	850°C- 4 hr.	87	8	6,100	0.5	6,800	-29	+6	-54
0.01 wt% MnO	850°C-10 hr.	93	6	8,700	0.3	9,600	-21	+9	-59
	900°C- 2 hr.	92	8	8,500	0.5	9,400	-28	+11	-56
	900°C-10 hr.	94	8	14,600	0.3	16,500	-38	+12	-64
	1000°C- 1 hr.	91	11	8,100	0.8	8,600	-30	+6	-53
	1000°C- 5 hr.	95	12	15,600	0.7	17,000	-40	+9	-64
0.576 PFN-0.384 PNN-	900°C- 2 hr.	92	22	10,800	0.8	11,000	-49	-7	-53
0.04 PT	900°C-10 hr.	94	22	13,300	0.8	13,600	-51	-5	-58
0.01 wt% MnO	1000°C- 1 hr.	91	23	12,500	1.0	12,700	-53	-8	-40
	1000°C- 4 hr.	95	26	13,300	1.0	13,500			
	1000°C-10 hr.	96	29	20,200	1.0	20,500	-68	-43	-65

*Temperature coefficients calculated using the following equation: $T.C.\ (\%) = [K_{(T)}-K_{(25°)}]/[K_{(25°)}]\times 100$.
**Theoretical densities of PFN, PNN and PT are 8.46 g/cc, 8.55 g/cc and 7.96 g/cc, respectively.

APPENDIX 8

A PHENOMENOLOGICAL GIBBS FUNCTION FOR $BaTiO_3$ GIVING CORRECT E FIELD DEPENDENCE OF ALL FERROELECTRIC PHASE CHANGES

A.J. BELL
Department of Ceramics, University of Leeds, Leeds LS2 9JT England

L.E. CROSS
Materials Research Laboratory, The Pennsylvania State University, University Park, PA 16802

Abstract The elastic Gibbs function for $BaTiO_3$ introduced by Buessem, Goswami and Cross[1] has been modified by including the last symmetry permitted sixth order term $HP_1^2P_2^2P_3^2$ with a coefficient $H = 4.91 \times 10^9$ Vm^9 C^{-5}. The function predicts the correct high electric field behavior of the low temperature ferroelectric:ferroelectric phase changes in the single crystal and suggests an interesting change of sign of the pyroelectric effect at high field levels in the induced tetragonal ferroelectric phase.

INTRODUCTION

The shift of Curie temperature (T_c) under high electric bias fields in simple proper ferroelectric crystals has been used quite frequently to characterize the nature of the phase change at T_c and to obtain information as to the sign, magnitude and temperature dependence of higher order terms in the Landau: Ginzburg:Devonshire phenomenological theory.

In single crystal barium titanate ($BaTiO_3$), Merz[2] observed a shift of Curie temperature

$$\left(\frac{\partial T_c}{\partial E}\right)_X = 1.43 \times 10^{-3} \text{ K/kV cm}^{-1}$$

where the subscript X indicates measurements at constant and in this case zero mechanical stress. This datum, and the corresponding double hysteresis loops observed at high AC fields in $BaTiO_3$ are in good agreement with appropriate Devonshire theory.

It should be possible to use the electric field dependence of the lower temperature ferroelectric:ferroelectric phase changes in $BaTiO_3$ to refine a more complete three dimensional elasto-dielectric free energy, however, in the past, data on macro-crystals has not extended to sufficiently large E field levels[3] to provide a useful range to verify the free energy function.

Very recently Fesenko and Popov[4] have used an optical method to determine the E field dependence of the low temperature phase

changes in $BaTiO_3$ crystals of less than 20 μm thickness. This excellent data extends to fields up to 650 kV cm^{-1} well above the previously recognized breakdown strength of bulk $BaTiO_3$.

It is the purpose of this paper to demonstrate that a slightly extended version of the elastic Gibbs function used previously by Buessem, Goswami and Cross (BGC)[1] gives good agreement between predicted and measured phase changes.

The basic reason for wishing to extend and refine the BGC function is to be able to calculate the internal stress effects in fine grain barium titanate[5,6] over the full range of ferroelectric stability to compare with recent measurements of grain size effects in pure $BaTiO_3$ ceramics[7]. This latter work is now in progress.

PHENOMENOLOGICAL THEORY

The Gibbs free energy of a perovskite type simple proper ferroelectric under zero mechanical stress ($X_{ij} = 0$) with a non zero electric field E_3 applied parallel to the x_3 axis may be expressed in terms of the polarization components P_i along the axial directions x_i (i = 1,2,3) of the cubic paraelectric phase in the form

$$\begin{aligned} G_1 - G_{10} = \Delta G_1 &= A(P_1^2+P_2^2P_3^2) + B(P_1^4+P_2^4+P_3^4) \\ &+ C(P_1^6+P_2^6+P_3^6) + D(P_1^2P_2^2+P_2^2P_3^2+P_3^2P_1^2) \\ &+ G(P_1^4P_2^2+P_1^2P_2^4+P_2^4P_3^2+P_2^2P_3^4+P_3^4P_1^1+P_1^2P_3^4) \\ &+ H(P_1^2P_2^2P_3^2) - E_3P_3 \end{aligned}$$

where G_{10} is the energy of the unpolarized undeformed crystal. It is the energy difference ΔG_1 which is of interest and which determines the ferroelectric stability.

The expression is complete in all symmetry permitted terms up to the 6th order, but E is considered only in the special direction of one of the cube axes. In Devonshire[8], only A is temperature dependent, but in BGC both B and C are also linear functions of temperature.

The polarization conditions (in the absence of an external field) which occur at different temperatures in the four stable ferroelectric phases in $BaTiO_3$ are:

$P_1 = P_2 = P_3 = 0$	paraelectric cubic m3m	(a)
$P_1^2 \neq 0$ $P_2 = P_3 = 0$	tetragonal 4mm	(b)
$P_1^2 = P_2^2 \neq 0$ $P_3 = 0$	orthorhombic mm2	(c)
$P_1^2 = P_2^2 = P_3^2 \neq 0$	rhombohedral 3m	(d)

If the coefficients A to H and their temperature dependencies are known, the function can be used to derive all the dielectric

properties of the single domain states and their ranges of stability in each phase.

For each phase region, the first derivative of ΔG_1

$$\left(\frac{\partial \Delta G_1}{\partial P_i}\right)_X = E_i$$

gives the field components E_i (taken to be zero). These equations can then be solved to yield the spontaneous values of P_i.

The second derivatives of ΔG_1

$$\left(\frac{\partial^2 \Delta G_1}{\partial P_i \partial P_j}\right)_X = \left(\frac{\partial E_i}{\partial P_j}\right) = \chi_{ij}$$

yield the dielectric stiffness χ_{ij} again at constant and zero stress.

To determine the modifications to the P_i, χ_{ij} and phase stability due to high non zero values of E_3, it is simple to substitute back into the original equations new values of P_3 of the form

$$P_3 = P_s + \Delta P_3$$

From the first derivative equations, values of E_3 corresponding to suitably chosen ΔP_3 increments can be found. These new values of P_3 and E_3 may then be substituted back into the equations for ΔG_1 and for the χ_{ij} to determine the modifications to the phase stability and to the dielectric stiffness in each phase.

RESULTS AND DISCUSSION

The values of the free energy coefficients A through G were taken from BGC. The coefficient H was chosen so as to give a rhombohedral:orthorhombic transition temperature of 202 K (-71°C) in close agreement with recent crystallographic determination. The full set of values is given in Table 1.

The spontaneous electric polarizations were determined by solution of the first derivative equations with $E_3 = 0$. Values of ΔP were then chosen and substituted back to derive the non zero E_3. The ΔP range was chosen to given E_3 values from 0 to 600 kV cm^{-1} in the temperature range from 50 to 300 K. New P_3 values were then used to calculate the ΔG_1 and χ_{ij} values and to determine the cross over between stable solutions.

Figure 1 shows the T vs E_3 phase diagram for $BaTiO_3$ derived in this manner. The measured transition values taken from the experiments of Fesenko and Popov are superposed for comparison. The trends of the two sets of values are in very good agreement. If we were to chose a modified value of H in the thermodynamic parameters the zero field rhombohedral:orthorhombic transition could be raised and the experimental and model values would agree precisely. Since, however, we wish later to model stress effects in high purity $BaTiO_3$ ceramics, it appeared advisable to fix on

values which reproduce the best data for low field dielectric and crystallographic determination of the zero field transition. In the orthorhombic:tetragonal phase change, the model predicts a smoothly non linear behavior without the abrupt termination of a shift observed above 450 kV cm^{-1} in the experimental data. We are tempted to believe that this arrest observed may be an artifact of the very difficult experimental conditions and that the model predicts a more rational response.

The predictions from the model function for dielectric permittivities ε_{33} and ε_{11}, and for the polarization P_3 are given in Figure 2. The value of ε_{11} in the induced tetragonal phase can be seen to increase markedly with increasing field. Presumably the energy minimum for the 001 direction of P decreases faster than that for the 011 minimum, thus the saddle point between them is lowered and the slope at the minimum will be decreased. That ε_{33} is lowered as the minimum in the 100 direction is lowered is not at all surprising.

A result which is much more unexpected is the change of slope in the P vs T curve. Clearly this means that for fields above 200 kV cm^{-1}, the pyroelectric coefficient ($p(T) = dP_s/dT$) will be of opposite sign to that with $E_3 = 0$.

This trend suggests that due to the shape of ε_3 vs T, ΔP increases faster with temperature than P_s decays. Experiments are now being planned to test this prediction.

CONCLUSION

The introduction of a suitable sixth order term

$$HP_1^2P_2^2P_3^2$$

into the modified Devonshire function of BGC permits a phenomenological description of the electric field dependence of the low temperature ferroelectric:ferroelectric phase changes in $BaTiO_3$ and a T vs E phase diagram in good agreement with experiment.

An unexpected prediction from the model is that the pyroelectric coefficient p(T) should change sign at high fields in the induced tetragonal phase.

REFERENCES

1. W.R. Buessem, L.E. Cross and A.K. Goswami, J. Amer. Ceram. Soc. 49(1):33 (1966).
2. W.J. Merz, Phys. Rev. 91, 513 (1953).
3. E.J. Huibregtse and D.R. Young, Phys. Rev. 103, 1705 (1956).
4. O.E. Fesenko and V.S. Popov, Ferroelectrics 37, 729 (1981).
5. W.R. Buessem, L.E. Cross and A.K. Goswami, J. Amer. Ceram. Soc. 49(1):36 (1966).
6. R.C. Pohanka, S.W. Freiman and B.A. Bender, J. Amer. Ceram. Soc. 61, 72 (1978).
7. K. Kinoshita and A. Yamaja, J. Appl. Phys. 47, 371 (1976).
8. A.F. Devonshire, Adv. in Phys. 3, 85 (1954).

Table 1. Values of constants used in the modified Devonshire Free Energy Function.

$A = 3.34 \times 10^5 (T - 108)$	$Vm C^{-1}$
$B = 4.69 \times 10^6 (T - 120) - 2.02 \times 10^8$	$Vm^5 C^{-3}$
$C = -5.52 \times 10^7 (T - 120) + 2.76 \times 10^9$	$Vm^9 C^{-5}$
$D = 3.23 \times 10^8$	$Vm^5 C^{-3}$
$G = 4.47 \times 10^9$	$Vm^9 C^{-5}$
$H = 4.91 \times 10^9$	$Vm^9 C^{-5}$

T is expressed in ^{o}C.

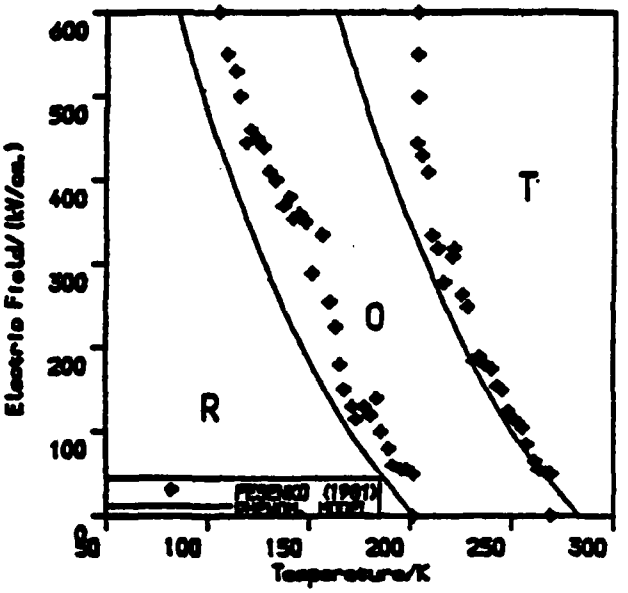

Fig 1. The temperature-electric field phase diagram for $BaTiO_3$ showing the calculated and measured boundaries of the rhombohedral (R), orthorhombic (O) and tetragonal (T) phases.

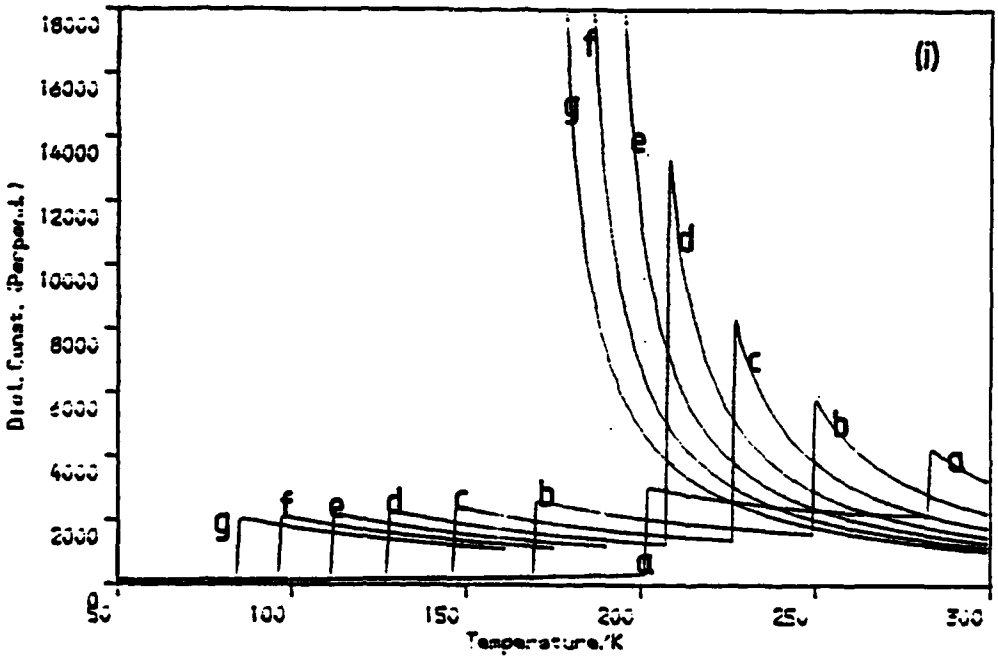
(i)
Temperature/K

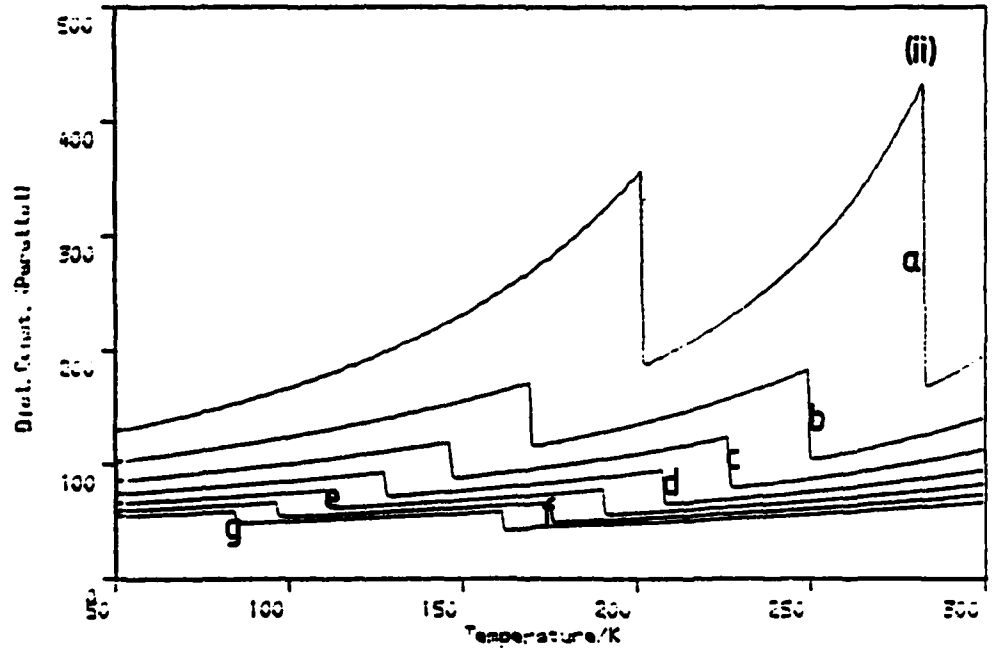
(ii)
Temperature/K

AD-A146 183 CENTER FOR DIELECTRIC STUDIES(U) PENNSYLVANIA STATE 2/2
UNIV UNIVERSITY PARK MATERIALS RESEARCH LAB
L E CROSS ET AL. MAY 84 N00014-82-K-0339

UNCLASSIFIED F/G 20/12 NL

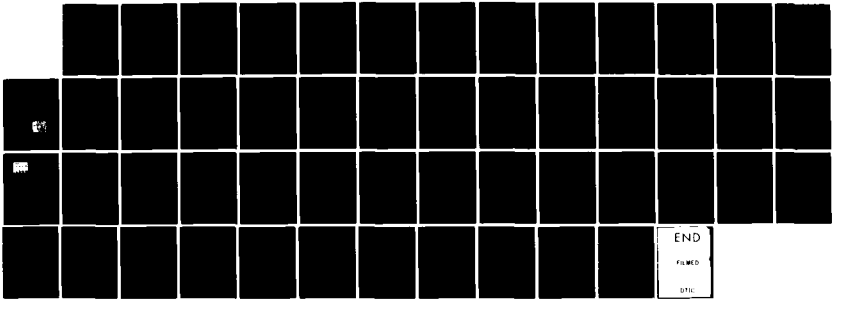

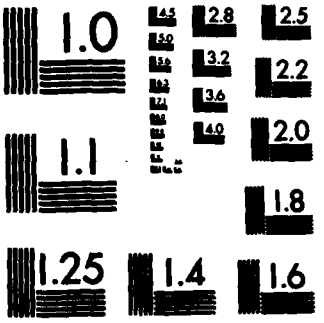

MICROCOPY RESOLUTION TEST CHART

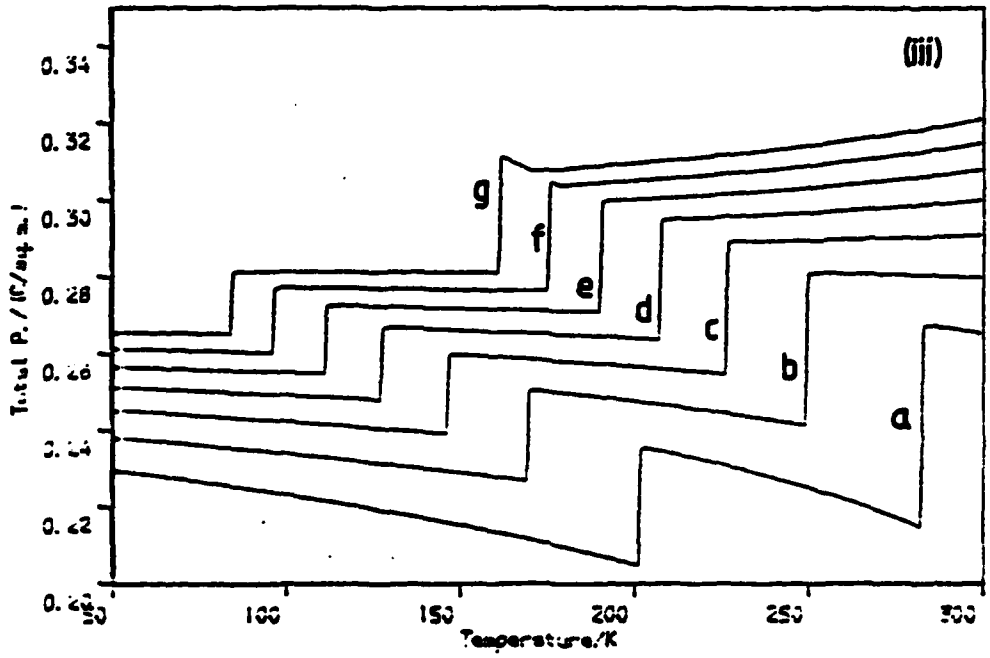

Figure 2

Calculated values of the dielectric permittivities

(i) ε_{11}

(ii) ε_{33}

(iii) the electric polarization $P_3 = P_s + \Delta P$

a - 0 kV cm^{-1}

b - 100 kV cm^{-1}

c - 200 kV cm^{-1}

d - 300 kV cm^{-1}

e - 400 kV cm^{-1}

f - 500 kV cm^{-1}

g - 600 kV cm^{-1}

APPENDIX 9

THE EFFECT OF GRAIN SIZE ON THE PERMITTIVITY OF $BaTiO_3$

A.J. BELL and A.J. MOULSON
Department of Ceramics, University of Leeds, Leeds, U.K.

and L.E. CROSS
Materials Research Laboratory, The Pennsylvania State University, University Park, Pa. 16802, U.S.A.

Abstract Grain size effects in polycrystalline $BaTiO_3$ are reviewed in terms of the "internal stress model". By considering polarization dependent terms in the Devonshire free energy expression, the dielectric constant may be calculated for the whole ferroelectric temperature region, under various stress systems. Encouraging comparisons with measured values may be made.

INTRODUCTION

Coarse grained $BaTiO_3$ (grain size > 50 μm) generally has a room temperature dielectric constant of approximately 2000, which may be considered to be some average of the single crystal constants, ε_{ij}[1]. Several authors have noted that the dielectric constant increases markedly with decreasing grain size, attaining a value of 6000 for bodies of grain sizes of 1 μm or less[2-4]. Kinoshita and Yamaji[5] have shown (Figure 1) that above the ferroelectric transition temperature, T_c, grain size has no observable effect on the dielectric constant, although T_c decreases by approximately 2°C in fine grained material. In addition the tetragonal/orthorhombic and the orthorhombic/rhombohedral transition temperatures are 10°C higher.

Based on observations (recently corroborated with Dy-doped material[6]) that fine grained $BaTiO_3$ contains very few 90° twins, compared to coarse grained material, Buessem et al.[7] have proposed an internal stress model to explain the dielectric measurements. The stresses caused by the deformation from cubic symmetry on passing through the ferroelectric transition are relieved by

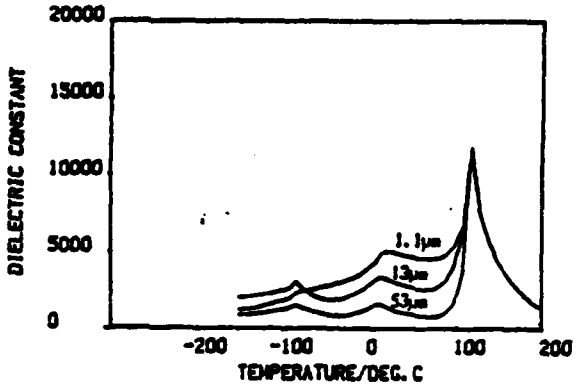

Fig.1 Effect of grain size on the dielectric constant of $BaTiO_3$. (Ref. 5)

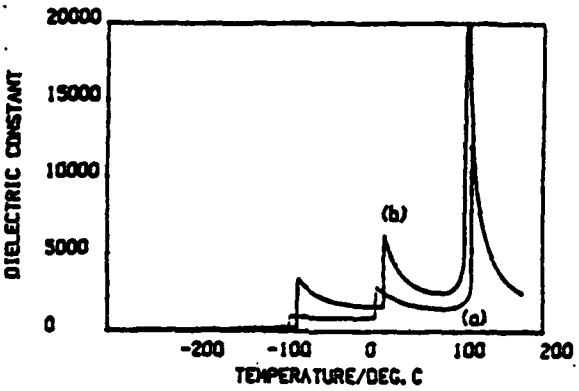

Fig.2 Results of the phenomenological model, (a) K=0, (b) K≠0 (see text).

Figure 2 shows $\bar{\varepsilon}$ for zero stress and for a phase dependent K, ($K_{(tetr.)} = 0.052$, $K_{(ortho)} = 0.082$, $K_{(rhomb)} = 0.205$). $\bar{\varepsilon}_{RT} \simeq 6000$, and the lower phase transition temperatures have increased by 10°C, similar to 1 μm grain size material[5]. However the large decrease in the ferroelectric transition temperature and the accompanying increase in $\bar{\varepsilon}_{max}$ predicted by the model but not seen experimentally, may infer that the stress system does not develop until several degrees below the transition, so that the onset of tetragonality is not suppressed; or that there is a polarisation-free stress system acting above T_c, increasing the energy of the cubic phase.

REFERENCES

1. M. Marutake, Jnl. Phys. Soc. Japan, 11, 807 (1956).
2. A.A. Anan'eva, B.V. Strizkov and M.A. Ugrymova, Bull. Acad. Sci. USSR Phys. Soc. 24, 1935 (1960).
3. H. Kniekamp and W. Heywang, Z. Angew Phys., 6, 385 (1854).
4. G.H. Jonker and W. Noorlander, in "Science of Ceramics" 1, 255 Academic Press, New York (1962).
5. K. Kinoshita and A. Yamaji, J. Appl. Phys., 47, 371 (1976).
6. A. Yamaji, Y. Enomoto, K. Kinoshita and T. Murakami, J. Am. Ceram. Soc., 60, 97 (1977).
7. W.R. Buessem, L.E. Cross and A.K. Goswami, J. Am. Ceram. Soc., 49, 33 (1966).

Consider the model of a single crystallite of $BaTiO_3$ constrained by an isotropic medium having the bulk properties of polycrystalline $BaTiO_3$. It is evident from the electrostriction relations,

$$X_{ij} = -c_{ijkl}x_{kl} - g_{ijkl}P_kP_l; \quad x_{ij} = -s_{ijkl}X_{kl} + Q_{ijkl}P_kP_l \qquad ..(4)$$

that the stresses on the constrained grain are a function of polarisation, where x_{ij} are the strains, c_{ijkl}, s_{ijkl} the elastic coefficients, and g_{ijkl}, Q_{ijkl} are the electrostriction coefficients (full notation). It may be possible to evaluate x_{ij} and hence X_{ij} by a full analysis of the model; however it is convenient to assume a proportional relationship

$$X_{ij} = -K g_{ijkl} P_k P_l \qquad ...(5)$$

where K is some constant. Substitution into equation 1 reduces the stress dependent terms to two terms in P_i^4 and $P_i^2P_j^2$ $(i \neq j)$. Thus the dielectric constant may be evaluated with K as the only independent variable.

RESULTS AND DISCUSSION

For convenient comparison with measured values, the polycrystalline dielectric constant, $\bar{\varepsilon}$, is taken as the arithmetic mean of the single crystal values;

$$\bar{\varepsilon} = (\varepsilon_{11} + \varepsilon_{22} + \varepsilon_{33})/3.$$

The free energy coefficients were taken from the literature[7], except the coefficient H, for which the value of 6.65×10^9 Vm^7C^{-5} was derived.

For K independent of phase the value of $\bar{\varepsilon}$ in the tetragonal and orthorhombic phases increases with increasing K. However, the tetragonal/orthorhombic and orthorhombic/rhombohedral phase transition temperatures also increase dramatically. $\bar{\varepsilon} = 6000$ is not attained at room temperature as the material becomes orthorhombic.

twinning in coarse grained material; however, if twinning does not occur each grain must be subjected to a stress system opposing that deformation. By including stress terms in the free energy expression for $BaTiO_3$, and using Devonshire thermodynamic methods, it was shown that a compressive stress along the c axis and equal tensile stresses along the a axes of 80 MPa produces a dielectric constant of 6000 at 25°C.

THEORY

The free energy of a ferroelectric in terms of stress, X_{ij}, and polarisation, P_i, may be given as:

$$G_1 - G_{10} = -\tfrac{1}{2}s_{11}(X_{11}^2+X_{22}^2+X_{33}^2)-s_{12}(X_{11}X_{22}+X_{22}X_{33}+X_{33}X_{11})-\tfrac{1}{2}s_{12}(X_{12}^2+X_{23}^2+X_{31}^2)+(Q_{11}X_{11}+Q_{12}(X_{22}+X_{33}))P_1^2+(Q_{11}X_{22}+Q_{12}(X_{11}+X_{33}))P_2^2+(Q_{11}X_{33}+Q_{12}(X_{11}+X_{22}))P_3^2+Q_{44}(X_{12}P_1P_2+X_{23}P_2P_3+X_{31}P_3P_1)+A(P_1^2+P_2^2+P_3^2)+B(P_1^4+P_2^4+P_3^4)+C(P_1^6+P_2^6+P_3^6)+D(P_1^2P_2^2+P_2^2P_3^2+P_3^2P_1^2)+G(P_1^4P_2^2+P_1^2P_2^4+P_2^4P_3^2+P_2^2P_3^4+P_3^4P_1^2+P_3^2P_1^4)+H\,P_1^2P_2^2P_3^2 \quad ...(1)$$

where s_{ij} are the elastic compliances, Q_{ij} are the electrostriction strain coefficients (reduced notation) and A,B,C,D,G,H are the free energy coefficients. The expressions for electric field and dielectric susceptibility are

$$E = \frac{\partial G_1}{\partial P_i} = 0 \qquad ...(2)$$

and

$$\chi_{ij} = \frac{\partial^2 G_1}{\partial P_i \partial P_j} = \frac{1}{\varepsilon_o \varepsilon_{ij}} \qquad ...(3)$$

By applying the symmetry conditions for polarisation in each phase, with each component, P_i, equal to zero or $\pm P_s$, equation 2 may be solved for P_s^2 at any temperature. Substitution of each solution which satisfies $\chi_{ij} > 0$ into equation 1 allows the minimum free energy state and the dielectric constants to be evaluated.

APPENDIX 10

The Pennsylvania State University

The Graduate School

The Modeling and Effects of Macrodefects in Monolithic Capacitors

A Thesis in

Solid State Science

by

David Craig Hardy

Submitted in Partial Fulfillment
of the Requirements
for the degree of

Master of Science

December 1983

ABSTRACT

Porosity in monolithic capacitors is known to be an electronically deleterious microstructural defect. However, the relation between the size, number, shape and location of these defects and the consequent dielectric properties of the monolith are not well understood from either a quantitative or fundamental perspective. To enable detailed investigations of these effects, a process has been developed for the fabrication of barium titanate multilayer ceramic capacitors with defects of known geometries, position and number.

The fabrication process involves placing either planar or spherical polymeric pore precursors at either intraceramic or at the ceramic-internal electrode interface during the lamination process. Details of the process, including binder, solvents, drying and firing conditions are presented. Scanning electron microscopy (SEM) is used to demonstrate the reliability of the process. Electrical property measurements indicate that increased degradation of the dielectric material occurs with increasing porosity and average pore size. Macrodefect location within the multilayer ceramic capacitor structure also determines the magnitude of the deleterious effect on the dielectric properties. When macrodefects are introduced solely on the same plane as the internal electrode the dielectric constant is greater than what is observed in a multilayer

ceramic capacitor with the same concentration of macrodefects which have been introduced only within the dielectric layers. These property effects are presented to permit a more detailed understanding into property effects due to processing related porosity.

APPENDIX 11

PREPARATION AND ELECTRICAL PROPERTIES OF THIN FILMS OF ANTIMONY SULPHUR IODIDE (SbSI)

P.K. GHOSH, A.S. BHALLA AND L.E. CROSS
Materials Research Laboratory, The Pennsylvania State University, University Park, PA 16802

Abstract The c-axis oriented thin films of SbSI are prepared by the recrystallization of the amorphous SbSI films. The recrystallized films show the pyroelectric properties and have a dielectric capacitance between 0.2-0.5 $\mu F/cm^2$ and the tan δ <1%.

INTRODUCTION

SbSI is one of the most important members of the large family of $A^{V}B^{VI}C^{VII}$ ferroelectric compounds[1-4]. In the ferroelectric phase below 22°C it belongs to an orthorhombic point group mm2, and has very large structural and growth anisotropy along the polar c-axis. In the case of single crystal, the growth rate along c-axis is about 50 times faster than that of along a or b-axis. SbSI has very interesting piezoelectric and pyroelectric properties. It also has a large anisotropy in the dielectric properties and the dielectric constant along the c-axis is $\sim 6 \times 10^4$ at the T_c. These interesting properties along with its growth anisotropic characteristics make SbSI an attractive candidate material for the study of c-axis oriented thin films. In the past, some attempts have been made to produce thin films of SbSI by the chemical vapor deposition and thermal evaporation of SbSI with the purpose of studying the switching behavior and the memory effect in the semiconductor-dielectric thin film junction[5-8].

In this paper we report the preparation of single crystal thin films of SbSI and their pyroelectric and dielectric properties.

EXPERIMENTAL AND RESULTS

Thin films of SbSI were prepared by the vacuum thermal evaporation of SbSI single crystals. SbSI single crystals used as the source material were gorwn by the Bridgman method. Evaporation was conducted through resistance heating of a tungsten filament in a vacuum of about 10^{-5} torr. Evaporation was done well below the decomposition temperature of SbSI in order to deposit a stoichiometric film.

SbSI films were deposited on a variety of substrates, such as, (a) Plain glass slides, (b) Au-coated glass slides, (c) SnO_2(F) coated glass slides, (d) Silicon wafers.

In most of the experiments, the substrate was kept at room temperature. During the evaporation process, the substrate temperature increased to about 80°C depending on the evaporation conditions (e.g. source temperature, source to substrate distance, etc.).

Films thus prepared were continuous, free of cracks and pinholes. X-ray diffraction studies showed a poor crystalline nature of the SbSI films.

Successive annealing was done to enhance the single crystal growth in the films. The samples were annealed in closed containers in a globar furnace. Several trial runs showed that the temperature range between 100°C - 200°C was suitable for the recrystalliza- of the films.

Two different atmospheric conditions were used for annealing, (a) Atmospheric conditions in a closed container, and (b) Iodine atmosphere.

The crystallized films were predominantly oriented along the polar c-axis as indicated by the x-ray diffraction studies (Figure 1).

The relative intensity of 002 x-ray diffraction peak was taken as the measure of the degree of preferred orientation of the c-axis in the SbSI film. The optical microscopic studies revealed no flaws such as cracks and pinholes in these films. SEM studies showed the microstructure of the films (Figure 2). There were needle-shaped crystallites of ∿0.2 μ diameter size throughout the film and those were oriented along the length of the needles From the typical growth behavior of SbSI crystals, x-rays and SEM studies, it was concluded that

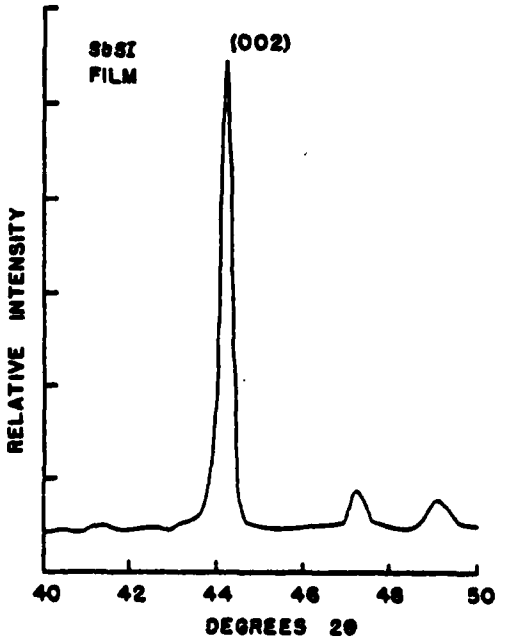

X-RAY DIFFRACTION PATTERN

Figure 1.

FIBERS ≤ 0.2 μm CROSS-SECTION

SEM IMAGES

Figure 2.

these needles were oriented parallel to the c-axis of SbSI. The different parts of the film did show some relative misorientation in the film. X-ray diffraction studies also indicated the presence of Sb_2S_3 in some of the films. Such films gave a strong (002) diffraction peak ($2\theta \sim 47°$) corresponding to the c-axis oriented Sb_2S_3 needles.

The recrystallization behavior of SbSI films deposited on the various substrates used in the studies was almost identical. The films deposited on the gold or SnO_2 coated substrates were used for the electrical measurements. Au electrodes were deposited on such films.

SbSI films were poled with a field of 1 KV/cm while cooling down through the phase transition. Pyroelectric response of these films was measured by the Byre Roundy technique. Figure 3 shows the temperature dependence of the pyroelectric current of recrystallized SbSI single crystal film on SnO_2 substrate. Pyroelectric current peaks up near 10°C, corresponding to the T_c in the SbSI film. The pyroelectric peak near the transition is rather broad. It could be due to the compositional variation in the SbSI crystallites. Although the effect of stresses in the film could also produce such shift in the T_c towards lower temperature. The dielectric measurements were made on several SbSI films deposited on Au or SnO_2 coated glass slides. A computer controlled HP 4274A multifrequency LCR meter was used for the measurements. The measurements were made at frequencies 1 KHz to 100 KHz with the 50 V/cm a.c. field. Figure 4 shows the temperature dependence of the dielectric constant. K vs T peak showed the $T_c \sim 10°C$, lower than the T_c observed in the single crystal of SbSI. Also there was a substantial broadening in the dielectric maxima. The dielectric loss in the film was $\sim$1% over the measured temperature range (Figure 5).

The broadening in the dielectric peak could be due to the lower packing density of the crystallites and the inhomogeneity in the chemical composition of the SbSI needles. It is also known that the shear stresses in SbSI single crystal shifts the T_c towards lower temperatures and since the heteroepitaxy films generally have the built in stresses, it does support the lower T_c observed in SbSI films. The low packing density, shear stresses and the crystalline misorientations may also be responsible for the lower dielectric constant of the SbSI film. Since the SbSI films are prepared on the amorphous substrates, the orientation and composition of the interfacial layer may also be

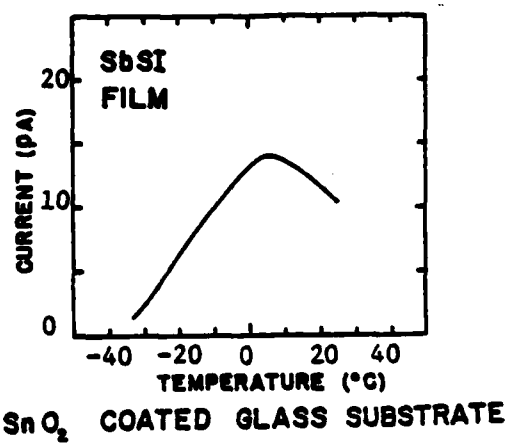

Figure 3.

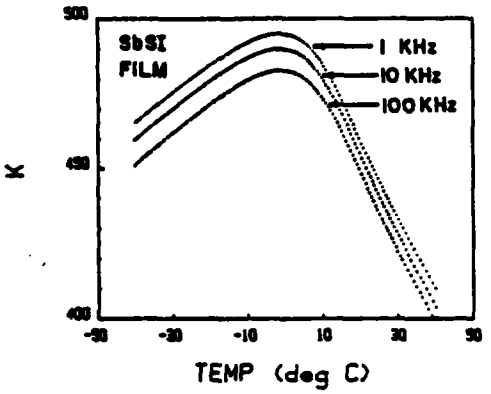

SnO_2 COATED GLASS

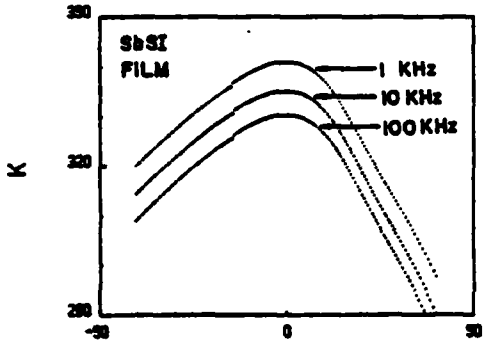

Au COATED GLASS

Figure 4.

playing an important role in influencing the dielectric properties of the films. There is a possibility of series connections of the SbSI needles in the film especially near the interface area. Detailed studies are in progress to investigate the effects of the interface layer on the dielectric constants of SbSI films. The capacitance of the SbSI films prepared was in the range ~0.2-0.5 $\mu F/cm^2$ and with a typical loss factor of 1%.

SUMMARY

1) SbSI films with a high degree of preferred orientation parallel to the c-axis are prepared on the amorphous and polycrystalline substrates by the thermal evaporation of SbSI and subsequently annealing the films between 100-200°C.

2) The recrystallized films could be poled and showed a pyroelectric response.

3) The well oriented films have the capacitance between 0.2-0.5 $\mu F/cm^2$ and the typical dielectric loss tangent <1%.

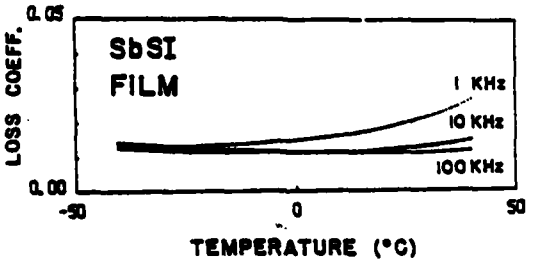

Au COATED GLASS SUBSTRATE

Figure 5.

REFERENCES

1. R. Nitsche and W.J. Merz, J. Phys. Chem. Solids 13, 154 (1960).

2. E. Fatuzzo, G. Harbeke, W.J. Merz, R. Nitsche, H. Roetschi and W. Ruppel, Phys. Rev. 127, 2036 (1962).

3. E. Dönges, Z. Anorg. Allgem. Chem. 263, 112 (1950).

4. T. Mori and H. Tamura, J. Phys. Soc. Jpn. 19, 1247 (1964).

5. Y. Hamakawa, M. Yoshida and K. Yamanaka, J. NonCryst. Solids 10, 868 (1972).

6. Y. Hamakawa and M. Yoshida, Jpn. J. Appl. Phys. 40, 80 (1970).

7. A.A. Agasiev, A.Kh. Zeinally and V.G. Silverstrov, Sov. Phys. Crystallogr. 18, 814 (1974).

8. R.N. Sheftal, A.G. Zhdan, K.V. Nikitin and E.S. Artobolevskaya, Sov. Phys. Sol. State 11, 2158 (1970).

APPENDIX 12

QUASI-STATIC CAPACITANCE AND ULTRA SLOW RELAXATION OF LINEAR AND NON-LINEAR DIELECTRICS

ZHANG LIANGYIXG, YAO XI, H.A. MCKINSTRY AND L.E. CROSS
Materials Research Laboratory, The Pennsylvania State University, University Park, PA 16802

Abstract The time dependence of quasi-static capacitance of linear and non-linear materials can be measured using a constant voltage ramp method. The measured data are consistent with a theoretical equation derived from a superposition theorem. The capacitance of fast polarization, saturated polarization and the time constant of the relaxation process can be obtained using a non-linear least squares method. Ultra slow relaxation for linear dielectrics and ferroelectrics are reported.

INTRODUCTION

Recently, the interest in quasi-static capacitance and ultra slow relaxation of linear and non-linear dielectrics has been increasing rapidly. Some important structural information including the macro-inhomogeneity of dielectrics and the ultra slow relaxation of ferroelectrics domain can be obtained from the time dependence of the quasi-static capacitance. In this new technique, the capacitance-time dependence of the sample is measured directly. The time constant of ultra slow relaxation of the material can be calculated and the ultra low frequency dielectric response of the material can be obtained using a simple Debye relaxation formula. This technique as well as the ultra low frequency dielectric measurement[1] and the DC transient measurement[2] are very useful techniques in studying the ultra slow dielectric response of the materials.

MEASURING SYSTEM AND RESULTS

Figure 1 is a schematic diagram of the measuring system. The sample under study is connected to a ramp voltage source through a high sensitivity picoammeter. Samples are held at the starting voltage for a time period long enough to saturate the dielectric at that voltage. Then the applied voltage starts to ramp down or up toward the finishing voltage. The voltage ramp is divided into many steps. The total current passing through the sample is taken at each step voltage. An integrating-averaging technique has been used to minimize the noise in the measurement of low currents. The measurement is under computer control.

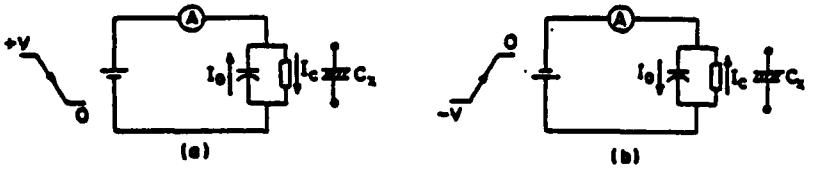

Figure 1. Schematic diagram of the constant voltage ramp method (a) voltage ramp from +V, (b) voltage ramp from -V.

At any instant of time, the current measured in a high sensitivity picoammeter I_T is the sum of a conduction current $I_C = V/R_i$ and a dielectric displacement current $I_D = dQ/dt$. The R_i is an instantaneous resistance at the voltage level V and the Q is the charge stored in the capacitor. The quasi-static capacitance C is defined as

$$C = I_D/(dV/dt) \tag{1}$$

In order to get an accurate measurement of the quasi-static capacitance, the separation of the displacement current from the conduction current is very important for the samples with low resistance measured at low voltage ramp rates. From the schematic diagram of the measurement circuits, Figure 1, it is clearly shown that the displacement current and the conduction current are always opposite in sign in spite of the voltage ramping up from a negative starting voltage or ramping down from a positive starting voltage. Therefore, a compensation point is expected, at which the displacement current and the conduction current are equal in magnitude but opposite in sign. Hence, the pseudo capacitance measured as the total current divided by the ramp rate at the compensation point is zero. Figure 2(a) is an example taken for a mica capacitor. The capacitance with respect to the applied voltage measured as the total current divided by the ramp rate is, in this case, clearly dominated by conduction. The compensation point moved toward higher voltage when the ramp rate was increased. For samples with high resistance or measured at a high ramp rate, the influence of the conduction current can be small. Figure 2(b) is an example taken for a polystyrene capacitor. The capacitance measured at different voltages does not change.

To separate the displacement current from the total measured current, the zero-crossing method has been used. Clearly, at any time when V = 0, the conduction component of current I_C must go to zero. Thus, by starting the voltage ramp from a fixed positive or negative voltage and by ramping at a fixed rate to zero voltage and measuring the instantaneous current exactly at zero crossing, the conduction may be eliminated, and the pure displacement current and quasi-static capacitance explored. Therefore only the

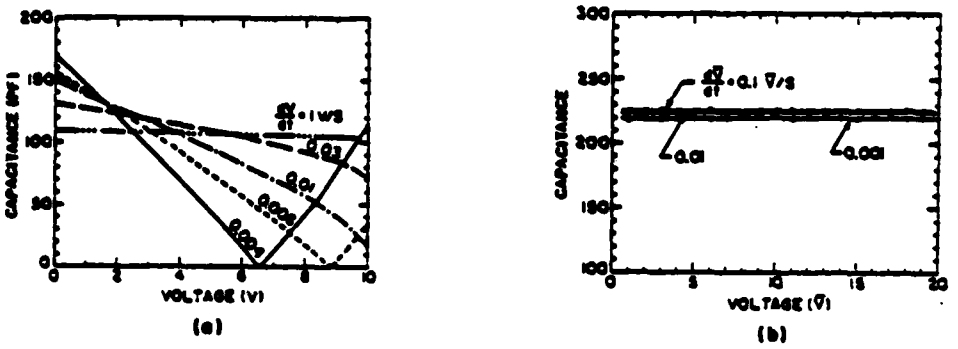

Figure 2. Relationship between the capacitance and applied voltage of the mica capacitor (a) and polystyrene capacitor (b).

capacitances on the zero voltage axis in Figure 2(a) and 2(b) are real quasi-static capacitances of the samples.

The time dependence of quasi-static capacitance can be obtained from the superposition theorem. For a linear dielectric, the electrical displacement D(t) is given by

$$D(t) = \varepsilon_\infty E(t) + \int_0^t E(t') \cdot f(t-t') \cdot dt' \qquad (2)$$

where E(t) is a function of the time that the electric field is applied, f(t) is a decay function of the dielectric polarization. For a constant voltage ramp and simple relaxation process, the time dependence of quasi-static capacitance can be obtained from equation (2)

$$C(t) = C_\infty + (C_s - C_\infty)\left(1 - \frac{\tau}{t} + \frac{\tau}{t} e^{-\frac{t}{\tau}}\right) \qquad (3)$$

where C_∞ is the capacitance of the fast polarization, C_s is the capacitance response to the total polarization, τ is the time constant of the relaxation process.

There are two alternative ways to measure the time dependence of the quasi-static capacitance - fixing the starting voltage and measuring the quasi-static capacitance at different ramp rates, or fixing the ramp rate and measuring the capacitance from different starting voltages. For a linear dielectric, the results of the two methods are identical. Figures 3(a) and 3(b) show the time dependence of the quasi-static capacitance of a mica capacitor and a ceramic capacitor. The slow relaxations explored in these capacitors are probably of the Maxwell-Wagner type originating from the inhomogeneity of the dielectric and the build-up of space charge within the dielectric. In contrast, the capacitance of polystyrene has almost no change up to 2000 sec.

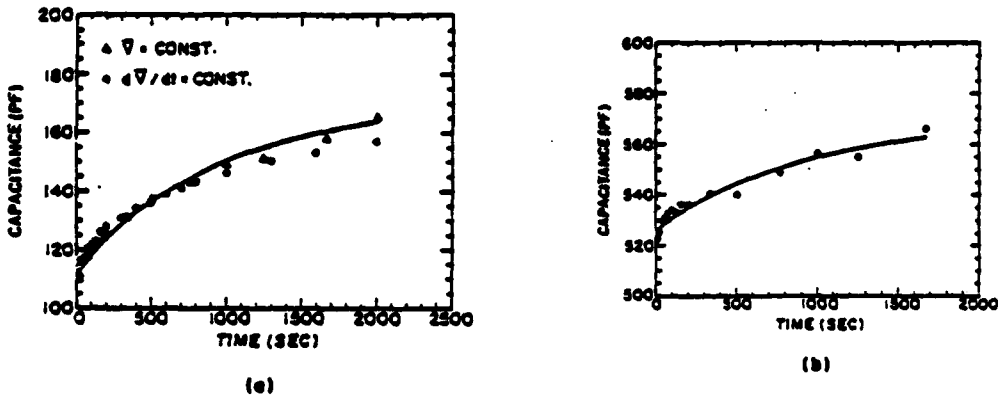

Figure 3. Time dependence of the quasi-static capacitance of a mica capacitor (a) and ceramic capacitor (b). The solid line is the calculated curve from equation (3) fitted by computer.

The experimental data of the time dependence of the quasi-static capacitance can be fitted to the theoretical (3) using the least squares method. The important parameters of dielectric, relaxation - C_∞, C_s, τ - can be obtained. The calculated fitting curves based on equation (3) are also plotted on the figures.

QUASI-STATIC CAPACITANCE OF FERROELECTRICS

It is expected that the time dependence of the quasi-static capacitance can be related to the very slow processes of the domain contribution to the total polarization. Measurements on some ferroelectrics have also been made. Figure 4(a) is the time dependence of the capacitance of a commercial soft PZT sample. For the poled sample, no significant change of capacitance can be observed, while for the depoled sample, a clear time dependence of capacitance is evident. The difference of the capacitance C_s-C_∞ obtained from the computer fitting calculation is a measure of the very slow domain contributions to the total polarization. The time constant τ can be related to the response of the domain adjustment process to the electric field applied. For the lead lanthanum zirconate titanate (PLZT) with composition 8:65:35, where 8 is the substitution ratio of lanthanum to lead, and 65:35 is the atom ratio of zirconium to titanium, the same result as the soft PZT is shown in Figure 4(b).

SUMMARY

The time dependence of the quasi-static capacitance can be measured using the constant voltage ramp method. The measured data of the time dependence of capacitances are consistent with the theoretical equation derived from the superposition theorem. The capacitance of fast polarization C_∞, the capacitance of the saturated capacitance C_s, and the time constant can be obtained

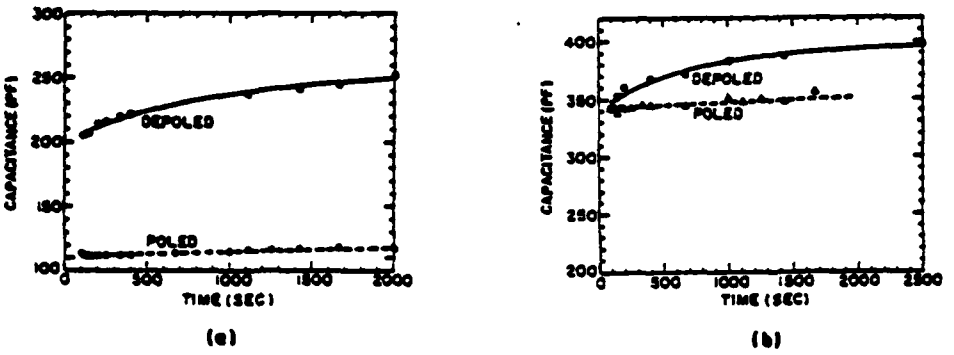

Figure 4. Time dependence of quasi-static capacitance of a soft PZT (a) and PLZT (b). For the depoled sample of soft PZT, C_∞ = 200.6 PF, C_s = 266.8 PF, τ = 524.1 S. For the depoled sample of PLZT, C_∞ = 338.7 PF, C_s = 405.6 PF, τ = 356.0 S.

using a non-linear least square method to fit the experimental data to the theoretical equation. The method can be used to study the ultra slow relaxation in dielectrics and the very slow domain process of ferroelectrics.

REFERENCES

1. H. Nakamura, Y. Husimi and A. Wada, J. Appl. Phys. 52, 3053 (1981).

2. S. Takeishi and S. Mashimo, Rev. Sci. Instrum. 53 (8), 1155 (1982).

APPENDIX 13

PYROELECTRIC PROPERTIES OF THE MODIFIED TRIGLYCINE SULPHATE (TGS) SINGLE CRYSTALS

A.S. BHALLA, C.S. FANG, L.E. CROSS AND YAO XI
Materials Research Laboratory, The Pennsylvania State University, University Park, PA 16802

Abstract—Several doping substitutions (Li^+, Mn^{+2}, D^+, P^{+5}, As^{+5}) in the TGS structure have been studied and the pyroelectric and dielectric properties measured. In the case of TGS single crystals modified by partial substitution of $(PO_4)^{-3}$ and $(AsO_4)^{-3}$ groups for the $(SO_4)^{-2}$, higher pyroelectric coefficients and an enhancement of the pyroelectric material figure of merit (p/K) > 2 x TGS have been observed.

Single crystal triglycine sulfate (TGS) is a widely used material in the pyroelectric devices. It shows the most attractive pyroelectric properties and has the basic pyroelectric material figure of merit $p/K \simeq 1.1 \times 10^{-5}$ C/m^2K (p is the pyroelectric coefficient and K is the dielectric constant of the crystal). Single crystals of modified compositions of TGS such as DTGS, TGFB, DTGFB, TGSe and solid solutions among these various family members have shown even more promising pyroelectric properties[1-7] (e.g., the figure of merit for DTGFB $\simeq$ 1.5xTGS).

Recently we have tried various ionic (Li^+, Mn^{+2}, D^+) and radical group (PO_4^{-3}, AsO_4^{-3}) substitutions in the TGS structure[8-9]. Doped single crystals of TGS are grown from the saturated solutions of TGS modified with specific concentrations of the respective dopants (Fig. 1). In this paper, we report the results of pyroelectric measurements Li^+ and Mn^{+2} doped and phosphate and arsenate substituted TGS single crystals.

Single crystals of TG(SP) and TG(SAs) were grown by slow cooling of the saturated solutions[7] with compositions

$$3(NH_2CH_2COOH)\cdot(1-x)H_2SO_4\cdot xH_3PO_4$$
and $$3(NH_2CH_2COOH)\cdot(1-x)H_2SO_4\cdot xH_3AsO_4$$

(+ a few % alanine) respectively. (010) plates of 0.5 mm thick were prepared and coated on both sides with gold electrodes. Pyroelectric and dielectric properties in the temperature range between -30°C to 70°C were measured by using the computer controlled set-up. The pyroelectric coefficients were measured by the Byer-Roundy Technique[10].

Figures 2 and 3 show the results of the pyroelectric and dielectric measurements on the ATG(SP) and ATG(SAs) single crystals. The computed values of the spontaneous polarization (Ps) and the figure of merit (p/K) at various temperatures are also shown in

Figures 2 and 3. The p, Ps and p/K values are larger by a factor of 2 than those of pure TGS.

Pyroelectric properties of some important single crystal materials of the TGS family along with ATG(SP), ATG(SAs), LTGS and MTGS (Li^+ and Mn^{+2} doped TGS respectively) are listed in Table 1. Clearly the $(PO_4)^{-3}$ and $(AsO_4)^{-3}$ substituted TGS crystals have the best pyroelectric properties at the most desirable operating temperature (~25°C).

The Curie constant ~$4x10^3$/°C of ATG(SP) and ATG(SAs) was calculated from the 1/K vs T plots in the paraelectric region to derive the Curie-Weiss law. The ratio of the slopes of the curves 1/K vs T (fig. 4) in the ferroelectric and paraelectric regions was typically between 2-3 indicating the dominantly second order transition.

It is rather interesting to note that at room temperature the spontaneous polarization in the case of ATG(SP) and ATG(SAs) has increased by a factor of almost two compared to that of TGS but there is essentially no change in the dielectric constant, transition temperature or the crystal structure. According to the thermodynamical model of Devonshire, the ferroelectric behavior of TGS can be described by the free energy expression

$$F(T) = F_0(T) + \beta(T-T_0)P^2 + \gamma/4\, P^4 + \delta/6\, P^6 + \text{higher order terms} \quad (1)$$

where β, γ, δ are related to the dielectric stiffness and higher order stiffness coefficients. Considering the temperature dependence of the coefficients β, γ, δ, the following thermodynamic relation can be derived

$$p/(K-1) = P_s/C + [(d\gamma/dT)P_s^3 + (d\delta/dT)P_s^5 + \text{higher order terms}] \quad (2)$$

For the case if β, γ and δ are independent of temperature, the expression simplifies to

$$p/(K-1) = P_s/C \quad (3)$$

and is independent of the number of higher order terms considered in equation (1).

By including the eight order terms in equation (1), Zerem and Halperin[12] showed a good agreement between the calculated and experimental values of P_s in TGS in the temperature range from T_c to 100K. By considering the isothermal dielectric susceptibility[13], Seymour et al. found a much closer agreement between the p/K and P_s/C up to 20°C below T_c.

It appears that the large increase in the P_s of ATG(SP) and ATG(SAs) must be contributed by the large temperature dependence of β, γ, δ and higher order terms in equation (1). This is also evident from the p/K vs T plots for ATG(SP) and ATG(SAs) (Figs. 2 and 3). The p/K vs T curve deviates to a great extent from the P_s vs T behavior suggesting that contributions from higher order terms

occur. The puzzling change of P_s and of p/K could then be due to either the change in the magnitude of β, γ, δ or their large temperature dependence in these modified TGS structure.

The powder x-ray diffraction studies of the modified TGS compositions indicate no major structural change due to $(PO_4)^{-3}$ and $(AsO_4)^{-3}$ substitution but the further verification is needed in this matter.

Thus the present studies suggest that ATG(SAs) and ATG(SP) are most useful pyroelectric materials and are quite inexpensive to produce. Various solid solutions of ATG(SAs)-ATG(SP) and the effect of deuterium substitution for hydrogen in these crystals are under investigation.

REFERENCES

1. P.J. Lock, Appl. Phys. Lett. 19, 390 (1970).
2. G.M. Loiacono, W.N. Osborne, M. Delfino and G. Kostecky, J. Cryst. Growth 46, 105 (1979).
3. P. Felix, P. Gamot, P. Lacheau and V. Raverdy, Ferroelectrics 17, 543 (1978).
4. E.T. Keve, K.L. Bye, P.W. Whipps and A.D. Annis, Ferroelectrics 3, 39 (1971).
5. K.L. Bye, P.W. Whipps, E.T. Keve and M.R. Josey, Ferroelectrics 7, 179 (1974).
6. G.M. Loiacono, A. Shaulov, D. Dorman, J. Jacco and G. Kostecky, J. Cryst. Growth 60, 29 (1982).
7. B. Brezina, M. Safrankova and J. Kvapil, Phys. Stat. Solidi 15, 451 (1976).
8. C.S. Fang, Y. Xi, A.S. Bhalla and L.E. Cross, Ferroelectrics (accepted).
9. C.S. Fang, Y. Xi, A.S. Bhalla and L.E. Cross, Mat. Res. Bull. 18, 1095 (1983).
10. R.L. Byer and C.B. Roundy, Ferroelectrics 3, 333 (1972).
11. S.T. Lai and J.D. Zook, Ferroelectrics 7, 171 (1974).
12. J.Z. Zerem and A. Halperin, Ferroelectrics 7, 205 (1974).
13. R.J. Seymour, J.P. Dougherty and A. Shaulov, Ferroelectrics 29, 163 (1980).

Table 1. Pyroelectric Properties of the TGS Family (Optimum Temp.).

Material	K	p $\mu C/m^2K$	P_s $\mu C/cm^2$	T_c (°C)	$x10^{-5}$ p/K C/m^2K
TGS	30	330	3.0	49	1.1
DTGS	19	270		62	1.4
TGFB	14-16	210-240		73	1.5
DTGFB	11-14	190-240	4.3	75	1.7
LTGS	40	400	3.7	49	1.0
MTGS	40	560	4.6	49	1.2
ATGSP (25°C)	30-32	650	5.0	51	2.0
ATGSAs (25°)	32	700	6.0	51	2.1-2.3

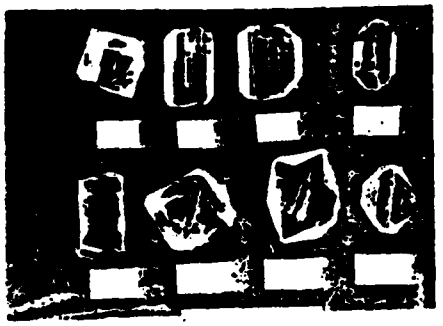

Fig. 1. Modified TGS single crystals.

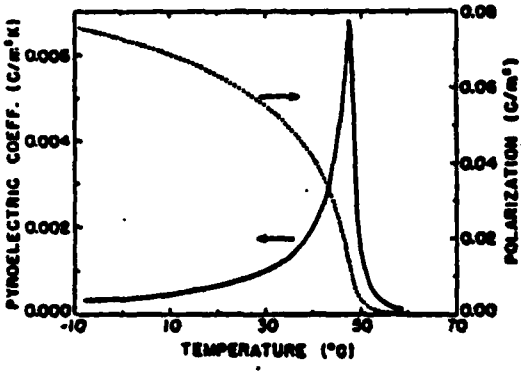

(a)

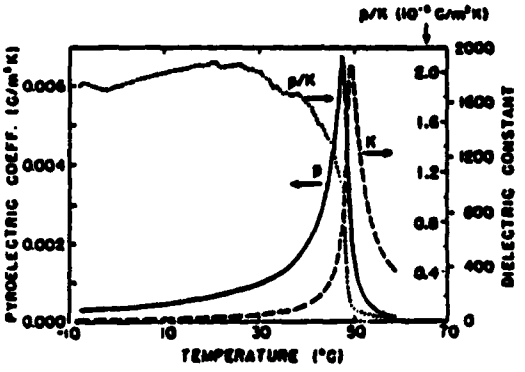

(b)

Fig. 2. ATG(SAs): Temperature dependence of polarization, p, K and p/K.

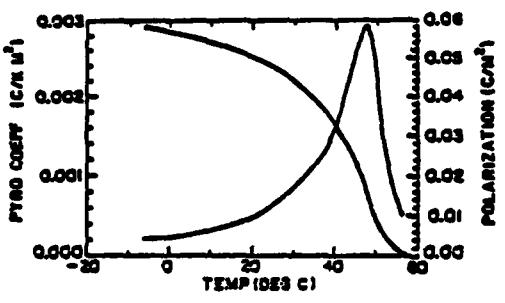

(a)

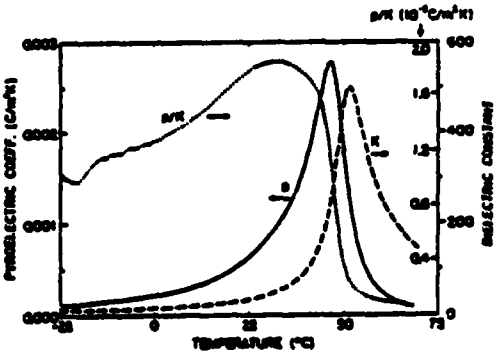

(b)

Fig. 3. ATG(SP): Temperature dependence of polarization, p, K, and p/K.

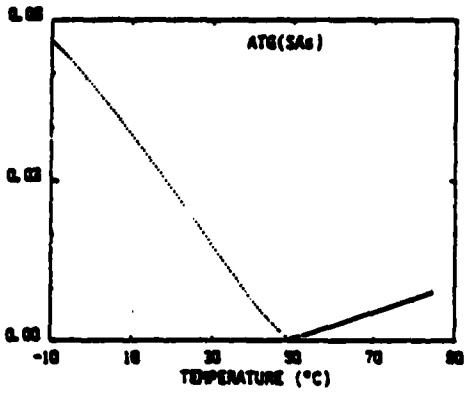

Fig. 4. ATGSP: 1/K vs T.

APPENDIX 14

Ferroelectrics, 1983, Vol. 51, pp. 9-13
0015-0193/83/5101-0009$18.50/0

THE GROWTH AND PROPERTIES OF A NEW ALANINE AND PHOSPHATE SUBSTITUTED TRIGLYCINE SULPHATE (ATGSP) CRYSTAL

C.S. FANG*, YAO XI**, A.S. BHALLA AND L.E. CROSS
Materials Research Laboratory, The Pennsylvania State University, University Park, PA 16802

Abstract A modified alanine doped triglycine sulphate (ATGS) crystal has been grown with partial substitution of H_2SO_4 with H_3PO_4. Growth of the ATGSP crystal from a unipolar ATGS seed in the temperature range 30-40°C gives a unipolar bulk crystal with lower permittivity ($\varepsilon_r \sim 30$) and higher pyroelectric coefficient ($6.5 \cdot 10^{-4}$ c/k.m^2) than pure TGS. In the doping range used, the higher pyroelectric coefficient is traced to a significantly larger spontaneous polarization P_s ($\sim$5 μc/cm^2 at room temperature). Tangent δ is below 0.01 over the whole frequency range from 100 Hz to 100 Khz.

INTRODUCTION

Triglycine sulphate is a well known ferroelectric crystal which is widely used in pyroelectric applications. Large crystals of very good optical quality can be grown from water solution and have been extensively studied. In order to modify and improve properties for application a range of 'dopings' have been tried including deuterium substitution (DTGS), alanine substitution (ATGS) and substitution of the sulphate group with fluoberyllate (DTGFB)[1-7]. By some of these substitutions, thermal depoling can be reduced and the Curie temperature raised.

In the following experiments, we have explored the effects of partial substitution of sulphuric acid with phosphoric acid in the growth system, demonstrating that the phosphate ion can be incorporated in the structure to form $(NH_2CH_2COOH)_3(H_2SO_4)_{(1-x)}(H_3PO_4)_x$ abbreviated ATGSP.

Comparing ionic radii S^{+6}(0.26Å), Se^{+6}(0.43Å), Be^{+2}(0.41Å) and P^{+5}(0.31Å), it is perhaps not surprising that low levels of H_3PO_4 can be incorporated without structural change. More surprising is the rather major effect of such low level substitution upon the bulk polarization and pyroelectric coefficients.

*Permanent Address: Shandong University, Jinan, China.
**Permanent Address: Xian Jiaotong University, Xian, China.

EXPERIMENT

Single Crystal Growth

Triglycine sulphate is usually formed by the chemical reaction

$$3NH_2CH_2COOH + H_2SO_4 \rightarrow (NH_2CH_2COOH)_3H_2SO_4$$

In the case of phosphoric acid substitution, the reaction is

$$3\ NH_2CH_2COOH + (1-x)H_2SO_4 + xH_3PO_4$$
$$\rightarrow (NH_2CH_2COOH)_3(1-x)H_2SO_4xH_3PO_4$$

For the alanine substitution a small amount of the levo alanine is substituted for glycine to prepare the ATGSP composition. The saturated point of solution is controlled at 42°C and the pH value is in range of 2.3-2.5.

A seed crystal of single domain ATGS is used to initiate growth which proceeds by slow cooling in the temperature range from 42-35°C. Cooling rate and growth conditions are quite similar to those used in pure TGS[1,2].

At high H_3PO_4/H_2SO_4 ration, the growth slows markedly, but for ration up to unity large optically clear crystals are readily obtained. Reproducibility is excellent and a typical crystal is shown in Figure 1(a). It will be noted that the shape is different from that of normal TGS, the (010) face is very well developed and so cutting normal to the ferroelectric b axis can be economically accomplished, Figure 1(b).

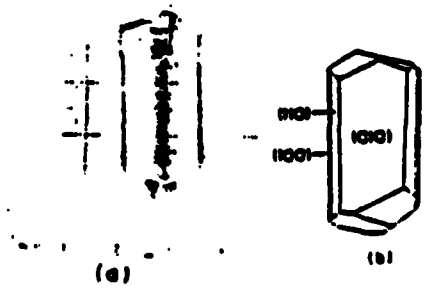

Figure 1. The growth shape of ATGSP crystal.

Atomic absorption analysis shows that the H_3PO_4 incorporated into the crystal is much below the mole fraction in the solution, but even at these low levels there are significant changes in lattice parameters from pure TGS. Table I summarizes data from three concentrations. It can be seen that the lattice parameter c and monoclinic angle β increase with phosphorous content while the b spacing decreases. At high phosphorous concentration, the structure changes from monoclinic (C_2^2) and ferroelectric behavior is lost.

Table 1. The lattice parameters of ATGSP with different P content.

Samples		H_3PO_4 in solution	P in crystal (mol)	Lattice parameters (A^0)
TGS		0	0	a=9.419, b=12.65, c=5.732, β=110.36°*
ATGSP	1	1/5	0.02	a=9.396, b=12.62, c=5.723, β=110.4°
	2	1/2	0.16	a=9.436, b=12.58, c=5.739, β=110.7°
	3	1	0.21	a=9.547, b=12.50, c=5.745, β=113.8°

* from ASTM card.

Dielectric and Pyroelectric Properties

Parallel plate samples of ATGSP for dielectric studies were cut with major surfaces normal to the ferroelectric b axis and polished to thicknesses in the range of 0.5 to 1 mm. Sputtered gold electrodes 5 mm in diameter were applied using special care to protect the sample from overheating during sputtering.

The dielectric properties were measured by a computerized automatic measuring system with Hewlett Packard's new generation of microprocessor based equipment. The temperature dependence of dielectric constant and loss tangent were measured with a multi-frequency LCR meter, HP 4274A and HP 4275A with basic accuracy of 0.1%. The temperature dependence of the pyroelectric coefficient and spontaneous polarization were measured with the HP 41408 picoampere meter. A HP 9825A desktop computer was used for on-line control of automatic measurement through a HP 69048 multi-programmer interface. Special softwares were developed for automatic measurement. Linear temperature change with specified rates was easily achieved. The reproducibility of measurements was excellent.

The dielectric and pyroelectric behavior of ATGSP with low phosphorous content (sample 1)shows no significant improvement on TGS; while the crystal with high phosphorus content (sample 3) exhibits very low ferroelectricity, hence only a very low pyroelectric coefficient is achieved. Only the crystal with appropriate phosphorus content (sample 2) exhibits excellent dielectric and pyroelectric properties. Most of our measurement has been done on this crystal.

Figure 2 is the temperature dependence of dielectric constant K_{22} and loss tangent of the ATGSP crystal. The Curie temperature of ATGSP is 51°C. Because of the chemical bias effect of the alanine group, no significant depolarization can be observed. The dielectric constant at room temperature is about 30, which is lower than that of well polarized TGS crystals. The frequency dependence of dielectric constant at room temperature in the wide frequency range

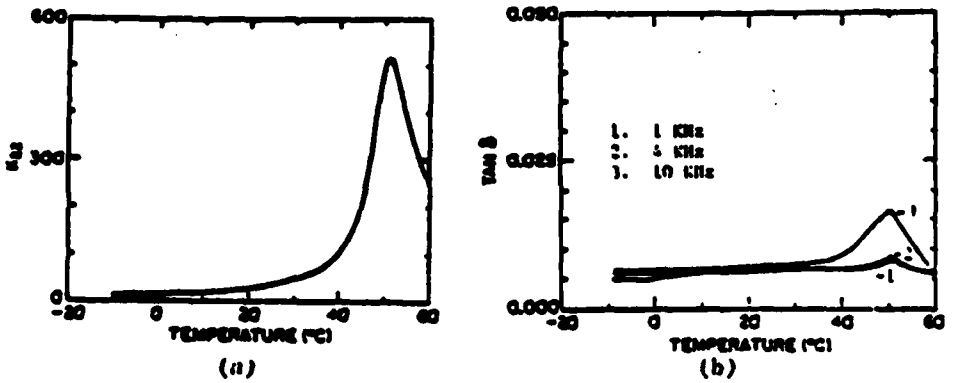

Figure 2. The temperature dependence of dielectric constant K_{22} (a) and loss tangent (b) of ATGSP crystal.

of 10^2-10^5 is negligible. The loss tangent of the ATGSP crystal at room temperature is lower than $1 \cdot 10^{-2}$ in the same frequency range, which is comparable with the best TGS crystals.

The pyroelectric response of the ATGS crystal is improved significantly by the partial substitution of phosphate for sulfate group in TGS. Figure 3 and Figure 4 are the temperature dependence of spontaneous polarization and pyroelectric coefficient of ATGSP crystal. Because of the chemical bias effect, the ATGSP crystal is permanently poled below the Curie temperature. Therefore, no prepoling is needed. At room temperature, the spontaneous polarization of ATGSP is about $5 \cdot 10^{-2}$ C/m^2, which is higher than $2.8 \cdot 10^{-2}$ C/m^2 of TGS. The pyroelectric coefficient of ATGSP at room temperature is about 6-$7 \cdot 10^{-4}$ C/K·m^2, which is more than twice that of TGS's (2-$3.5 \cdot 10^{-4}$ C/K·m^2).

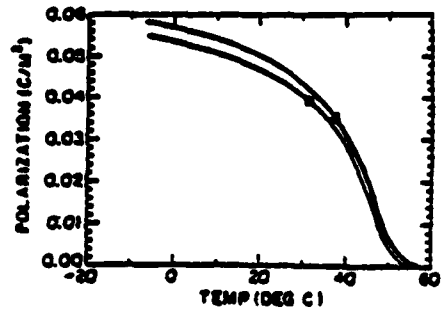

Figure 3. The temperature dependence of spontaneous polarization of ATGSP crystal.

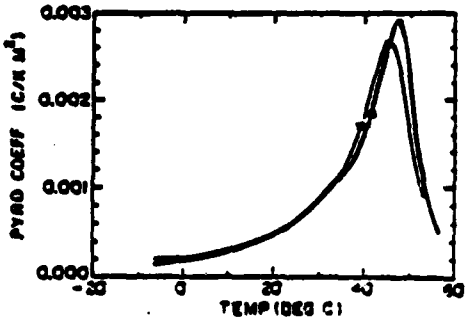

Figure 4. The temperature dependence of pyroelectric coefficient of ATGSP.

In view of the rather low actual incorporation of the phosphate group in the TGS structure, the very major change in P_s and pyroelectric coefficient is quite surprising. Most modifications to TGS result in a large value of the crystallographic b parameter, and a lowering of P_s. It may be noted, however, that in the fluoberyllate TGFB which has both higher T_c and larger P_s than TGS, again the b parameter is smaller.

With such significant improvement in pyroelectric parameters, an obvious next step is to explore deuteration of the ATGSP and this work is now in progress.

A comparison of ATGSP and TGS crystals is given in Table 2.

Table 2. Dielectric and pyroelectric properties of doped TGS crystals at room temperature.

crystal	ϵ_{22}	tg δ	T_c(°C)	P_s(x10^{-2}C/m^2)	P(x10^{-4}C/m.K)	Depolarization	Figure of merit $\frac{P}{C_v}$(x10^{-5}C/m^2)
TGS	35-50	0.004-0.01	49	2.8	2-3.5	Yes	1
ATGS	30		49	3.0	3.6	No	1.1
[illegible]	25		75	4.3	4.0	Yes	1.5 (at 50°C)
ATGSP	30	0.004	51	3.0	6-7	No	2.3

ACKNOWLEDGEMENT

We wish to thank Mr. H. Gong for atomic absorption spectrum analysis.

REFERENCES

1. B. Brezina, Mat. Res. Bull. 6, 401 (1971).

2. K.L. Bye, P.W. Whipps, E.T. Keve and H.R. Josey, Ferroelectrics 7, 179 (1974).

3. J.E. Gordon and D.G. Boal, Ferroelectrics 17, 411 (1977).

4. V. Winterfeldt, G. Schanck and A. Klopperpieper, Ferroelectrics 15, 21 (1977).

5. E.H. Puity, Optics and Laser Tech. 3, 150 (1971).

6. P.J. Lock, Applied Physics Letters 19(10), 390 (1970).

7. E.T. Keve, K.L. Bye, P.W. Whipps and A.D. Annis, Ferroelectrics 3, 39 (1971).

APPENDIX 15

Ferroelectrics, 1983, Vol. 50, pp. 257-262
0015-0193/83/5001-0257$18.50/0

QUANTUM - FERROELECTRIC PRESSURE SENSOR

C.F. CLARK AND W.N. LAWLESS
CeramPhysics, Inc., Westerville, Ohio 43081

S.L. SWARTZ
Materials Research Laboratory, Pennsylvania State University, State College, Pennsylvania 16802

Abstract Quantum ferroelectrics are characterized by a temperature-independent dielectric constant at low temperatures ($\partial\varepsilon/\partial T=0$), yet in this temperature range the Clausius-Mossotti relation requires that the dielectric constant have a non-zero pressure dependence ($\partial\varepsilon/\partial p\neq 0$). Consequently, a quantum ferroelectric can be used as a cryogenic pressure sensor which is independent of temperature and intense magnetic fields and would be useful as a solid-state device for sensing overpressures in superconducting magnets. Research in the ceramic system $(Cd_{1-x}Pb_x)_2\ (Nb_{1-y}Ta_y)_2\ O_7$ has revealed a compositional range where quantum effects dominate below 15K (i.e., $\partial\varepsilon/\partial T=0$). A sensor made from these ceramics will have $\varepsilon^{-1}\propto p$ up to 30 kbar, and such sensors can be made in the form of small (e.g., 2x2x5 mm) multilayer capacitors. Such devices are anticipated to have pressure sensitivities $\Delta C/\Delta p \approx 450$ pF/kbar at 4.2K.

The purpose of this paper is to present the results of work being done to develop a solid-state, ceramic pressure sensor useful at liquid helium temperatures and at pressures up to at least 30 kbars.[1] The devices would be made from a quantum ferroelectric compound and would have almost no temperature dependence over the 2-10 K range. This paper is divided into three parts: (1) The background of the concept; (2) Experimental results; and (3) A device model based on these results.

A quantum ferroelectric is distinguished from a "classical" ferroelectric in that quantum fluctuations (i.e., zero-point motion) suppress the transition to a polarized state. The result is a plateau in the dielectric constant over some finite temperature

range as T→0. Recent studies have concentrated on crystals of $KTaO_3$ and $SrTiO_3$ and associated solid solutions which exhibit this quantum ferroelectric behavior.[2-5] The transition temperature in these systems can be changed by substitution of small amounts of different ions in the compound, e.g. Nb for Ta in $KTaO_3$.

The pressure dependence of the dielectric constant is unchanged and may be related to the compressibility of the material through the Clausius-Mossotti formula as given by Bosman and Havinga.[6]

$$\left(\frac{\partial \epsilon}{\partial p}\right)_T = (1/3)\ (\epsilon-1)\ (\epsilon+2)\beta\ \left(\frac{\partial \ell n \alpha}{\partial \ell n V}-1\right) \tag{1}$$

where β is the compressibility and α is the polarizability of a small macroscopic sphere of volume V. For $\epsilon \gg 1$

$$\left(\frac{\partial \epsilon}{\partial p}\right)_T = M\epsilon^2 \tag{2}$$

where $M = 1/3\,\beta\,\left(\frac{\partial \ell n \alpha}{\partial \ell n V}-1\right)$. Equation (2) is equivalent to:

$$\left(\frac{\partial (1/\epsilon)}{\partial p}\right)_T = -M \tag{3}$$

and Equation (3) has been verified experimentally for $KTaO_3$ by Abel.[7]

Neither the $KTaO_3$ system nor the $SrTiO_3$ system would be suitable for pressure sensors. Ceramics in the $KTaO_3$ system have uncontrollable losses of K_2O during formation and single crystals are expensive. $SrTiO_3$ ceramics have two disadvantages: (1) The refractory ceraming temperatures (~1500°C) lead to well-documented irreproducibilities and loss of dopant/substitutional ions; and, more seriously, (2) The quantum regime appears limited to ≤ 4 K with little hope of raising this boundary.

The recent work on the $KTaO_3$ system showed that a ferroelectric transition could be induced in a known quantum ferroelectric

by substituting Nb ions on the Ta site. By analogy it might be possible to make substitutions into a known ferroelectric and induce quantum ferroelectric behavior. The dielectric constant of $Cd_2Nb_2O_7$ pyrochlore system with Pb substitutions on the A site and Ta substitutions on the B site has been investigated by Jona, et al.[6] They found a suppression of T_c from 185 K to 50 K when the Pb or Ta substitutions were varied from 0 to 20 mole %. Our work has investigated this system by making both Pb substitutions on the A site and Ta substitutions on the B site. The system has the general formula $(Cd_{1-x}Pb_x)_2(Nb_{1-y}Ta_y)_2O_7$.

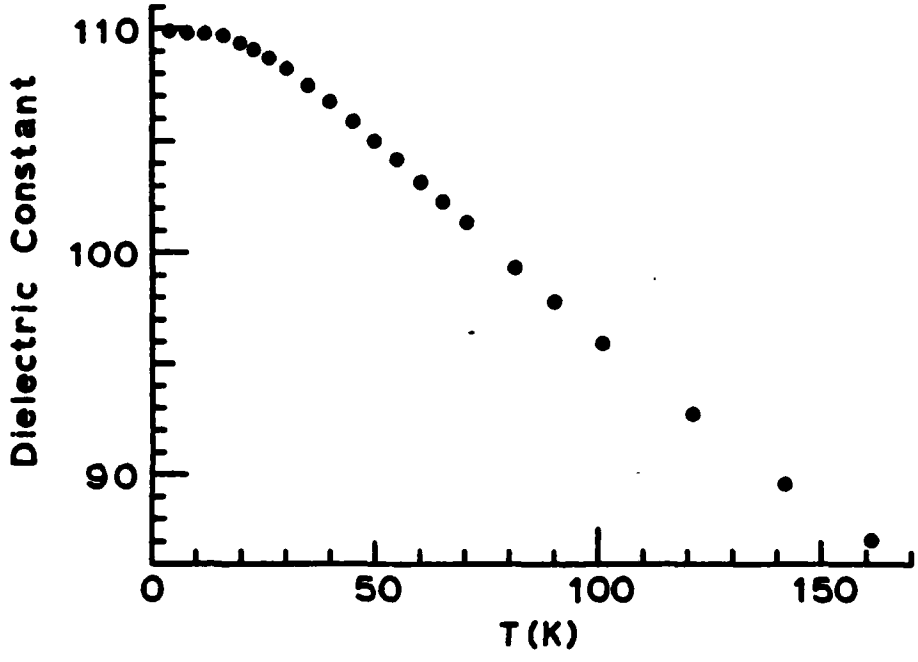

FIGURE 1 Dielectric constant versus temperature for $(Cd_{.80}Pb_{.20})_2\ (Nb_{.20}Ta_{.80})_2\ O_7$.

Our work has been successful in moving the system into the quantum regime. Figure 1 shows the dielectric constant as a function of temperature for a typical compound in the quantum regime,

x=0.20, y=0.80. Figure 2 shows data for a smaller temperature range of the best compound found so far, x=0.60, y=0.50.

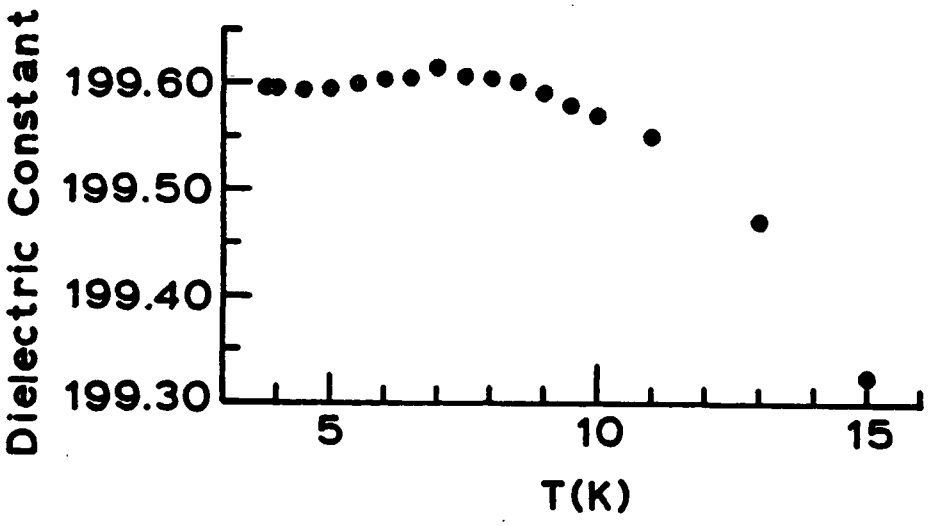

FIGURE 2 Dielectric constant versus temperature for $(Cd_{.40}Pb_{.60})_2(Nb_{.50}Ta_{.50})_2O_7$.

In general, making either Pb or Ta substitutions lowers the transition temperature until a limit of about 7-8 K is reached. All the compounds have shown a slight peak even when Tc is low (cf. Fig. 2), but the peak never is below 7-8 K even when the compound is clearly in the quantum regime. This behavior also holds for single-crystal, quantum ferroelectric, $KTaO_3$ which has a slight peak around 3 K.[9] For the $Cd_2Nb_2O_7$ system the maximum dielectric constant (i.e., at T_c) is lowered as x and y increase, but ε remains high enough (>200 for x=0.60, y=0.50) for a pressure sensor to have a large pressure sensitivity (cf. Eq. 2).

The selection criteria for the best material for a pressure sensor not only take into account the flatness over as large a temperature range as possible, but also include keeping the dielectric constant as large as possible and keeping the Ta content as

low as possible. The dielectric constant should be high in order to maximize the pressure sensitivity (cf. Eq. 2), and keeping the Ta concentration low keeps the ceramic sintering temperature low. Of the combinations analyzed, the compound with x=0.60, y=0.50 was the best choice given the above criteria.

With the measurements on this material as shown in Fig. 2, it is possible to describe the characteristics of a real device. For a 2x2x5 mm device size it would be possible to manufacture a multilayer device of 66 layers, each with a dielectric thickness of .002921 cm and an overlap area of electrodes of .0570 cm. The capacitance of the device at 4.2 K would be 22.77 nF.

The pressure sensitivity depends on the value of M in Eq. 2. This parameter has yet to be determined for our system. However, it has been determined for other ferroelectrics over a range of temperatures[7] and for $Cd_2Nb_2O_7$ at room temperature.[6] M does not vary greatly and a reasonable assumption would be $M = -10^{-4}$ $(kbar)^{-1}$ for our material. Then for our model device at 4.2 K

$$(\partial C/\partial p)_T = 450 \text{ pF/kbar}$$

On a six place General Radio capacitance bridge the smallest detectable capacitance change would be 0.1 pF or, equivalently, 0.22 bars. If the temperature is between 4 and 9 K, but otherwise unknown, then the uncertainty in capacitance would be 2.8 pF due to the slight temperature variation of ε in this temperature range, and the corresponding uncertainty in pressure would be 6.2 bars. Around 4 K the temperature sensitivity of the capacitance is 0.7 pF/K. A typical temperature uncertainty for a system at liquid helium temperatures might be .050 K. This uncertainty would be equivalent to a pressure uncertainty of .077 bars, i.e., less than the maximum readable sensitivity of a six-place bridge.

There are a number of tests to be run before a practical device is available. Actual multilayer devices are presently being

fabricated and these will need to be tested for stability within a single cool-down and for reproducibility from cool-down to cool-down. The magnetic field dependence will be determined at the National Magnet Laboratory at MIT and measurements of the constant M in Eq. 2 will be made at Sandia National Laboratories.

REFERENCES

(1) This work is supported under a grant from the NSF SBIR program Contract No. DMR-8113317.
(2) U.T. Hochli and L.A. Boatner, Phys. Rev. B20, 266(1979).
(3) D. Rytz, U.T. Hochli, and H. Bilz, Phys. Rev. B22, 359(1980).
(4) U.T. Hochli, H.E. Weibel, and L.A. Boatner, Phys. Rev. Lett. 39(1977).
(5) K.A. Miller and H. Burkhard, Phys. Rev. B19, 3593(1979).
(6) A.J. Bosman and E.E. Havinga, Phys. Rev. 129, 1593(1963).
(7) W.R. Abel, Phys. Rev. B4, 2696(1971).
(8) F. Jona, G. Shirane, and R. Pepinsky, Phys. Rev. 98, 903(1955).
(9) W.N. Lawless, unpublished.

APPENDIX 16

NATIONAL CENTER FOR DIELECTRIC STUDIES

The Pennsylvania State University

Full Member Companies	Representative
AVX Corporation	Dr. Kim Ritchie
Corning Glass Works	Dr. H. Garfinkel
E.I. DuPont	Dr. I. Burn
Hewlett Packard Corporation	Dr. W.F. Mooy
IBM Corporation	Dr. J. Humenik
San Fernando Electric Company	Dr. M. Rosenberg
Sprague Electric Company	Dr. G. Love
TAM Ceramics	Dr. C.E. Hodgkins
Union Carbide Corporation	Dr. J. Piper
Vitramon Corporation	Dr. J. Soong

Associate Member Companies	Representative
American Technical Ceramics	Dr. V. Capozzi
AMP, Inc.	Dr. J. Diener
Cabot Corporation	Dr. R.A. Hard
Centre Engineering	Dr. J.W. McCrea
Dow Chemical	Dr. E.F. Engles
Electro-Science Labs, Inc.	Dr. S.J. Stein
Engelhard Industries	Dr. J. Constantine
Ferro Corporation	Dr. G. Braun
Heraeus Cermalloy	Dr. K.R. Bube
Metz Metallurgical	Dr. M. Metz
Norton Company	Dr. A.K. Agarwal

APPENDIX 17

Responsible DOD Organization:	**Office of Naval Research Department of the Navy Arlington, VA 22217**
Contract No.:	**N00014-82-0190**
Performing Organization:	**Lehigh University 203 E. Paker Ave. Bethlehem, PA 18015**
Principle Investigator:	**Dr. Donald Smyth**

25. (U) Degradation rates of $BaTiO_3$-based ceramic dielectrics have been measured at stresses of 4 Kv/cm at 100°C and 1 Kv/cm at 200°C as a function of composition and microstructure. The results are consistent with previous suggestions that degradation is caused primarily by the migration of oxygen vacancies. BaO-rich and highly donor-doped samples both show particular resistance to degradation, with excess BaO having a capability for counteracting the usual deleterious defects of acceptor impurities. These two compositional types are related through the mode of compensation for donor impurities, and similarities in their microstructure have been observed. Grain size variations from 1-10 microns had no effect on the degradation rate of undoped $BaTiO_3$ with Ba/Ti = 1.000. Ca-doped $BaTiO_3$ has been studied due to reports of a commercial dielectric capable of being cofired with nickel electrodes and which showed excellent stability. It has been shown that Ca acts as an acceptor-dopant when Ba+Ca/Ti greater than 1, i.e. when there is an excess of alkaline earth cations, apparently by partial occupation of Ti-sites in the structure. This has been confirmed by comparison of the intensities of characteristic x-rays as a function of electron beam orientation in individual grains (a technique known as ALCHEMI). These Ca-doped materials showed very poor degradation resistance, however.

TR Degradation Mechanisms in Ceramic Dielectrics, D.M. Smyth and M.P. Harmer, August 1, 1983

Responsible DOD Organization: Office of Naval Research
Department of the Navy
Arlington, VA 22217

Contract No.: N00014-82-K-0313

Performing Organization: Rutgers University
College of Engineering
P.O. Box 909
Piscataway, NJ 08859

Principle Investigator: Dr. W. Roger Cannon

25. (U) A series of screening tests on approximately seventy dispersants led to only three which showed excellent dispersion effectiveness. These were Emphos 21-A, a phosphate ester (Whitco Chemical Co.) Menhaden fish oil (Kellog), a fatty acid and zonyl A (DuPont) an ethoxylate. Further studies on the phosphate ester indicated that 0.8% addition was optimum and that settling factors as high as 70% could be achieved. It was proposed that the excellent dispersion effectiveness of the phosphate ester was related to the ionization of the ester which imparted a larger positive charge to the surface and helped anchor the long chained molecules to the surface as well as helped achieve double layer repulsion.

TR Deflocculants for Tape Casting Barium Titanate Dielectrics, W. Roger Cannon, July, 1983.

Responsible DOD Organization:	Office of Naval Research Department of the Navy Arlington, VA 22217
Contract No.:	N00014-82-K-0312
Performing Organization:	Rutgers University College of Engineering P.O. Box 909 Piscataway, NJ 08859
Principle Investigator:	Dr. John B. Blum

25. (U) The dispersion of a slurry by ultrasonic agitation was compared to that of ball milling. It was found that the ultrasonically dispersed slurry settled slower and to a denser compact. Further is has a lower viscosity and was less agglomerated. Mixtures of two different particle-size distribution $BaTiO_3$ powders were made. The mixtures were incorporated into a tape casting slurry and the slurry viscosity, green tape density and green tape strength were evaluated. Broadening the particle-size distribution of a fine, narrowly distributed powder resulted in lower slurry viscosities and higher green tape densities. The broadened distribution also resulted in a green tape with a lower tensile yield stress and greater deformation before failure. A deep level spectroscopy (DLTS) system has been designed and assembled. Calibration fo the components of the system and preliminary.

TR Improved Particle Size Distribution for Tape Casting $BaTiO_3$ and a DLTS Study of Grain Boundaries in $BaTiO_3$, by John B. Blum, June, 1983.

Responsible DOD Organization:	**Office of Naval Research Department of the Navy Arlington, VA 22217**
Contract No.:	**N00014-82-K-0336**
Performing Organization:	**University of Missouri-Rolla 222 Fulton Hall Rolla, MO 65401**
Principle Investigator:	**Dr. Harlan V. Anderson**

25. (U) A computer interfaced current-voltage system was developed. The system allows for the simultaneous measurement of current-voltage characteristics on ninety different specimens under ten different conditions. An apparatus to measure thermally stimulated currents for capacitor dielectric materials was also developed. Initial measurements of thermally stimulated currents on a variety of dielectric compositions (X7R, Z5U, NPO) were carried out. The interpretation of the measurements remains to be done.

T.R., H. Anderson, 'Current Status of Dielectric Studies,' August, 1983

Responsible DOD Organization:	Office of Naval Research Department of the Navy Arlington, VA 22217
Performing Organization:	University of Illinois Department of Ceramic Engineering Urbana, IL 61801
Principle Investigator:	Dr. R.C. Buchanan

23. (U) The objective of this work is to investigate the feasibility of fabricating dense, optically transparent ceramic compounds by liquid phase sintering.

24. (U) Several compounds have been identified in other research programs as having potential for optical (IR) window applications. Among these are ZrO_2, $3Al_2O_3$, $2SiO_2$ and complex germanates. Fabrication paths using reactive liquid phase sintering of these refractory ceramic compounds will be explored. This would entail selection and/or development of suitable liquid phase additives for the different compounds and optimization of process variables to achieve maximum densification. Sintering kinetics, process characterization, microstructure and properties are also a focus of this study.

Responsible DOD Organization:	Office of Naval Research Department of the Navy Arlington, VA 22217
Contract No.:	N00014-83-K-0168
Performing Organization:	Virginia Polytechnic Institute and State University Blacksburg, VA 24061
Principle Investigator:	Professor L. Burton

25. (U) The voltage and temperature dependence of leakage currents were measured on new and degraded X7R and Z5U dielectric materials. Ohmic, Schottky and space change limited currents were observed. Above 1 volt space charge limited currents were the dominant type of current for degraded materials. Activation energies were typically 1 eV for pristine materials and zero for degraded materials. The electrical measurements data were modelled in terms of grain boundary or trap activation energies. New and degraded capacitors were cross sectioned (both by fracture and polishing) and characterized by SEM/EDAX methods. No lead penetration into the ceramic body was observed.

L.R. 'Conductivity in Dielectrics,' L. Burton, September, 1983.

Responsible DOD Organization: Office of Naval Research
Department of the Navy
Arlington, VA 22217

Performing Organization: Purdue University
West Lafayette, IN 4790

Principle Investigator: Professor R. Vest

23. (U) Missile guidance systems require one hundred percent reliable operation of their electronic components. The objective of this research is to explore new methods for fabricating high quality multilayer ceramic dielectrics.

24. (U) The approach will involve the exploration of metallo-organic precursors as a means of engineering the molecular and microstructural characteristics of the dielectric material. Research on organic precursors and solvents will be carried out. The effects of thermal treatments on the resultant chemistry, microstructure, and structure will be defined. The required ink chemistry and processing condition to produce high quality, uniform, continuous films will be determined.

Responsible DOD Organization:	**Office of Naval Research Department of the Navy Arlington, VA 22217**
Contract No.:	**N00014-83-C-0141**
Performing Organization:	**Honeywell Ceramics Center 5121 Winnetka Avenue North New Hope, MN 55428**
Principle Investigator:	**Dr. Barry Koepke**

25. (U) All samples for the first phase of the work have been received. These included approximately 300 special $BaTiO_3$ multilayer ceramic plates which will be used for determining the effects of chemical and electrical environments on slow crack growth as a function of orientation. Remnants of these specimens after test will be used for stress reaction measurements. In addition, 200 $BaTiO_3$ multilayer capacitors were received which will be used for static fatigue measurements. The testing equipment has been fabricated, installed and calibrated. Full scale testing will be started as soon as a new strip chart recorder has been received.

TR Progress Report on Multilayer Cracking by Kelly D. McHenry, August 15, 1983.

END

FILMED

10-84

DTIC